Department of Electrical and Electronic Engineering

Resource Allocation in Heterogeneous Networks

Nakrop Jinaporn

A dissertation submitted to the University of Bristol in accordance with the requirements for award of the degree of PhD in the Faculty of Engineering

EPSRC Centre for Doctoral Training in Communications

December 2019

Abstract

Due to the heterogeneity and new capacity demands in fifth generation (5G) networks, a heterogeneous network (HetNet) is being considered by the long-term evolution (LTE)-advanced to satisfy these network requirements. Due to a mix of high and low power base stations, spectral and energy efficiencies could be improved as compared with the traditional cellular network. Whereas the HetNet seems to be an efficient approach, there are still research questions on how resource allocation in such a network could be enhanced. Another challenge is the usage of unlicensed bands in future wireless networks. The coexistence between the LTE and WiFi networks within the unlicensed spectrum should be considered.

In this thesis, a system-level (SL) simulator has been developed based on the Monte Carlo simulation approach to model downlink LTE cellular networks. Key user throughput statistics such as peak, mean and edge throughputs are used for the performance evaluation throughout this thesis. The small cell deployment is first investigated by this developed simulator. By increasing the number of femtocells, the peak throughput could be around eight times as large as the conventional cellular network. User throughputs can be gained by the resource block (RB) scheduling as well. The best-channel quality indicator (CQI) scheduler appears to be the best choice to boost mean and peak throughputs as compared to the round-robin (RR) scheduler.

The simulator is further developed to model the carrier aggregation (CA). Component carrier (CC) selection and RB scheduling are considered separately. Because of the

different load balance across CCs, the peak throughput of the RR CC selector could be around three times as large as the reference signal received power (RSRP) CC selector. The combination of frequency bands and RB scheduling in the CA deployment are also investigated.

Another focus of attention is the usage of unlicensed spectrum in the LTE network. It is called the unlicensed-LTE (U-LTE) in this thesis. The frame-based listen-before-talk (LBT) algorithm is included in the developed simulator to coexist the LTE and WiFi networks in the unlicensed spectrum. The novel resource allocation for the U-LTE is proposed. The LTE transmission probability on CCs derived from the WiFi network is defined for the clear channel assessment (CCA) and CC selection. The transmission probability threshold is used instead of the energy detection (ED) threshold. Subsequently, the proposed CC selectors, including maximum probability (MaxProb), random and RR, are examined. Due to the best CC load balance, the RR CC selector could offer around a twofold increase in mean and peak throughputs of the MaxProb CC selector. To investigate the impact of RB scheduling on the performance metrics in the U-LTE, user throughputs, including minimum, mean and maximum, between the macro and femto networks are compared. For the femto network, the highest user throughput could be obtained by the best-CQI scheduler.

In summary, key user throughput statistics can be significantly enhanced by the small cell deployment and CA as mentioned above. Load balancing across CCs is preferable to offer higher user throughputs. It is found that the choice of RB scheduling should be considered in connection with user throughput, fairness and computational complexity. In addition to CC selection and RB scheduling, there is still room for improvement in the coexistence between the LTE and WiFi networks within the unlicensed spectrum for both modelling and real implementation.

Dedication and Acknowledgements

I owe my deepest gratitude and sincere thanks to my supervisors, Dr Simon Armour and Professor Angela Doufexi, for their valuable guidance and encouragement to complete this PhD thesis. I would like to show my gratitude to Dr George Oikonomou, Miss Suzanne Binding and all CSN/CDT friends for their useful suggestions and support. I would like to thank my scholarship provider, the Royal Thai Government, for financial support. And last but not least, I would like to thank my parents, wife and daughter for their understanding and support on me. I would like to dedicate my PhD thesis to all of them.

Author's Declaration

I declare that the work in this dissertation was carried out in accordance with the requirements of the University's *Regulations and Code of Practice for Research Degree Programmes* and that it has not been submitted for any other academic award. Except where indicated by specific reference in the text, the work is the candidate's own work. Work done in collaboration with, or with the assistance of, others, is indicated as such. Any views expressed in the dissertation are those of the author.

SIGNED: Nakrop Jinaporn DATE: 14 December 2019

Contents

List of Figures

List of Tables

List of Abbreviations

2G Second Generation. 1

3G Third Generation. 1

3GPP Third-Generation Partnership Project. 1

3GPP2 Third-Generation Partnership Project 2. 1

4G Fourth Generation. 1

5G Fifth Generation. i

ACK Acknowledgment. 61

AI Artificial Intelligence. 113

AP Access Point. 35

BCCH Broadcast Control Channel. 11

BCH Broadcast Channel. 11

BICM Bit-Interleaved Coded Modulation. 119

BLER Block Error Rate. 39

CA Carrier Aggregation. i

CC Component Carrier. i

CCA Clear Channel Assessment. ii

CCCH Common Control Channel. 11

CDMA Code-Division Multiple Access. 1

CP Cyclic Prefix. 9

CQI Channel Quality Indicator. i

CRC Cyclic Redundancy Check. 123

CSAT Carrier-Sensing Adaptive Transmission. 23

CSG Closed Subscriber Group. 16

CSMA/CA Carrier-Sense Multiple Access with Collision Avoidance. 24

DCCH Dedicated Control Channel. 11

DCS Dynamic Channel Selection. 23

DFS Dynamic Frequency Selection. 25

DFT Discrete Fourier Transform. 9

DL Downlink. 3

DL-SCH Downlink Shared Channel. 12

DRS Discover Reference Signals. 26

DTCH Dedicated Traffic Channel. 11

DTMC Discrete-Time Markov Chain. 36

DTX Discontinuous Transmission. 94

eCCA Extended Clear Channel Assessment. 24

ecdf Empirical Cumulative Distribution Function. 62

ED Energy Detection. ii

EDGE Enhanced Data Rates for Global Evolution. 1

eLAA Enhanced License Assisted Access. 25

eMBB Enhanced Mobile Broadband. 2

eNB Evolved Node B. 15

EPA Extended Pedestrian A. 53

ERAA Efficient RB Allocation Algorithm. 34

ESM Effective SINR Mapping. 119

ETU Extended Typical Urban. 53

EV-DV Evolved Data Voice. 1

EVA Extended Vehicular A. 53

FDD Frequency-Division Duplexing. 12

FFT Fast Fourier Transform. 10

FOSS Free and Open Source Software. 113

GA Greedy Algorithm. 33

GERAN GSM EDGE Radio Access Network. 1

gNB gNodeB. 112

GPRS Generalised Packet Radio System. 1

GSM Global System for Mobile Communications. 1

HARQ Hybrid Automatic Repeat Request. 26

HD High-Definition. 2

HeNB Home eNB. 15

HetNet Heterogeneous Network. i

HSPDA High Speed Downlink Packet Access. 1

IFFT Inverse Fast Fourier Transform. 10

ILP Integer Linear Programming. 34

IMT-A International Mobile Telecommunications-Advanced. 16

IoT Internet of Things. 4

ISM Industrial, Scientific, and Medical. 21

ITU International Telecommunication Union. 53

L2S Link-to-System. 118

LAA License Assisted Access. 12

LBT Listen-Before-Talk. ii

LL Link Level. 39

LP Linear Programming. 34

LTE Long-Term Evolution. i

LTE-A LTE-Advanced. 2

MAC Medium Access Control. 11

MaxProb Maximum Probability. ii

MCH Multicast Channel. 12

MCL Minimum Coupling Loss. 47

MCS Modulation and Coding Scheme. 26

MI Mutual Information. 119

MIESM Mutual Information Effective SINR Mapping. 41

MIMO Multiple-Input Multiple-Output. 2

mMTC Massive Machine Type Communications. 2

mmWave Millimetre-Wave. 21

MSUL Minimising System Utility Loss. 33

NACK Negative Acknowledgement. 27

NL Network Level. 39

NR New Radio. 4

OFDM Orthogonal Frequency-Division Multiplexing. 2

OFDMA Orthogonal Frequency-Division Multiple Access. 9

OOP Object-Oriented Programming. 42

OSG Open Subscriber Group. 16

PAPR Peak-to-Average Power Ratio. 9

PBCH Physical Broadcast Control Channel. 12

PCC Primary Component Carrier. 19

PCCH Paging Control Channel. 11

PCell Primary Serving Cell. 19

PCFICH Physical Control Format Indicator Channel. 12

PCH Paging Channel. 12

PDCCH Physical Downlink Control Channel. 12

PDCP Packet Data Convergence Protocol. 11

pdf Probability Density Function. 55

PDP Power Delay Profile. 53

PDSCH Physical Downlink Shared Channel. 12

PedA Pedestrian A. 53

PF Proportional Fair. 28

PHICH Physical Hybrid Automatic Repeat Request Indicator Channel. 12

PHY Physical Layer. 11

PMCH Physical Multicast Channel. 12

PRB Physical Resource Block. 13

PUSCH Physical Uplink Shared Channel. 19

QoS Quality of Service. 21

RAT Radio Access Technology. 20

RB Resource Block. i

RE Resource Element. 13

RF Radio Frequency. 17

RI Rank Indicator. 122

RLC Radio Link Control. 11

ROI Region of Interest. 40

RR Round Robin. i

RRC Radio Resource Control. 19

RRH Radio Remote Head. 15

RRM Radio Resource Management. 39

RSRP Reference Signal Received Power. ii

RSRQ Reference Signal Received Quality. 112

SC-FDMA Single-Carrier-Frequency-Division Multiple Access. 9

SCC Secondary Component Carrier. 19

SCell Secondary Serving Cell. 19

SDL Supplemental Downlink. 25

SINR Signal-to-Interference-plus-Noise Ratio. 25

SISO Single-Input Single-Output. 65

SL System-Level. i

TB Transport Block. 61

TDD Time-Division Duplexing. 12

TDM Time-Division Multiplexing. 23

TDMA Time-Division Multiple Access. 1

TPC Transmit Power Control. 25

TTI Transmission Time Interval. 58

TU Typical Urban. 53

U-LTE Unlicensed LTE. ii

U-NII Unlicensed National Information Infrastructure. 21

UE User Equipment. 12

UL Uplink. 9

uRLLC Ultra-Reliable and Low Latency Communications. 2

UWB Ultra-Wideband. 21

WCDMA Wideband CDMA. 1

WiMAX Worldwide Interoperability for Microwave Access. 1

ZF Zero Forcing. 116

Chapter 1

Introduction

1.1 Background and Motivations

In the late 1980s the global system for mobile communications (GSM), the first digital cellular network, was introduced. Based on time-division multiple access (TDMA), the theoretical peak rate of 9.6 kbps could be provided by the second generation (2G). To achieve higher peak rates and spectral efficiency, the generalised packet radio system (GPRS) and enhanced data rates for global evolution (EDGE) were presented based on GSM technology while IS-95 code-division multiple access (CDMA) was developed in the early 1990s. The third generation (3G) began around the end of the 1990s. Wideband CDMA (WCDMA) and GSM EDGE radio access network (GERAN) standards were defined under the third-generation partnership project (3GPP). CDMA2000 was launched concurrently by the third-generation partnership project 2 (3GPP2). Subsequently, high speed downlink packet access (HSPDA) and CDMA2000 1x evolved data voice (1xEV-DV) systems were the two examples of 3.5G technologies introduced by 3GPP and 3GPP2, respectively. Around 2006 the worldwide interoperability for microwave access (WiMAX) based on the IEEE 802.16 and long term evolution (LTE Rel-8) were presented in the fourth generation (4G), both employing orthogonal frequency-division

multiplexing (OFDM). To enhance not only system performance metrics but also user experience, LTE-advanced (LTE-A) Rel-10 and WiMAX (IEEE 802.16m) have been considered for 4.5G systems. A peak rate of 3 Gbps could be offered by LTE-A Rel-10 with 100-MHz bandwidth and 8 $\times$ 8 multiple-input multiple-output (MIMO) configuration [3], a substantial increase when compared with GSM.

Unlike the traditional cellular networks, heterogeneous networks and increasing capacity demands have been considered resulting from dynamic radio topologies in the fifth generation (5G) systems. In [2], the UK mobile data traffic per month (in Petabytes) in 2019 is nearly a twofold gain over three years, as shown in Table 1.1. 90 percent of data traffic and 21 percent of voice traffic[1] are carried by 4G. 2G and 3G are still deployed with 6 percent and 73 percent of voice traffic, respectively. Whereas the majority of traffic is produced in urban areas, the traffic consumption in rural areas has also increased significantly.

In addition, the usage of mobile data is predicted to raise exponentially, resulting from a dramatic growth of mobile devices and bandwidth-greedy applications such as streaming high-definition (HD) video and gaming. According to [8], 5G services and applications can be classified into three groups: enhanced mobile broadband (eMBB), massive machine type communications (mMTC) and ultra-reliable and low latency communications (uRLLC). This means that future networks are needed to satisfy these different network requirements.

Another issue is on how to provide not only higher network capacity but also wider coverage, better user experience and lower costs, as compared to existing network deployments. Through ultra-densification and offloading, heterogeneous networks (HetNets), including high power (macro base stations) and low power (picocells, femtocells and relays) nodes, considered by the LTE-A are viewed as the network evolution to satisfy 5G requirements [3, 9, 10]. Although HetNets appear to be one promising solution, open

[1]The proportional of total minutes of originated calls is used for the measurement.

Table 1.1: The total mobile data traffic per month in the UK (adapted from [2]).

Year	**Total traffic (Petabytes)**
2017	156
2018	211
2019	294

challenges are also raised such as uncontrolled interference and resource sharing.

To model a cellular network, the system-level (SL) simulation has been widely used for radio planning and optimisation purposes [11]. Based on this SL approach, the aggregate interference can be generated resulting in accurate results, in particular interference scenarios. In addition, potential algorithms, including scheduling and power control, may be included in this simulation. The system performance such as throughput and spectral efficiency could be analysed.

In this thesis, the main aim is to study on how resource allocation in HetNets can be enhanced. This results in the three network scenarios of LTE cellular networks, including small cell deployment, carrier aggregation (CA) and the usage of unlicensed spectrum in the LTE network, are modelled and investigated by means of the developed SL simulator in Chapters 3 - 5. First, LTE homogeneous and heterogeneous cellular networks in downlink (DL) transmission are modelled in Chapter 3. Building blocks of the SL simulator are described step-by-step. For the simulation verification, the results from the simulator developed in this thesis are compared with a reference simulator [6]. The impact of small cell deployment and resource block (RB) scheduling techniques on the network performance is addressed. Second, the CA is analysed based on the simulation results for a homogeneous network in Chapter 4. Component carrier (CC) selection and RB scheduling are modelled by this developed simulator. Third, the SL simulation for HetNets with the unlicensed LTE (U-LTE) is performed in Chapter 5. A

novel resource allocation, including the clear channel assessment (CCA), CC selection and RB scheduling, using the LTE transmission probability on CCs is proposed for the simulation to enable LTE and WiFi networks to coexist in the (same) unlicensed spectrum. For all network scenarios above, the performance metrics are evaluated for the LTE network in terms of user throughputs and fairness index.

Note that the LTE standard is the focus of interest which is applied to the simulator developed in this thesis for comparison purposes. However, this work could be further modified for other standards and network deployments such as 5G new radio (NR) and cellular internet of things (IoT). The simulation stage such as network element placement, fading and resource allocation can be adapted for these later standards. Thus, there are still various challenges and future work on this research area.

1.2 Objectives

This thesis aims to examine resource allocation (RB scheduling and CC selection) and the coexistence issue within the unlicensed bands for LTE cellular networks in DL transmission by means of the SL simulation[2]. The main objectives include

- Creating the system model for modelling resource allocation in LTE network scenarios: small cell deployment, CA and U-LTE.
- Developing a novel algorithm of resource allocation for the U-LTE.
- Building a SL simulator based on the Monte Carlo approach for LTE cellular networks.

[2]In [7], the SL simulation is widely used to model a cellular network and evaluate the performance of the entire network in connection with the radio resource management. As compared with the analytical modelling, the SL approach appears to be more accurate and reliable. Besides, more complex cellular networks can be modelled by the SL simulation. However, the computing capability is the challenge of this SL approach to obtain a statistically representative result of the network performance.

- Evaluating the impact of resource allocation in the above network scenarios on the performance metrics: user throughputs and fairness index.

1.3 Contributions

The SL simulator based on the Monte Carlo approach developed in this thesis offers new functionalities and the main contributions by the author are as follows:

Although this developed simulator and the existing simulator [6] have the same approach of CA modelling where CC selection and RB scheduling are considered independently, the more variety of practical CC selectors, including round-robin, random and reference signal received power, is implemented in this thesis as compared with the existing work. In [6], either all active CCs are assigned to every UE with CA support or these active CCs are assigned cyclically to the UEs. Furthermore, the channel quality is included in the case of reference signal received power CC selector presented in Chapter 4 while the two CC selectors of the existing simulator are performed regardless of the channel condition.

Due to the limitation of existing simulator, the usage of unlicensed bands in LTE cellular networks cannot be modelled by the latest version of [6]. This results in a new simulator for the U-LTE which is further developed from the CA modelling discussed above. In addition to the CC selection and RB scheduling, the coexistence between the LTE and WiFi networks is included in this simulation. The frame-based listen-before-talk is selected for this coexistence mechanism.

To the best of this author's knowledge, a novel resource allocation of the U-LTE modelling is proposed in Chapter 5. The LTE transmission probabilities on all active CCs and transmission probability threshold are introduced to facilitate the clear channel assessment and CC selection. The LTE transmission probability threshold is used instead of the energy detection threshold. The three CC selectors based on the LTE transmission probabilities on CCs are presented. As compared to the existing energy

detection-based clear channel assessment, the proposed clear channel assessment using the LTE transmission probability threshold could offer a more straightforward and flexible way to coexist the LTE and WiFi networks in the unlicensed bands. Only the WiFi transmission probabilities and number of WiFi devices within the (shared) unlicensed bands are required by the centralised LTE base station to determine the LTE transmission probabilities on active CCs for this proposed channel assessment. Note that a CC is free if its corresponding LTE transmission probability is greater than or equal to the LTE transmission probability threshold.

Besides, the three CC selectors (maximum probability, round-robin and random) proposed in this thesis could be more suitable for the U-LTE deployment as compared with the conventional CC selection (round-robin, random and reference signal received power). This is because the LTE transmission probabilities on CCs derived from the WiFi transmission condition are included in the proposed CC selection while the conventional CC selectors are performed regardless of the WiFi network. The CC selection in the U-LTE is probably improved by means of the transmission condition from both LTE and WiFi networks.

Furthermore, there are conference publications resulting from this thesis (related to Chapters 3 and 4):

- N. Jinaporn, S. Armour, and A. Doufexi, "System-Level Simulation for Homogeneous and Heterogeneous Cellular Networks," in *2019 IEEE 89th Vehicular Technology Conference (VTC2019-Spring)*, 2019 [12].

- N. Jinaporn, S. Armour, and A. Doufexi, "Performance Evaluation on Resource Allocation with Carrier Aggregation in LTE Cellular Networks," in *2019 IEEE 90th Vehicular Technology Conference (VTC2019-Fall)*, 2019 [13].

1.4 Thesis Organisation

The remaining chapters of this thesis are organised as follows: background and related work are presented in Chapter 2. Subsequently, the methodology of the SL simulator developed in this thesis for homogeneous and heterogeneous networks is discussed in Chapter 3. The simulation verification is shown. Small cell deployments and scheduling are then investigated by this simulator. The CA-based resource allocation is modelled in Chapter 4. In the penultimate chapter, the resource allocation for the U-LTE is examined. Finally, a summary of the thesis and future work are concluded in Chapter 6.

Chapter 2

Background

The basic background and proposed work related to this thesis are presented. All relevant information in this chapter such as the LTE standard and resource allocation is applied to model the LTE cellular network in DL transmission by means of the SL simulation under different network scenarios in Chapters 3 - 5. The principle of LTE is first described in Section 2.1. Subsequently, the concept of HetNet is briefly outlined in Section 2.2. The CA and U-LTE are discussed in Sections 2.3 and 2.4, respectively. In Section 2.5, the review of resource allocation with LTE, CA and U-LTE is provided including existing algorithms and related work. Finally, the main points in this chapter are concluded in Section 2.6.

2.1 LTE

The 3GPP LTE [3, 14] has become the main standard of current cellular networks in 4G and is the main focus of attention in this thesis. The LTE environment, including transmission scheme and frame structure, is reviewed here, in particular the DL transmission.

2.1.1 LTE Overview

In [15], a comprehensive review of system and radio protocol architectures is presented. For the LTE transmission scheme, the orthogonal frequency-division multiple access (OFDMA) has been selected for DL transmission. Owing to the use of a cyclic prefix (CP) and the orthogonality in the frequency domain, the inter-symbol and intra-cell interference can be avoided [16, 17]. This results in the high spectral efficiency. Moreover, potential configurations can be supported such as multiple system bandwidth, low-complexity receivers, frequency-selective scheduling and MIMO [3].

However, the high peak-to-average power ratio (PAPR)[1] is the major drawback of this OFDMA scheme [16, 18]. This leads to a large back-off and the degraded efficiency of the power amplifier at the transmitter. Hence, the single-carrier-frequency-division multiple access (SC-FDMA) with a low power amplifier back-off has been used for the uplink (UL) transmission instead of the OFDMA. In this SC-FDMA scheme, a discrete Fourier transform (DFT) precoder is added to the conventional OFDMA processing, resulting in a single-carrier transmit signal. This implementation is also known as the DFT-spread OFDM. The PAPR problem of OFDMA signals can be alleviated by this additional precoder [18]. Because of the reduction in PAPR, the SC-FDMA results in many benefits to the mobile terminal such as transmitter power efficiency and low-power (less expensive) power amplifiers.

According to [3, 16], the total system bandwidth is divided into parallel subcarriers in OFDMA. A subchannel is then formed by a set of different subcarriers for the basic unit of data transmission. To generate a single OFDM symbol, the (input) data symbols are mapped to subcarriers in the frequency domain. Each data symbol is modulated and transmitted over one of the subcarriers as presented in Figure 2.1. Note that a RB is the basic transmission unit in LTE consisting of a group of 12 subcarriers with a frequency

[1]The PAPR is the ratio of peak to average power of a (OFDM) signal (in dB) where the power amplifier back-off requirement can be determined by this ratio.

spacing Δf of 15 kHz. Alternatively, the OFDM transmission and OFDMA can be illustrated in the time-frequency grid [19, 20, 21].

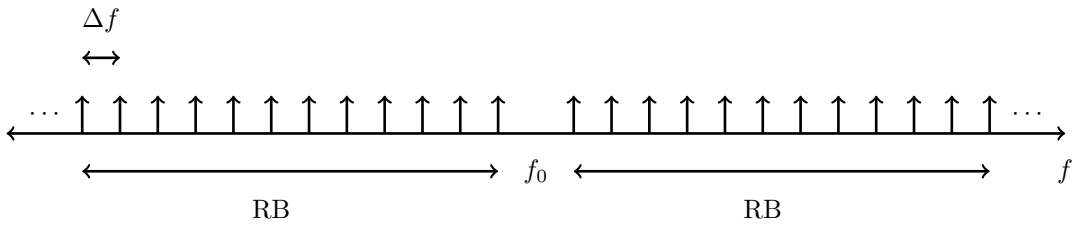

Figure 2.1: The OFDM transmission in the frequency domain. Let f_0 and Δf be the centre frequency and a frequency spacing, respectively. The usable subcarriers are placed around this f_0. A single RB is formed by 12 subcarriers with Δf of 15 kHz in this illustration.

Subsequently, these modulation symbols are converted into the time domain by the inverse fast Fourier transform (IFFT) algorithm. The sequence of time samples (output) from the IFFT is called an OFDM symbol [17]. Then a CP is added to the OFDM symbol before transmission. Figure 2.2 shows the OFDM symbol comprising of CP and data. Note that a subframe consisting of multiple OFDM symbols can be defined as the basic transmission unit in LTE. For instance, there are 14 OFDM symbols within a subframe in the case of normal CP. The reverse operation is performed at the receiver. For example, the modulation symbols in the frequency domain are obtained by the fast Fourier transform (FFT).

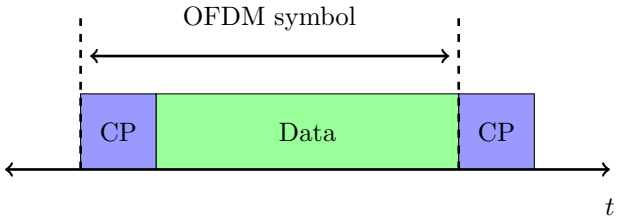

Figure 2.2: The OFDM symbol in the time domain.

2.1.2 LTE Downlink Transmission

In this section, the user-plane protocols and frame structure are described. The physical layer resource grid in DL transmission is also outlined.

2.1.2.1 Logical, Transport and Physical Channels

A simplified version of the protocol stack, including packet data convergence protocol (PDCP), radio link control (RLC), medium access control (MAC) and physical layer (PHY), is shown in Figure 2.3. Only the interaction among the last three layers is discussed. The logical channels are used to transfer data (user- and control-plane information) between the RLC and MAC layers. The dedicated traffic channel (DTCH) is reserved for user-plane data while four control logical channels, including the broadcast control channel (BCCH), paging control channel (PCCH), common control channel (CCCH) and dedicated control channel (DCCH), are provided for control-plane data.

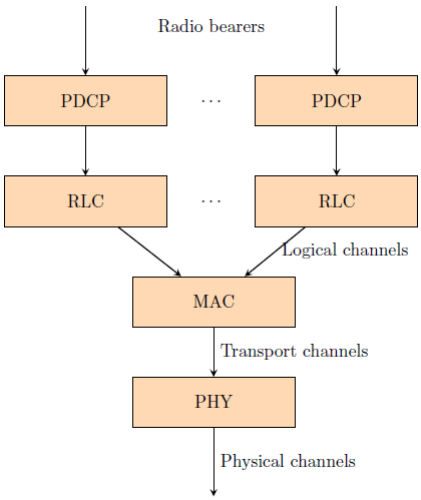

Figure 2.3: The user-plane data flow chart.

According to [22], the mapping between the MAC and PHY layers in DL is facilitated by four transport channels, including the broadcast channel (BCH), downlink

shared channel (DL-SCH), paging channel (PCH) and multicast channel (MCH). At the PHY, six physical channels are defined: the physical downlink shared channel (PDSCH), physical downlink control channel (PDCCH), physical control format indicator channel (PCFICH), physical hybrid automatic repeat request indicator channel (PHICH), physical broadcast control channel (PBCH) and physical multicast channel (PMCH). Also, the physical signals of synchronisation, cell-specific reference and user equipment (UE)-specific dedicated reference are supported.

2.1.2.2 Frame Structure

In LTE, data transmissions (DL, UL and sidelink) are performed within radio frames with $T_{\mathrm{f}} = 307200 \times T_{\mathrm{s}} = 10$ ms where $T_{\mathrm{s}} = \frac{1}{15000 \times 2048}$ seconds. Let T_{f} and T_{s} be the radio frame duration and basic time unit, respectively. Three frame structures are supported for frequency-division duplexing (FDD), time-division duplexing (TDD) and license assisted access (LAA) secondary cell operation [22]. To establish the duplex communications, two different carrier frequencies (channels) are assigned to UL and DL transmissions in FDD while different time slots in the same frequency band are used for each communication direction between the transmitter and receiver in TDD. For the LAA, the unlicensed spectrum can be utilised by the LTE system. The coexistence between the LTE and existing WiFi deployments in the unlicensed spectrum is strongly required. Therefore, the radio frame structures should be designed and selected in connection with these operation modes.

In this thesis, the frame structure of FFD (type 1) is the main focus of attention where each frame consists of 10 DL subframes (subframe 0 to 9) of length $T_{\mathrm{sf}} = 30720 \times T_{\mathrm{s}} = 1$ ms each as illustrated in Figure 2.4. Denote the subframe duration by T_{sf}. For the frequency spacing of 15 kHz, each DL subframe can be divided into two slots of length $T_{\mathrm{slot}} = 15360 \times T_{\mathrm{s}} = 0.5$ ms each. Let T_{slot} be the slot duration. For each slot, there are seven OFDM symbols in the case of normal CP type (a length of 5.21 μs for the first

symbol and 4.7 μs for the remaining six symbols) while a single slot is formed by six OFDM symbols in connection with extended CP type (a length of 16.6 μs).

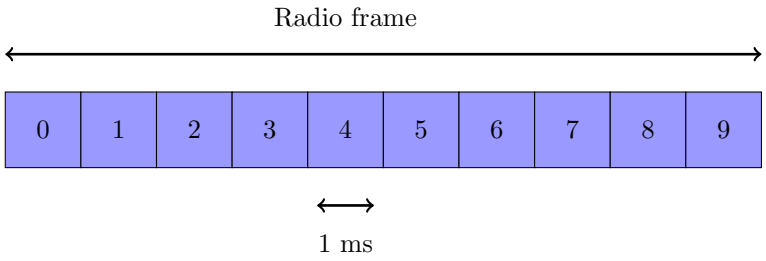

Figure 2.4: The FDD downlink radio frame.

Figure 2.5 shows the DL resource grid for each subframe. Each data symbol is mapped to one of the subcarriers being a resource element (RE) in LTE. This can be identified by the slot index (k, l) where k and l are the subcarrier and OFDM symbol index, respectively. Let $N_{\text{RB}}^{\text{DL}}$ be the number of RBs depending on the transmission bandwidth in the cell. Denote the number of OFDM symbols and subcarriers by $N_{\text{symb}}^{\text{DL}}$ and $N_{\text{sc}}^{\text{RB}}$, respectively.

Therefore, the total grid size is $N_{\text{RB}}^{\text{DL}} N_{\text{sc}}^{\text{RB}}$ subcarriers by $N_{\text{symb}}^{\text{DL}}$ OFDM symbols. A single RB is known as a physical RB (PRB) consisting of $N_{\text{sc}}^{\text{RB}} = 12$ and $N_{\text{symb}}^{\text{DL}} = 7$ [22]. Alternatively, a pair of RBs has a size of $N_{\text{sc}}^{\text{RB}} = 12$ by $N_{\text{symb}}^{\text{DL}} = 14$ defined as the minimum resource unit[2]. The subframe parameters under different system bandwidths are summarised in Table 2.1.

2.2 Heterogeneous Networks

Owing to the limitation of conventional cellular networks, HetNets have been introduced by the LTE-A defined as the network evolution for 5G [3, 9, 10]. In this section, the

[2]This definition of RB could be adequate for the purpose of the simulation in each 1-ms subframe.

[3]The PAPR is proportional to the number of subcarriers (or resource blocks) resulting in a high PAPR in the OFDM system.

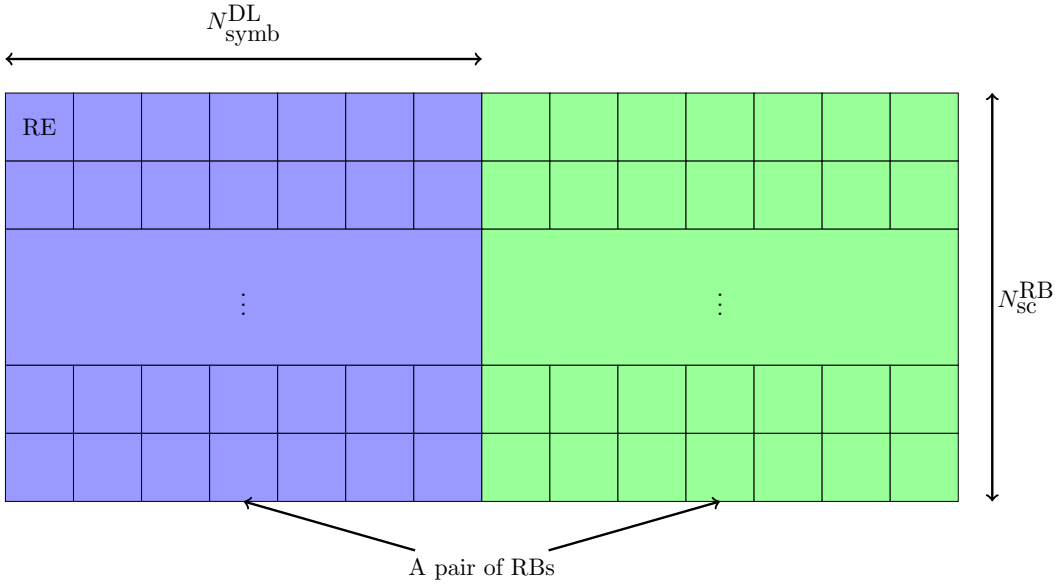

Figure 2.5: The downlink resource grid.

Table 2.1: The parameters for DL transmission (adapted from [3]).

Channel bandwidth (MHz)	1.4	3	5	10	15	20
Subframe duration (ms)	1.0	1.0	1.0	1.0	1.0	1.0
Subcarrier spacing (kHz)	15	15	15	15	15	15
Sampling frequency (MHz)	1.92	3.84	7.68	15.36	23.04	30.72
FFT size	128	256	512	1024	1536	2048
Number of RBs[3]	6	15	25	50	75	100
Number of data subcarriers	72	180	300	600	900	1200
Number of OFDM symbols per subframe	14/12 (normal/extended CP)					

concept of HetNet and small cells (low-power base stations) are discussed.

2.2.1 HetNet Architecture

As illustrated in Figure 2.6, a HetNet is formed by a mix of high-power (macro) base stations (or eNB) and various types of low-power nodes, including radio remote heads (RRH), relays, picocells and femtocells [4]. Hence, home base stations or femtocells are sometimes known as HeNB. The macro network provides an umbrella coverage while an underlay network is produced by the deployment of low-power base stations.

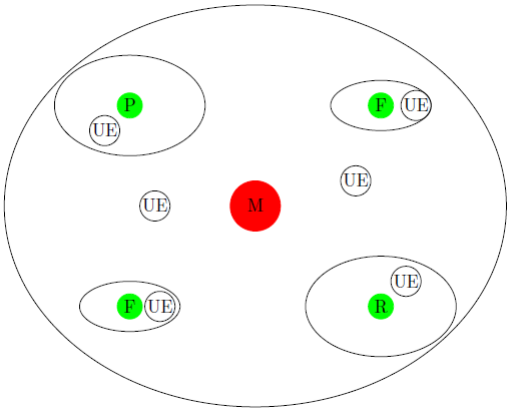

Figure 2.6: A HetNet architecture (M:macro eNB, R:relay, P:picocell and F:femtocell).

By increasing the number of low-power nodes within the local area, the separation distance among transceivers is reduced, resulting in the enhanced radio link quality. Indeed, more efficient spectrum reuse and extended coverage are probably obtained by the larger number of cells. This means higher data rates and lower energy consumption could be provided.

This architecture appears to be one of potential solutions for future networks where dynamic ultra-dense topologies are considered. However, it is still meaningful to emphasise that this approach also raises the number of research challenges such as interference management and resource allocation.

2.2.2 Small Cells

As compared with the macro base station, the lower transmit power and cost are required by small cells. For example, picocells with omni-directional antennas have the transmit power from 250 mW to 2 W for outdoor use and 100 mW or less for indoor use. This deployment is the same planned manner as the traditional macrocell. Unlike the picocells, femtocells are an unplanned deployment for indoor use. The omni-directional antennas are typically employed and the transmit power is 100 mW or less. Besides, femtocells can be divided into two types of access control: closed subscriber group (CSG) and open subscriber group (OSG). The properties of small cells are identified in Table 2.2.

Table 2.2: Small cell deployments (adapted from [4]).

Small cell type	**Transmit power**	**Antenna pattern**	**Deployment**	**Classification**
Picocell	250 mW - 2 W (outdoor) 100 mW or less (indoor)	Omni-directional	Planned manner	Open access
Femtocell[4]	100 mW or less (indoor)	Omni-directional	Unplanned manner	Open and closed access
Relay	250 mW - 2 W (outdoor) 100 mW or less (indoor)	Directional (backhaul link) Omni-directional (access link)	Planned manner	In-band and out-of-band Half- and full-duplex

2.3 Carrier Aggregation

Due to a dramatic increase in the capacity demand in future networks, wider bandwidths are required to provide higher data rates. However, potential resources for the international mobile telecommunications-advanced (IMT-A) seem to be non-continuous. While the number of continuous spectrum bands is restricted as regards various regional regulations, resources with different bandwidths over different (operating) frequency bands are probably available. For example, the band 1 (2100) refers to the frequency range

[4]It is also called the enterprise cell which enhances the mobile voice and data service in any indoor private or public places [23].

of 2110 - 2170 MHz with the bandwidth of 60 MHz and the band 255 (unlicensed national information infrastructure-3) is the frequency range of 5725 - 5850 MHz with the bandwidth of 125 MHz for DL transmission in LTE [24]. To fulfill the requirement for higher bandwidths, CA was introduced by the 3GPP within LTE-A standards to support IMT-A systems. A review of CA, including CA types, deployment and configuration, is provided here.

2.3.1 Classification of Carrier Aggregation

According to the concept of CA in LTE-A (LTE Rel-10), two or more CCs with different bandwidths and bands can be aggregated to provide wider bandwidth for the transmission between the eNB and UE. In [25], CA could be divided into three types: intra-band contiguous, intra-band non-contiguous and inter-band non-contiguous CA. As illustrated in Figure 2.7(a), multiple contiguous CCs in the same band are combined and the spacing between centre frequencies of CCs is a multiple of 300 kHz. On the contrary, non-contiguous CCs in the same band can be aggregated when the contiguous CCs are not available as shown in Figure 2.7(b). Inter-band non-contiguous CA, shown in Figure 2.7(c) for the case where non-contiguous CCs from different frequency bands are combined.

Lee et al. [25] indicates that whereas enhanced mobility is probably achieved by this approach resulting from different radio characteristics, there are still considerable challenges of implementation in connection with physical layer and resource allocation. For example, a single FFT module and a single radio frequency (RF) unit are required for an individual UE to implement the contiguous CA. For the non-contiguous CA, multiple FFT modules and RF chains are needed. Additionally, RF design challenges of terminals for CA are addressed such as transmitter and receiver architectures [26]. Because of the implementation complexity, intra-band non-contiguous CA appears to be the focus of interest in the UL while both intra- and inter-band types have been developed for the

DL.

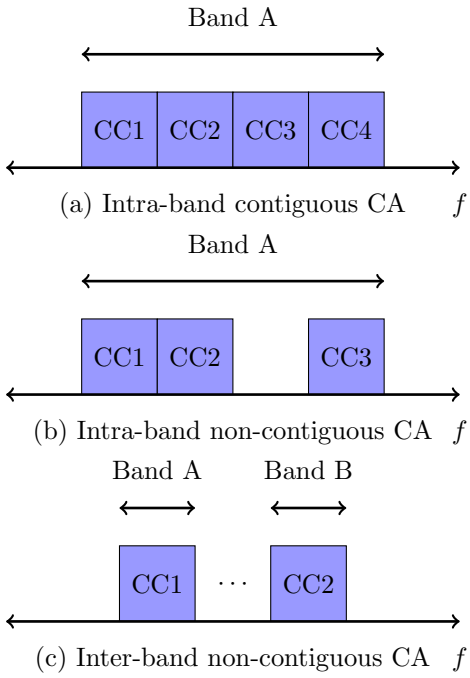

Figure 2.7: Three types of carrier aggregation.

2.3.2 Deployment Scenarios

Figure 2.8 shows the possible deployment of LTE-A CA where there are two CCs at frequencies of F1 and F2. For scenario 1, the antennas located at eNBs have the same radiation pattern for different CCs. When they operate on the same band, the same coverage could be obtained for them. On the other hand, the coverage of CCs is different in scenario 2 due to a large frequency separation between them. By using different radiation patterns for different CCs in scenario 3, the beams can be shifted across CCs, resulting in enhanced cell edge user throughput. For scenario 4, a single CC at a low frequency (F1) is used by the eNB (macrocell) to provide a large coverage. To serve the traffic from hotspots, another CC at a higher frequency (F2) is utilised by the number of RRH units connected to the eNB via optical links.

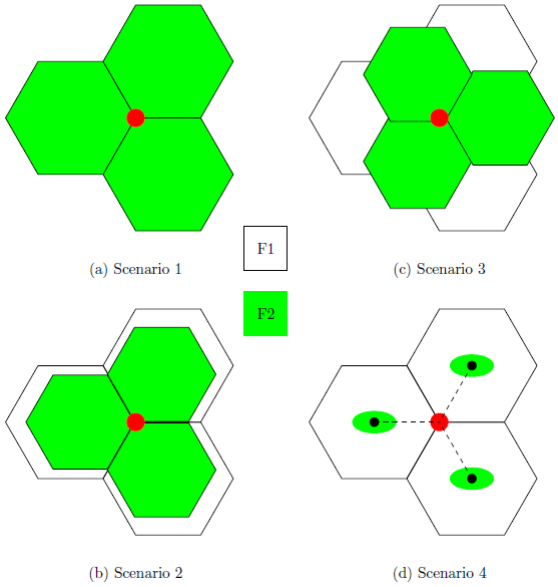

Figure 2.8: Deployment scenarios of CA.

2.3.3 Configuration of Component Carriers

To comprehend the configuration of CCs, a primary CC (PCC) is configured for a LTE-A UE connected with the primary serving cell (PCell), when the UE starts radio resource control (RRC) connection. This CC is utilised by either DL or UL considered as the DL PCC and UL PCC, respectively. Basic functionalities are included in the PCC such as link failure monitoring.

Subsequently, to meet the traffic load and network requirements, additional CCs can be configured for the UE. This refers to the secondary CCs (SCC) corresponding to secondary serving cells (SCell). Similarly, the CCs for DL and UL are named as the DL SCCs and UL SCCs, respectively. Unlike the PCC, dedicated signalling information, PDSCH, physical UL shared channel (PUSCH) and PDCCH are facilitated by the SCCs.

In fact, the usage of PCC and SCCs by UEs is managed by the eNB where different UEs could be configured with different numbers of CCs. In the same eNB, a CC seems to be the PCC for a specific UE. Meanwhile, it could be a SCC for another UE. Besides,

the same PCC is not required by different UEs as illustrated in Figure 2.9.

Therefore, CA appears to be a potential approach to improve network performance. For example, due to the knowledge of scheduling information in the PDCCH, the DL control channel of PCC can be applied to schedule resources on DL and UL SCCs. This results in the enhanced interference management and load balancing across different carriers. Also, the DL and UL PCCs may be changed to provide the best signal quality and coverage in connection with moving UEs. To deal with energy efficiency of UEs, DL SCCs are likely to be activated and deactivated dynamically.

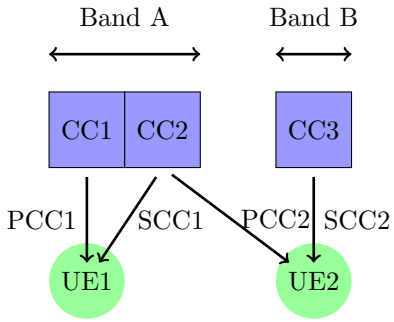

Figure 2.9: An example of CC configuration.

2.4 Unlicensed LTE

Because of an exponential growth of subscribers and wireless traffic, a lack of licensed spectrum for 5G cellular networks is expected in the near future. The use of unlicensed bands for LTE and other radio access technologies (RAT) has been investigated by academia and industry. Figure 2.10 shows the U-LTE deployment operated within the coverage of licensed (LTE) spectrum. If higher capacity is required, the unlicensed bands may be utilised and shared by various base stations (or cells) and RATs, in particular LTE and WiFi. From the point of view of CA, the licensed and unlicensed spectrum can be viewed as the primary and secondary carriers, respectively.

In [5], the authors discuss the benefits of LTE in the unlicensed spectrum. First,

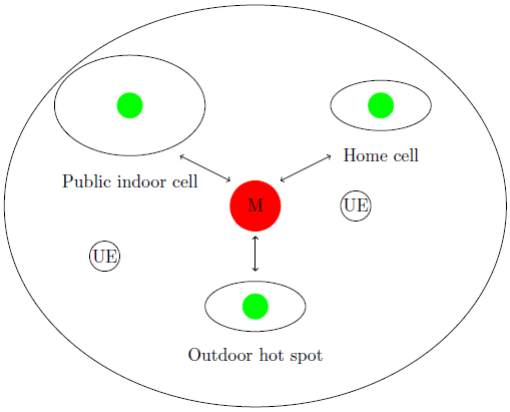

Figure 2.10: An example of U-LTE deployments.

the number of UEs, throughput and network coverage could all be enhanced. Second, the existing radio networks can be used regardless of extra network management and infrastructures. Third, both licensed and unlicensed bands are combined by means of CA resulting in the better quality of service (QoS) and user experience.

Although this U-LTE appears to be a promising solution, the coexistence between LTE and other wireless systems within the unlicensed spectrum is required. Also, the co-operation with licensed LTE networks is still important for network coverage and control information. In this section, a survey of U-LTE such as unlicensed bands, coexistence mechanisms and standards is provided.

2.4.1 Unlicensed Spectrum

According to [5, 27], there are unlicensed bands released by regional regulators. For example, the 2.4 GHz industrial, scientific, and medical (ISM) and 5 GHz unlicensed national information infrastructure (U-NII) bands have been widely utilised by WiFi, Bluetooth, Ultra-Wideband (UWB) and ZigBee. The 60 GHz millimetre-wave (mmWave) bands are arranged for unlicensed use as well. Owing to the large available bandwidth and radio characteristics, the 5 GHz spectrum has been considered by 3GPP to support not only the U-LTE but also small cell deployments. For instance, 5.15 - 5.25 GHz

(UNII-1), 5.25 - 5.35 GHz (UNII-2A), 5.47 - 5.725 GHz (UNII-2C) and 5.725 - 5.85 GHz (UNII-3) bands can be accessed in the US. The available 5 GHz unlicensed bands in different countries are summarised in Table 2.3. The authors of [5, 27] also identify that the extra regulation for each unlicensed band is required such as transmit power control and dynamic frequency selection.

Table 2.3: The available 5 GHz unlicensed spectrum (adapted from [5]).

Country	**Band (GHz)**
US	5.15 - 5.35 5.47 - 5.85
China	5.15 - 5.35 5.725 - 5.85
Europe, Korea and Japan	5.15 - 5.35 5.47 - 5.725

2.4.2 Coexistence Mechanisms

In this context, coexistence approaches in the unlicensed spectrum between LTE and WiFi are examined, divided into three domains: frequency, time and power [27].

2.4.2.1 Frequency Domain

The 5 GHz unlicensed bands may be separated into the number of channels (or CCs). No more than five channels can be aggregated for LTE while a single channel is accessed by WiFi [27]. According to [28], if any remaining (free) channels are detected, the U-LTE transmissions are established on them. On the contrary, the interference on each channel measured by energy and specific detection is considered if there are no free channels. The user-assisted information is probably used to facilitate this measurement. In this way, the channel(s) with the minimum interference level can be identified by LTE

for unlicensed transmission. This approach is also known as dynamic channel selection (DCS).

2.4.2.2 Time Domain

There are two ways to separate LTE and WiFi transmissions in the time domain: deterministic and random sharing. For the former approach, carrier-sensing adaptive transmission (CSAT) [28] can be applied to partition time into time-division multiplexing (TDM) cycles as illustrated in Figure 2.11. Each CSAT cycle includes on and off periods of U-LTE. Owing to the known utilisation of WiFi, the ratio between these two periods could be adapted. Thus, the fairness of time sharing between LTE and WiFi could be improved. The delay performance of WiFi could be enhanced by means of punctured subframes during on periods. The delay-sensitive and control data in WiFi can be transmitted to the channel during these small gaps unused by the LTE. Also, the use of a shorter CSAT cycle is able to improve the delay performance of WiFi.

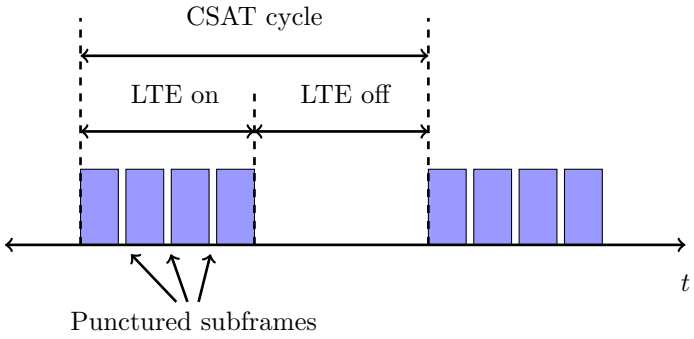

Figure 2.11: CSAT cycles.

Blank-subframe allocation is another deterministic mechanism [29]. A set of blank-subframes determined by the WiFi traffic load is inserted in a LTE radio frame. Only WiFi can access these silent subframes while LTE transmission is paused. The number of blank-subframes is proportional to the air time sharing. Unlike CSAT, this allocation is performed at frame level and the consecutive blank-subframes are not required as

shown in Figure 2.12.

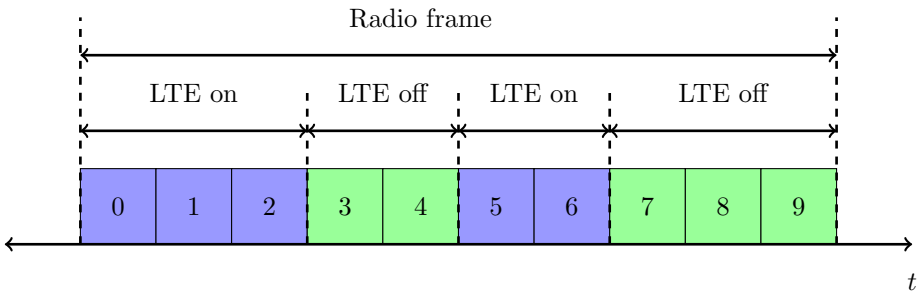

Figure 2.12: The blank-subframe allocation.

In the random sharing, listen-before-talk (LBT) has been used in LTE. This contention-based medium access is similar to carrier-sense multiple access with collision avoidance (CSMA/CA) in WiFi. Hence, LBT has been globally accepted by various regulators and communities. Frame- and load-based LBT are the two current versions [30]. Under the frame-based LBT, the time is first divided into frames. There are two periods within each frame: idle and channel occupancy periods. No LTE transmission is allowed during an idle period. At the end of this period, the CCA is performed. If the idle channel is sensed, the LTE transmission will begin during a following channel occupancy period. Otherwise, LTE data cannot be transmitted.

An alternative random sharing method is load-based LBT where a fixed frame structure is not needed. The CCA is initiated when there is any active LTE node. During this carrier sensing interval, the LTE data can be sent instantly if the idle channel is detected. Otherwise, the process of extended CCA (eCCA) is executed further.

2.4.2.3 Power Domain

The aggregated received energy can be used to determine the availability of channel for WiFi nodes. If this energy on a channel is higher than an energy detection threshold, the channel becomes busy and the WiFi transmission is deferred. To enhance the coexistence between LTE and WiFi, the output power of LTE nodes may be adjusted

by means of transmit power control (TPC). The wider transmission window of a WiFi node is obtained with the lower LTE transmit power. This results in the reduction of signal-to-interference-plus-noise ratio (SINR) and throughput in LTE. Therefore, a compromise between transmission opportunity of WiFi and LTE throughput seems to be an important consideration.

2.4.3 Standards

From the point of view of standardisation, there are a few standards proposed for U-LTE such as LTE-U, LAA, enhanced LAA (eLAA) and MulteFire [27]. For example, LTE-U is introduced by 3GPP Release 10/11 where any change of LTE protocols is not required. By using CA, LTE can be operated in both licensed and unlicensed bands. If the traffic demand is not satisfied by only licensed spectrum, supplemental downlink (SDL) mode for DL transmission in the unlicensed spectrum can be used. For the coexistence issue in LTE-U, the DCS mechanism is first performed to determine the number of free (cleanest) channels during SDL transmission. The operating channel can be adapted based on an (predefined) interference energy threshold. However, the free channel(s) may be either unavailable or limited. The same unlicensed channel is likely shared by multiple users from LTE-U and other networks. Thus, the CSAT could be applied to set the on and off periods for LTE-U transmission. The SDL mode will be suspended when no data is available in a transmission queue.

Unlike LTE-U, the LAA standard with LBT approach is launched by 3GPP Release 13 which aims to offer a single framework for various regional regulators. This means the LTE protocols should be modified to meet the global requirements. Only DL transmission in unlicensed bands is supported. Huang et al. [27] identifies the main features in LAA, including LBT, maximum duration for transmission, downlink-only transmission, DCS, dynamic frequency selection (DFS) and TCP. To achieve both DL and UL transmissions in the unlicensed spectrum, eLAA being the extension of LAA has been

developed under 3GPP Release 14. LBT, DCS and eNB's UL signalling are the key function in eLAA.

Another standard is MulteFire based on 3GPP Release 13/14. Both UL and DL transmissions in the unlicensed spectrum can be supported. Unlike the previous standards, the operation of MulteFire in the unlicensed spectrum could be maintained regardless of the licensed spectrum. There are three main points in this latest standard, including access modes, LBT channel access and enhanced discover reference signals (DRS).

2.5 Resource Allocation

In this section, a review of LTE scheduling and resource assignment being the main focus of interest is provided. The general process of scheduling in DL transmission is firstly described. Subsequently, the existing scheduling algorithms are discussed in connection with CA and U-LTE.

2.5.1 DL Scheduling

For DL transmission, either dynamic or semi-persistent scheduling can be deployed [3]. If the former scheduler is selected, LTE resource allocation for different UEs can be performed every 1-ms subframe at a granularity of 180 kHz (a single RB). After the eNB receives the DL channel quality feedback from UEs, a (channel sensitive) scheduler at the eNB is applied to select UEs with good channel conditions on given time, frequency and spatial resources. Because of the link adaptation, the transmission format such as modulation and coding scheme (MCS) is adapted to the current channel conditions on resources allocated by the scheduler. For example, different MCS schemes can be used by different scheduled UEs on different RBs in the same subframe. Due to the possibility of inaccurate link adaptation, a hybrid automatic repeat request (HARQ) being an (packet) error control mechanism by means of acknowledgement messages and timeouts

is used. Transmission data rates could be maintained regardless of errors in channel quality estimation and prediction. Therefore, these three mechanisms appear essential for modern wireless systems. For more details, comprehensive reviews are provided in [3, 31].

Figure 2.13 represents an example of a DL scheduling timeline. At the beginning, resources are assigned by the eNB to UE i for the first transmission. The scheduling grant is carried over PDCCH while the actual data is conveyed over PDSCH within subframe 0. To notify the success of the first transmission, the acknowledgement message is sent back to the eNB by the UE in subframe 5. If the negative acknowledgement (NACK) is received, the earliest subframe 8 can be used for the packet retransmission. The process is repeated in connection with the success of packet transmission and the maximum number of retransmissions.

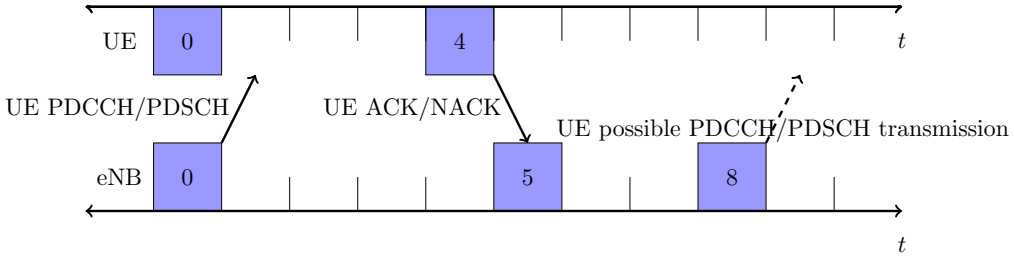

Figure 2.13: The downlink scheduling process.

In [32], the terms rate prediction and link adaptation are interchangeable where the MCS is determined for the UE by the recent channel quality indicator (CQI) report in each new transmission. The authors also indicate possible procedures of LTE scheduler as follows

- The selection of scheduled UEs
- The number of assigned RB
- The transmission power of each RB

- The MCS scheme for packet transmission

2.5.2 Resource Allocation in LTE

In this section, state-of-the-art scheduling algorithms in LTE are first described, including round-robin (RR), maximum SINR and proportional fair (PF). Although these schedulers are suitably used for comparison purposes in this thesis, there are lots of alternatives and variations in the research literature. Then, related work on LTE scheduling will be reviewed.

2.5.2.1 Scheduling Algorithms

Scheduling is required to select which UEs can be assigned RBs in the next subframe. Round-robin, maximum SINR (also known as best-CQI) and proportional fair scheduling have been widely used [3]. In round-robin, all UEs are equally scheduled regardless of the channel condition. This means the same number of RBs should be allocated to each UE, resulting in a high degree of fairness. The cell-edge user throughput can be enhanced while the system throughput is poor. For the maximum SINR scheduler, only UEs with good channel conditions seem to be scheduled, causing the low fairness. Not only very high system throughput but also very poor cell-edge throughput are achieved. To compromise between fairness and throughput, the proportional fair scheduling has been considered. In every subframe, a UE with the highest system utility function is first scheduled. This metric is derived from possible data rate in the current subframe and average achieved throughput in the past for this UE.

According to [31], the UE m^* is scheduled in the nth subframe based on the proportional fair manner as follows

$$m^*(n) = \underset{m=1,2,\ldots,M}{\arg\max} \frac{R_m(n)}{T_m(n)}, \tag{2.1}$$

where $R_m(n), m = 1, 2, \ldots, M$ is the data rate for the mth UE in the nth subframe. Let $T_m(n)$ be the average throughput for the mth UE in a past window. At each subframe,

this throughput is updated

$$T_m(n+1) = \begin{cases} \left(1 - \frac{1}{t_c}\right) T_m(n) + \left(\frac{1}{t_c}\right) R_m(n) & m = m^*(n) \\ \left(1 - \frac{1}{t_c}\right) T_m(n) & m \neq m^*(n), \end{cases} \tag{2.2}$$

where t_c is the window length. For very large t_c, this scheduling aims to maximise $\sum_{m=1}^{M} \ln(T_m)$. T_m and $\ln(T_m)$ can be viewed as the long-term average throughput and the utility of UE m, respectively. Hence, the proportional fair algorithm can be considered as regards the system (network) utility function

$$U(n) = \sum_{m=1}^{M} \ln\big(T_m(n)\big). \tag{2.3}$$

The UE m in the nth subframe with the largest (instant) reward in the system utility is scheduled. Alternatively, the scheduling expression could be generalised as

$$m^*(n) = \underset{m=1,2,\ldots,M}{\arg\max} \frac{\big(R_m(n)\big)^{\alpha}}{\big(T_m(n)\big)^{\beta}}, \tag{2.4}$$

where the factors α and β are used to balance between the fairness and throughput. Obviously, the round-robin ($\alpha = 0, \beta = 1$), maximum SINR ($\alpha = 1, \beta = 0$) and proportional fair ($\alpha = 1, \beta = 1$) schedulers can be obtained from this generalised expression.

The next step is to determine how many RBs can be assigned to the scheduled UE. The transmission format (MCS and MIMO schemes), power level and transport block size should be identified as well. Ghosh and Ratasuk [3] suggest that resource assignment (allocation) could be performed by a greedy approach. In each subframe, if a scheduled UE is selected, it can obtain as many RBs as possible subject to a power constraint.

2.5.2.2 Related Work

To the best of this author's knowledge, most related work has focused on how subcarriers are assigned in the OFDMA system such as [33, 34]. However, the explicit instruction of RB allocation in LTE has not been described. This seems to be the vital challenge

where the additional information, including channel quality feedback, QoS requirements and traffic models, could be included in the LTE scheduler [35, 36, 32].

For instance, based on the proportional fair approach, the UE with the largest scheduling metric is scheduled where the metric for the ith UE on the jth RB can be defined as [36]

$$m_{ij} = \frac{r_{ij}}{r^{\text{avg}} + \sum_{j=1}^{J} \delta_{ij} r_{ij}}. \tag{2.5}$$

Note that a physical RB being 180 kHz of bandwidth for a time duration of 0.5 ms (a timeslot) is used in [36]. As discussed before, each 1-ms subframe is divided into two slots. Let K and N be the number of OFDM symbols and subcarriers in each slot, respectively. Therefore, a single RB consists of $N \times K$ OFDM symbols being the smallest unit for the LTE scheduling in this work.

Let r_{ij} be the (instantaneous) achievable throughput of the ith UE on the jth RB. Denote the average throughput of this UE up to the current slot by r^{avg}. The term $\sum_{j=1}^{J} \delta_{ij} r_{ij}$ indicates assigned RBs of the ith UE in the current slot. If the UE has been scheduled on the jth RB, δ_{ij} equals one. Otherwise, this indicator equals zero.

Furthermore, $r_{ij} = 2cNK$ is determined by the spectral efficiency (c) in bit per channel use of the corresponding CQI, the number of subcarriers (N) and the number of OFDM symbols (K) in a single subframe, that is, two physical RBs are considered for this computation.

2.5.3 Resource Allocation with CA

According to [37], the structure of a LTE-A system with CA is illustrated in Figure 2.14. Firstly, a set of served UEs is picked by admission control at the eNB. CCs are then selected for the UEs by means of RRC signalling. Subsequently, the RB (or packet) scheduling and HARQ are performed on each CC. Thus, resource allocation with CA may be divided into two parts: CC selection and RB scheduling. This process and related work are discussed.

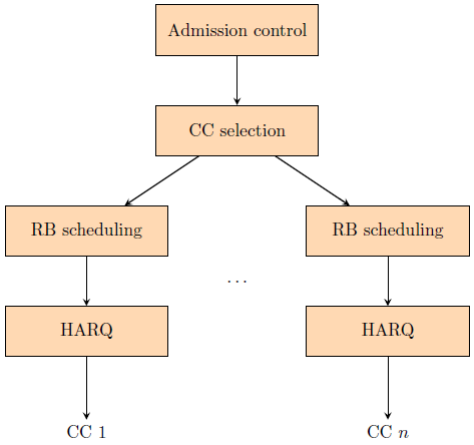

Figure 2.14: A LTE-A with CA structure.

2.5.3.1 CC Selection

The eNB allocates CCs to UEs in connection with the traffic load balance. In this way, there are two common methods: random and round-robin selection. In the former manner, the available CCs are randomly assigned to each UE resulting in the (long-term) load balance. This is because the number of UEs on each CC could be the same in the long-term period. Alternatively, CCs with the least number of UEs are allocated to a specific UE in the round-robin selection. The load may be uniformly distributed to all CCs. This results in the small variation in the traffic load among the available CCs.

When the inter-band non-contiguous CA as shown in Figure 2.7(c) is considered, the random and round-robin CC selection seem not to be the appropriate method. This is because the channel condition from different frequency bands is not considered in these two schemes.

In [37], the received reference signal received power (RSRP) is used to indicate the channel quality. Let rsrp_c^i be the RSRP of UE i on CC c. Due to a higher rsrp_c^i, the UE i can experience a better channel condition on the CC c. Note that every served UE is able to access all active CCs within the cell. Thus, the CC(s) with maximum rsrp_c^i is

assigned to UE i as follows

$$c^* = \arg\max_{c \in C} \text{rsrp}_c^i, \tag{2.6}$$

where C is the set of supported CCs per cell. This leads to not only the load imbalance but also CC underuse if the same (a low frequency band) CC(s) with better channel quality is always allocated. To overcome this potential imbalance, (2.6) is then revised

$$c^* = \arg\max_{c \in C} \frac{\text{rsrp}_c^i}{\sum_{1 \leq j \leq N} \text{rsrp}_c^j}, \tag{2.7}$$

where N is the number of served UEs per cell. The sum of RSRP from all UEs on the same CC is considered in (2.7). Moreover, this CC selection as regards the fairness can be defined

$$c^* = \arg\max_{c \in C} \frac{\text{rsrp}_c^i / R^i}{\sum_{1 \leq j \leq N} \text{rsrp}_c^j / R^j}, \tag{2.8}$$

where R^i is the average data rate of UE i. The better CC(s) will be assigned to the UE with small data rate.

Another challenge is on how CCs are dynamically configured: PCCs and SCCs. Also, the UE capability such as LTE and LTE-A UEs seems to be an important consideration. These two points result in the different number of supported CCs per UE. In other words, some UEs cannot access all active CCs within the serving cell.

2.5.3.2 RB Scheduling

After the CC selection, the scheduling is performed where RBs are assigned to a specific UE on each CC. The round-robin scheduler being a benchmark has been widely used. Furthermore, the proportional fair scheduling with CA can be implemented as follows [37]

$$i^* = \arg\max_{i \in U_c} \frac{r_{c,k}^i(t)}{R^i(t)}. \tag{2.9}$$

Let $RB_{c,k}$ be the RB k on CC c. At each subframe t, $RB_{c,k}$ will be scheduled to the UE i with maximum UE utility function. $r_{c,k}^i(t)$[5] is the achievable data rate of UE i on

[5]The achievable data rate defined in [38] is used in this thesis.

$RB_{c,k}$ and $R^i(t)$ is the average data rate of UE i at time t. Denote the set of UEs on CC c by U_c. Moreover, the average data rate could be defined

$$R^i(t) = \left(1 - \frac{1}{t_c}\right) R^i(t-1) + \frac{1}{t_c} \sum_{c \in C_i} T_c^i(t-1), \tag{2.10}$$

where $T_c^i(t-1)$ is the actual data rate (throughput) of UE i on CC c at time $(t-1)$. Let t_c and C_i be the average window size and the set of allocated CCs for UE i, respectively.

2.5.3.3 Related Work

Related work on resource allocation with CA can be classified into two groups: separate and joint allocation problems. For instance, CC selection and RB allocation are considered independently in [37, 6]. The CCs are selected before assigning RBs to scheduled UEs. In [6], there are two methods for CC selection. First, all active CCs are allocated to every UE with CA capability. If there is a UE without CA support, only its primary CC is picked. Second, the active CCs is cyclically assigned to UEs in the cell. Although the low computational complexity is obtained by this separate resource allocation, the network performance may be degraded.

To enhance the system performance, joint CC selection and RB allocation is considered. In [39], there are two user types, including narrowband and broadband users, which have the different CA capability. The joint resource allocation is formulated as a non-linear integer programming problem. Due to the high complexity, a sub-optimal algorithm is proposed to maximise the network utility function. RB allocation on each CC is firstly performed based on the proportional fair approach. A minimising system utility loss (MSUL) algorithm is then used to satisfy the CA capability constraint of narrowband users.

The modulation and coding scheme constraint is included in the joint CC selection and RB allocation problem [40]. At each subframe, a greedy algorithm (GA) is proposed to determine the largest gain assignment (utility function) resulting from all combinations of UEs, CCs and MCSs. RB allocation is then performed in connection with the

weighted data rate of UE. In [41], the MSUL proposed in [39] is modified to support MCS assignment. As compared with the MSUL and GA, this efficient RB allocation algorithm (ERAA) can provide the better network utility function and fairness index. The computational complexity of these three algorithms is also analysed.

Another (possible) constraint is the PCC and SCC selection. In [38, 42], the joint resource allocation problem with RB, MCS and SCC constraints is formulated as an integer linear programming (ILP). Owing to the linear programming (LP) relaxation, this ILP problem can be optimally solved by means of LP techniques. A comparison of recent resource allocation with CA is also presented in [42].

Due to the high computational complexity, this joint resource allocation should be considered carefully in practice. Lee et al. [25] also argues that there are potential challenges in resource allocation with CA such as joint optimisation between resource allocation and link adaptation, large overhead, power consumption, mobility management and user multiplexing.

2.5.4 Resource Allocation with U-LTE

Unlike the previous resource allocation, Huang et al. [27] indicates there are two significant considerations in the unlicensed spectrum. First, the transmission appears to be discontinuous and greedy in manner. Another point is the interference is probably unforeseeable and uncontrollable. Each U-LTE node may suffer from other interfering systems such as WiFi in the same unlicensed band. Therefore, the challenge is on how resources (or RBs) can be allocated optimally across both licensed and unlicensed spectrum. The use of unlicensed spectrum in LTE and related work are presented here.

2.5.4.1 The Use of Unlicensed Spectrum

The unlicensed spectrum may be integrated with the LTE licensed spectrum in different ways. For example, Figure 2.15 shows the SDL mode. Only the unlicensed band in DL

transmission is used to support the data traffic originating from the licensed band, while both control and data traffic are served by the license spectrum in UL transmission. From the point of view of CA, one of CCs within the licensed spectrum is viewed as a PCC and the extra CCs from the unlicensed spectrum are considered as the SCCs. Moreover, a PCC is managed by the PCell such as a LTE macro eNB. SCCs are operated by their corresponding SCells such as small cells.

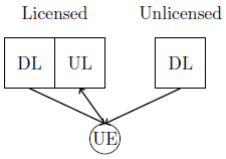

Figure 2.15: The integration of licensed and unlicensed spectrum: SDL mode.

There is the variety of U-LTE deployment scenarios resulting from small cells. For instance, macro coverage, outdoor/indoor environment, backhaul and spectrum seem to be the important factor. An example of LAA deployment with the ideal backhaul is shown in Figure 2.16. The licensed carriers are connected to the unlicensed carriers by means of the RRH. In this case, the LTE macro eNB is viewed as the PCell to offer the basic functionalities while RRHs appear to be a set of SCells to enhance the data rate for the UE.

2.5.4.2 Related Work

Because of a single (potential) framework for worldwide regulation, the LAA with LBT mechanism is the main focus of interest in this thesis. Related work on coexistence and resource allocation with LBT is discussed. The LBT scheme is first proposed for LTE heterogeneous networks in [43]. The placement of picocells and WiFi access points (AP) is considered. The UL performances, including LTE cell throughput and picocell user throughput, are evaluated under varying the WiFi activity factor. This factor refers to the fraction of WiFi transmission time. According to [44], the coexistence between

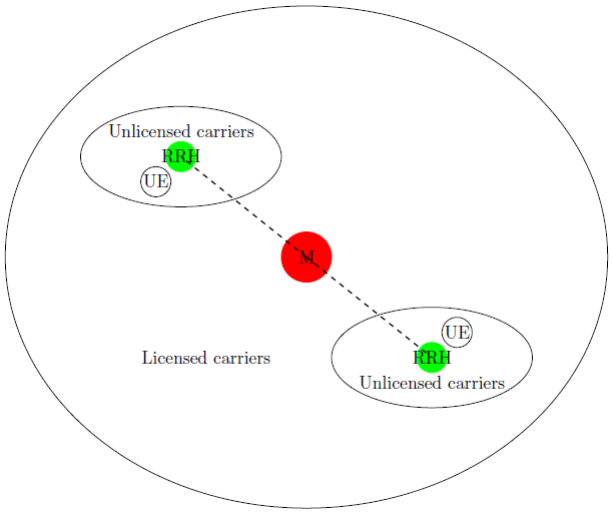

Figure 2.16: An example of LAA deployment: Ideal backhaul.

LTE and WiFi with LBT in DL is examined. The served load and user throughput are investigated under different network deployments. Note that these two works are simulated based on the system-level approach.

Another work is the system-level simulation based on stochastic geometry to analyse the coexisting network in [45]. The medium access priority and sensing threshold are considered in connection with the LBT. The throughput of LTE and WiFi users is then evaluated under indoor and outdoor scenarios.

For the analytical framework, according to [46], the work from [44] is analysed by Markov chain model resulting in the downlink throughput calculation. Furthermore, the channel access and successful transmission probabilities of LTE and WiFi are investigated. The performance analysis of the IEEE 802.11 distributed coordination function in [47] is applied to this work.

In [48], an analytical model of frame-based LBT based on a discrete-time Markov chain (DTMC) is studied. Then, a LBT algorithm is performed to determine the number of WiFi nodes and idle subframes. Not only the enhanced total system throughput but also the fairness between LTE and WiFi could be obtained.

The joint optimisation problem, including CC selection and RB scheduling based on frame-based LBT, is formulated to maximise the LTE throughput and maintain the fairness in [49]. To reduce the computational complexity, a heuristic algorithm is proposed for a sub-optimal solution in practice. This sequential algorithm consists of CC selection, determination of the number of idle subframes and RB allocation. As compared with the optimal solution, the comparable LTE throughput and fair coexistence could be obtained.

2.6 Summary

In conclusion, a survey of LTE, HetNets, CA, U-LTE and resource allocation was provided in this chapter. The related work will be considered in the remaining chapters. The aim of research is to examine resource allocation in heterogeneous cellular networks. This results in the SL simulator developed in this thesis. The SL simulation, system model, simulation model, simulation verification and network scenarios of small cell deployments and scheduling will be discussed in Chapter 3.

Chapter 3

System-Level Simulation

This chapter is an outline of the research methodology published in [12]. The SL simulation being the main approach is first discussed. A few existing tools and challenges in SL simulation are identified. To develop a SL simulator, system and simulation models for both homogeneous and heterogeneous LTE networks in DL transmission are described step-by-step. The performance metrics are then defined. For the simulation verification, the results from this developed simulator are compared to a reference simulator[1]. Finally, small cell deployments and scheduling techniques are investigated in terms of the UE throughput.

3.1 System-Level Simulation

In a HetNet, there are a large number of base stations (or eNBs) and UEs. Moreover, there is the variety of network elements and characteristics. As compared to the traditional cellular network, the HetNet results in the more complicated network operation such as interference and resource management. To model this complex network, simu-

[1]The Vienna SL simulator [6] is selected as a reference due to the prerequisite knowledge (coding language), open-source nature, user community, the number of primary publication citations and licensing [11].

lation has been widely used before the real implementation. In this section, the concept of simulation is briefly described, in particular SL. The existing SL simulators are then discussed. Furthermore, the research challenges in SL are identified resulting in the simulator developed in this PhD project.

3.1.1 Simulator Types

According to [11], simulators can be divided into three types: link level (LL), SL and network level (NL) simulators. They relate to the layers of the protocol stack. Firstly, a single link between two transceivers is investigated by LL simulation as regards the PHY performance. Based on link level abstraction, the block error rate (BLER) curves can be determined by this simulator which are used for SL and NL simulators. Secondly, SL simulators focus on the air interface to examine wireless networks with a large number of base stations and user terminals. Coverage, spectral efficiency and throughput can be analysed in connection with interference from other eNBs or UEs. Thus, the SL simulators could assist in the study of radio resource management (RRM), interference coordination and scalability. Thirdly, NL simulators focus on specific protocols and interfaces between layers. Base stations can be viewed as network entities which are able to exchange messages between each other. For example, backhaul can be modelled by NL simulators.

To select a suitable simulator, Alvarez et al. [11] outlines important technical features that should be considered such as link level abstraction, traffic types, scheduling and backhaul. Operational considerations for users, including prerequisite knowledge, network deployment scenarios and modularity, could be addressed as well. The authors also indicate the comparative analysis of three LTE simulators: Vienna SL, ns-3 and HetDensim.

In [7], the SL simulation can be classified into two groups: static and dynamic

simulations. For the static simulation, Monte Carlo approaches[2] have been widely used in the network planning and optimisation to evaluate the average performance of a large network for a long period (a sufficient number of snapshots). In each snapshot, network elements such as UEs are randomly placed over the region of interest (ROI) regardless of the time domain. Then, the performance metrics, including throughput and outage probability, could be obtained. Another approach is dynamic simulation where the network evolution is considered as a function of time. The dynamic of UEs, traffic and channel may be included in this simulation. In this way, the performance of a small network for a short period is often examined, such as throughput and delay.

3.1.2 Existing SL Simulators

There are both commercial and free simulators for radio planning and optimisation. Only existing SL tools for LTE networks are the focus of attention. ICS telecom [51] being a commercial simulator is used globally by various institutions to model such cellular networks. Some features are offered such as network coverage, interference analysis, throughput calculation, MIMO and network coexistence.

Alternatively, the Vienna downlink SL simulator [6] is designed to examine LTE-A homogeneous and heterogeneous scenarios. This non-commercial tool for academic use is based on MATLAB. Wideband SINR and throughput are the example of performance metrics. The technical features are summarised in Table 3.1. Fortunately, the source code is allowed to be accessed resulting in potential modification and new functionalities.

Although the Vienna simulator appears to be a reference simulator as mentioned at the beginning of this chapter, there is the limitation of CA and U-LTE implementation.

[2]Monte Carlo simulation is also known as the multiple probability simulation. In different simulations (or iterations) the random variables (inputs) are modelled based on appropriate probability distributions such as normal and uniform, resulting in the different outcomes. The statistically representative result is then determined by repeated random (outcome) sampling and statistical analysis [50].

Table 3.1: The technical feature of the Vienna simulator (adapted from[6]).

Feature	**Vienna LTE-A downlink SL simulator**
Performance metrics	Throughput, spectral efficiency, wideband SINR and fairness
Transmission mode	Single antenna, transmission diversity, open and closed loop spatial multiplexing
Path loss model	Free space, Cost 231, TS 36.942, TS 25.814 and TR 36.873
Shadow fading	2D correlated log-normal distribution
Small-scale fading	Based on power delay profile (e.g., ITU Typical Urban)
Antenna gain pattern	Omnidirectional, Berger, TR 36.873 and TS 36.942
Scheduling	Round robin, best channel quality indicator and proportional fair
Link level abstraction	Mutual information effective SINR mapping (MIESM)

First, only the RSRP discussed in Section 2.5.3 is applied to the CC selection in the Vienna simulator. Second, the usage of unlicensed spectrum in the LTE network presented in Section 2.4 cannot be modelled by the latest version of this simulator.

Therefore, a new SL simulator is developed in this thesis based on the Monte Carlo approach as discussed in Section 3.1.1 to model both LTE homogeneous and heterogeneous cellular networks. Most modules of this developed simulator stemming from the Vienna simulator will be discussed further in Section 3.2. Note that the Vienna simulator is used for the verification of simulation models in this Chapter 3 only, due to the simulation modification as mentioned below.

More options of CA selection and the use of unlicensed spectrum in LTE are implemented and modelled by this developed simulator, as compared with the Vienna simulator. These extensions will be presented in Chapters 4 and 5. Because of the Monte Carlo simulation, the number of UEs and their states are generated within different simulations (snapshots). The network performance which relies on repeated random sampling is then evaluated in terms of UE throughput and fairness index. This simulation approach will be discussed further in Section 3.2.

For a straightforward way of programming, another change is that separate MAT-

LAB functions are used in this developed simulator instead of the object-oriented programming (OOP) approach in the Vienna simulator. Each individual task such as the placement of network elements and scheduling algorithms can be flexibly modified.

3.2 System Model

The system model of SL simulation, including pre-processing, main simulation and post-processing for both homogeneous and heterogeneous networks, is described in this section.

3.2.1 Pre-Processing

The building blocks, including network layout, large-scale fading, wideband SINR, UE placement and small-scale fading, are presented. The pre-generated data from each stage is required by the main simulation which is discussed in Section 3.2.2.

3.2.1.1 Network Layout

According to [52], a hexagonal grid of 19 macro sites (red dots) with three sectors each is first generated as shown in Figure 3.1. This homogeneous network results in 57 sectors in total. Only the adjustable ROI is investigated (a rectangle of approximately 2000 $\times$ 1732 metres) for the SL simulation.

To examine a heterogeneous network, femtocells[3] can be generated on top of the existing macro network layout. There are two possible models for femtocell placement, including homogeneous density and a fixed number of femtocells per macro sector as shown in Figures 3.2 and 3.3. For example, Figure 3.2 shows the femtocell placement resulting from the homogeneous density model. There are 33 femto sites (green dots) uniformly dropped within the ROI of approximately 3.3 km^2 with an average density of 10 femtocells/km^2. Alternatively, a single femtocell per (active) macro sector is randomly

[3]Note that the terms femtocell and femto site are interchangeable throughout this thesis.

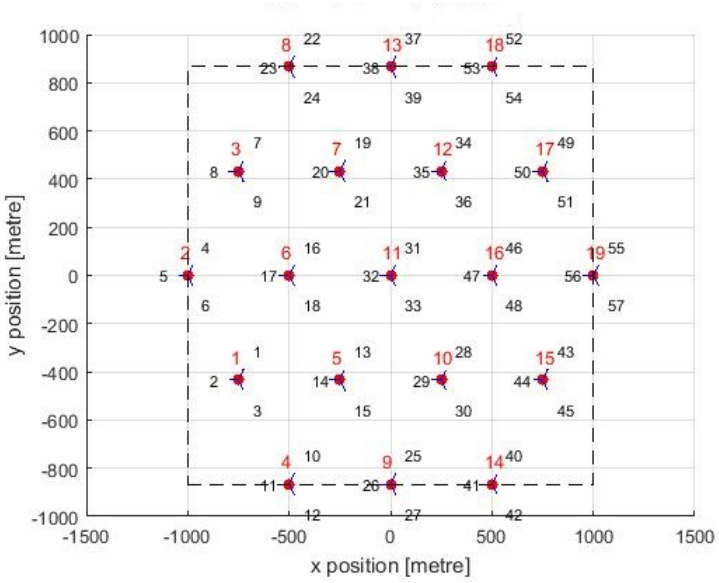

Figure 3.1: A homogeneous network (19 macro sites).

placed within the coverage area of its corresponding sector resulting in 53 femto sites (green dots) in Figure 3.3.

3.2.1.2 Large-Scale Fading

The ROI can be viewed as a (two-dimensional) pixel map with a given resolution of p metres per pixel. The large-scale fading, including antenna gain, path loss and shadow fading, can be generated and then stored on each pixel of $p \times p$ metres. Therefore, these time-invariant and position-dependent fading parameters can be pre-computed offline resulting in the reduced computational complexity.

3.2.1.2.1 Antenna Gain

Based on [52, 53], the eNB antenna pattern (horizontal) for each macro sector (in dB) is defined

$$A_{\mathrm{H}}(\theta) = -\min\left[12\left(\frac{\theta}{\theta_{3\mathrm{dB}}}\right)^2, A_{\mathrm{m}}\right], \tag{3.1}$$

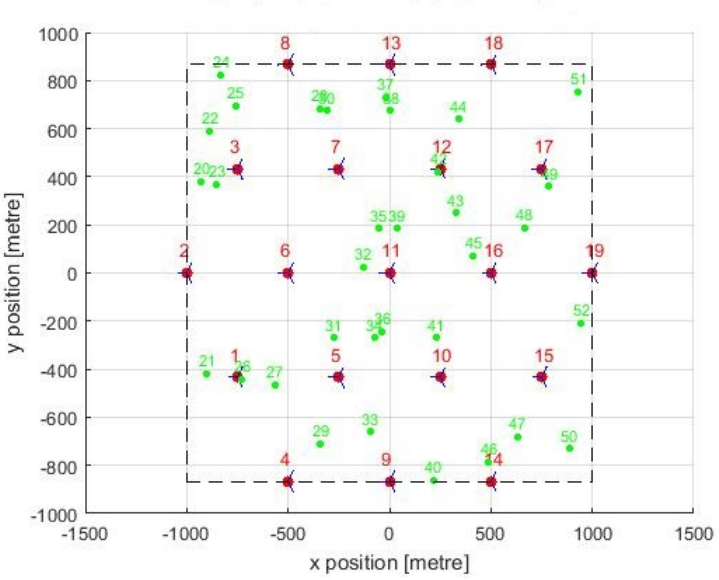

Figure 3.2: A heterogeneous network with the homogeneous density of femtocells (10 femtocells/km^2).

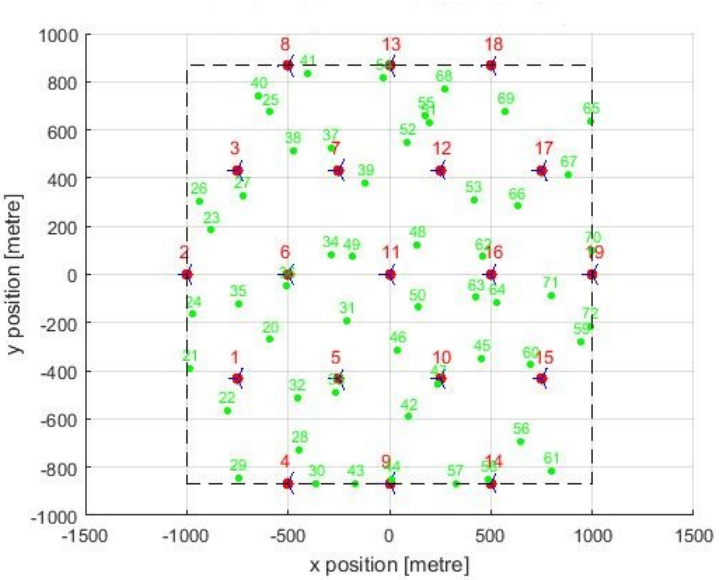

Figure 3.3: A heterogeneous network with a fixed number of femtocells per macro sector (a single femtocell per active sector).

where $-180^\circ \leq \theta \leq 180^\circ$. Let $\theta_{3\text{dB}}$ and A_m be the 3dB beamwidth and the maximum attenuation, respectively. For instance, the antenna pattern for tri-sectorised sites with $\theta_{3\text{dB}} = 65^\circ$ and $A_\text{m} = 20$ dB is shown in Figure 3.4. Note that a three-dimensional antenna pattern proposed by the 3GPP may be employed to consider both horizontal and vertical antenna patterns in practice [7]. In this way, the transmit antenna gain of eNB for any UEs is computed (in dB)

$$G_\text{TX} = G_\text{m} + A_\text{H}(\theta), \tag{3.2}$$

where the maximum base station antenna gain $G_\text{m} = 15$ dBi. Unlike the macro eNB, the antenna pattern (horizontal) of each femtocell is assumed to be omnidirectional ($A_\text{H}(\theta) = 0$ dB).

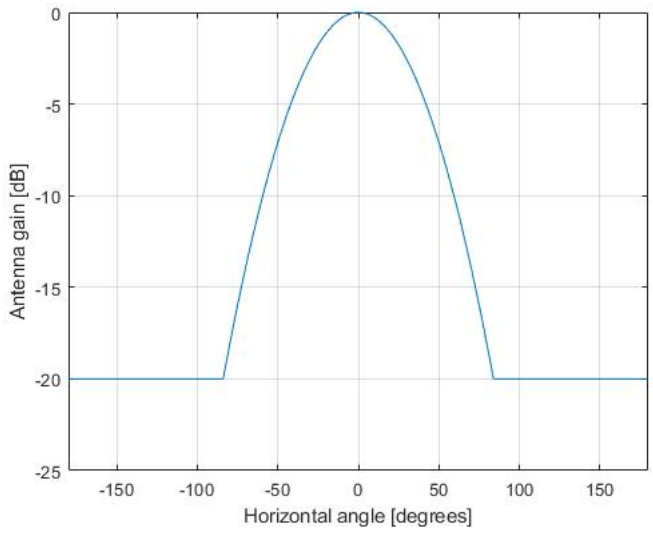

Figure 3.4: The antenna pattern for each sector in tri-sectorised sites ($\theta_{3\text{dB}} = 65^\circ$ and $A_\text{m} = 20$ dB).

3.2.1.2.2 Path Loss

The path loss model for a homogeneous network deployment (in dB) is expressed as [52]

$$L(R) = 128.1 + 37.6 \log_{10}(R), \tag{3.3}$$

where R is the distance between transmitter and receiver (in km). A carrier frequency of 2000 MHz and an eNB antenna height of 15 m above the average rooftop level are applied to (3.3).

According to [9], for a heterogeneous deployment, the path loss of femtocell to UE links (in dB) is obtained as follows

$$L(R) = 127 + 30 \log_{10}(R). \tag{3.4}$$

In this simplified model, any walls between a femtocell and its attached UEs are omitted. Moreover, the model from (3.3) is used for other links between a UE and other femtocell and macro sites. Figure 3.5 represents these two path loss models in this simulation.

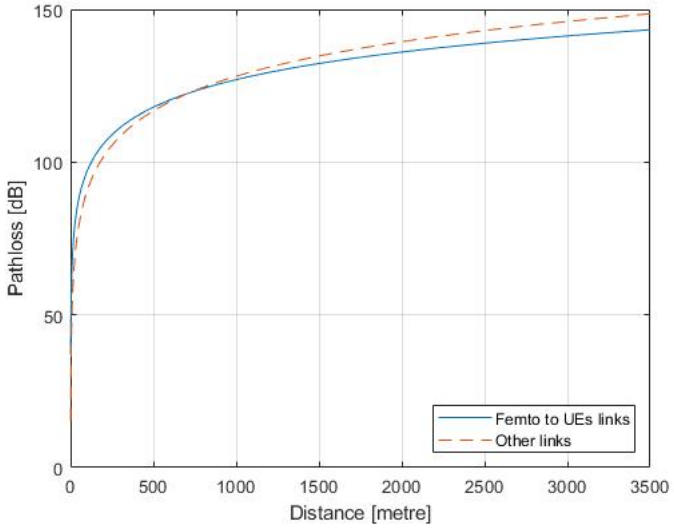

Figure 3.5: The path loss model (dashed red line from (3.3) and green line from (3.4)).

Subsequently, the antenna gain, path loss and minimum coupling loss (MCL) are combined. This MCL is defined as the minimum signal loss between the network elements in the worst case [52]. Thus, the received power is then determined

$$P_{\mathrm{RX}} = P_{\mathrm{TX}} - \mathrm{Max}(L_{\mathrm{total}}, \mathrm{MCL}), \tag{3.5}$$

where the total loss $L_{\mathrm{total}} = L(R) - G_{\mathrm{TX}} - G_{\mathrm{RX}}$. Let $P_{\mathrm{RX}}, P_{\mathrm{TX}}$ and G_{RX} be the received signal power, transmitted signal power and receiver antenna gain, respectively. The MCL is 70 dB for urban and 80 dB for rural area deployments. This results in the large-scale fading (antenna gain, path loss and MCL) maps for a given macro sector and femto site (transmitter) as illustrated in Figures 3.6 and 3.7, respectively.

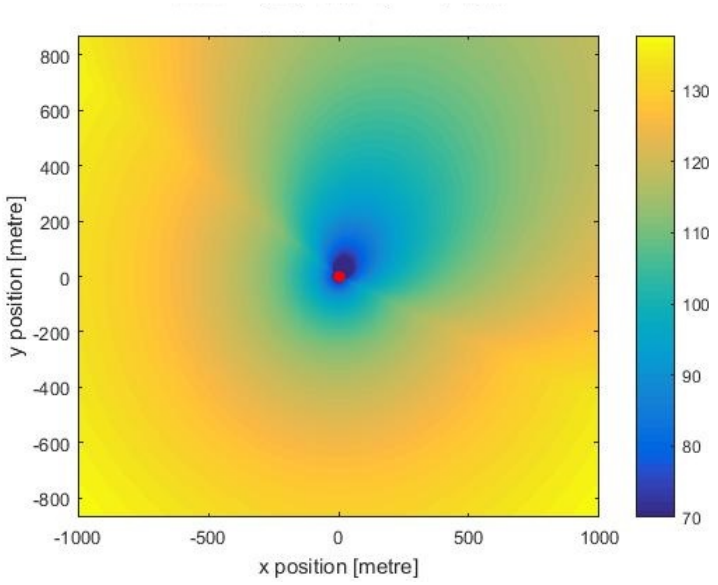

Figure 3.6: A large-scale fading map (in dB) for a macro sector (the site number 11 and sector number 31).

3.2.1.2.3 Shadow Fading

Shadow fading is modelled by a log-normal distribution, that is, the normal random variable with zero mean and a standard deviation of 10 dB is used [52]. Owing to the

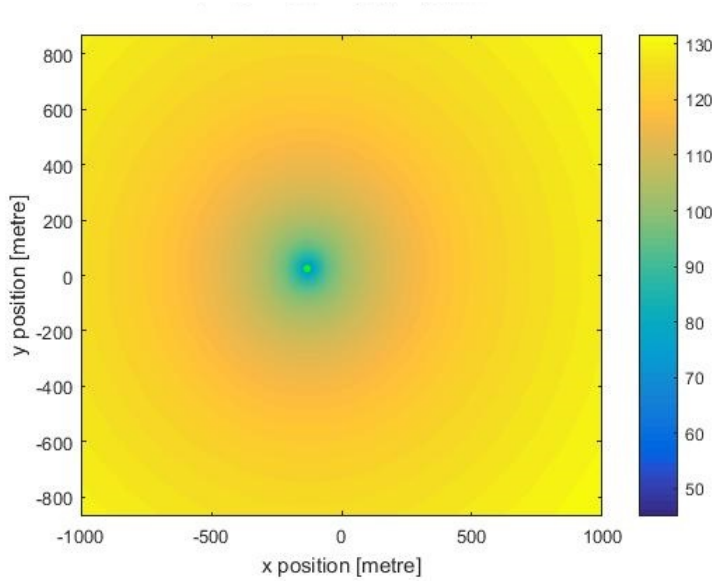

Figure 3.7: A large-scale fading map (in dB) for a femto site (the site number 32).

mobility of network elements (eNBs or UEs), the spatial correlation of shadowing values may be included in the modelling. The normalised correlation function is then defined

$$r(x) = e^{-\alpha x}, \tag{3.6}$$

where x denotes a distance between two points (or pixels) and $x \geq 0$. A value of $\alpha = 1/20$ has been used for a scenario between urban and suburban environments.

Typically, correlated shadow fading values ($\mathbf{s}$) are generated as follows

$$\mathbf{s} = \mathbf{L}\mathbf{a}, \tag{3.7}$$

where $\mathbf{a}$ is an uncorrelated shadow fading vector with $\mathbb{E}\{\mathbf{a}\mathbf{a}^{\mathrm{T}}\} = \mathbf{I}$. Each element in $\mathbf{a}$ is generated (in dB) as a normal random variable. The correlation matrix of $\mathbf{s}$ is $\mathbf{R} = \mathbb{E}\{\mathbf{s}\mathbf{s}^{\mathrm{T}}\} = \mathbf{L}\mathbf{L}^{\mathrm{T}}$ where $\mathbf{L}$ is the Cholesky decomposition of $\mathbf{R}$.

In [54], spatially correlated shadowing values are generated by means of the neighbouring pixels. For example, only four neighbouring values are required for the correlation process in Figure 3.8. As compared to the conventional approach, the computational complexity can be significantly decreased.

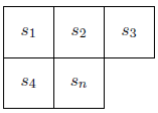

Figure 3.8: The generation of correlated shadowing value (s_n) with four neighbours.

A vector of correlated shadowing values $\tilde{\mathbf{s}} = (s_1, s_2, s_3, s_4)^\mathrm{T}$ with $\tilde{\mathbf{R}} = \mathbb{E}\{\tilde{\mathbf{s}}\tilde{\mathbf{s}}^\mathrm{T}\}$ can be extended to $\mathbf{s} = (s_1, s_2, s_3, s_4, s_\mathrm{n})^\mathrm{T}$ with $\mathbf{R} = \mathbb{E}\{\mathbf{s}\mathbf{s}^\mathrm{T}\}$. Each element in $\tilde{\mathbf{R}}$ and $\mathbf{R}$ is determined by (3.6). Thus, (3.7) can be revised

$$\begin{aligned} \mathbf{s} &= \mathbf{L}\mathbf{a} \\ &= \mathbf{L} \begin{bmatrix} \tilde{\mathbf{L}}^{-1}\tilde{\mathbf{s}} \\ a_\mathrm{n} \end{bmatrix}. \end{aligned} \tag{3.8}$$

This results in the new correlated shadow fading value as follows

$$s_\mathrm{n} = \lambda_\mathrm{n}^\mathrm{T} \begin{bmatrix} \tilde{\mathbf{L}}^{-1}\tilde{\mathbf{s}} \\ a_\mathrm{n} \end{bmatrix}, \tag{3.9}$$

where a_n is the generated normal random variable and $\lambda_\mathrm{n}^\mathrm{T}$ is the last row of $\mathbf{L}$. According to [52], an inter-site correlation of 0.5 and inter-sector correlation of 1 are assumed in order to generate $\mathbf{a}$. The shadowing map for a specific macro site (the site number 11) with 4 neighbouring correlation matrices is shown in Figure 3.9. A single map per site is generated in this simulation. Note that the same process is used for all macro and femto sites.

3.2.1.3 Wideband SINR

Due to the known large-scale fading, the wideband SINR (geometry) of the strongest signal on each pixel of the ROI (the two-dimensional pixel map) can be calculated

$$\Gamma = \frac{G_{\mathrm{TX},0} \cdot L_{\mathrm{M},0} \cdot P_{\mathrm{TX},0}}{\sigma_\mathrm{n}^2 + \sum_{l=1}^{N_\mathrm{int}} G_{\mathrm{TX},l} \cdot L_{\mathrm{M},l} \cdot P_{\mathrm{TX},l}}, \tag{3.10}$$

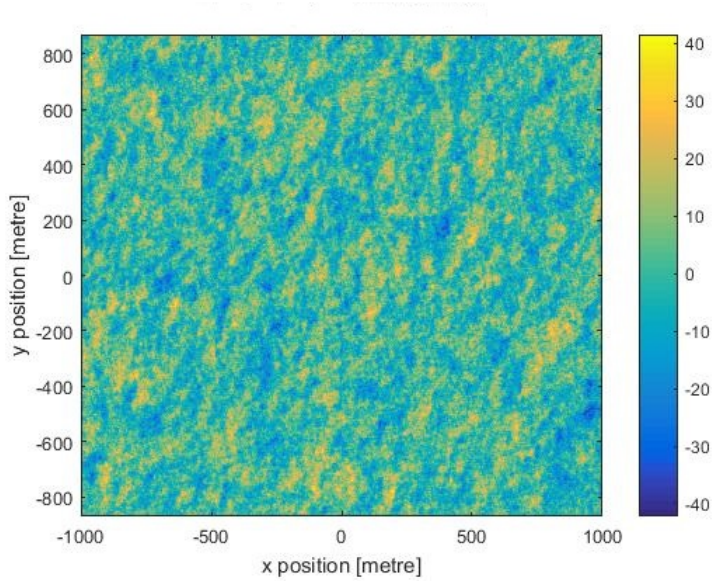

Figure 3.9: The shadow fading map (in dB) for the (macro) site number 11.

where $L_{\mathrm{M},i}$ is the large-scale fading loss (the index $i = 0$ for the desired transmitter and $i = 1, \ldots, N_{\mathrm{int}}$ for the interfering transmitters) and σ_{n}^2 is the receiver noise power.

For a macro network, if the shadow fading is not included in $L_{\mathrm{M},i}$, the wideband SINR map can be visualised in Figure 3.10. Otherwise, the resulting wideband SINR map is shown in Figure 3.11. Similarly, the calculation from (3.10) can be applied to a scenario of heterogeneous network. Because of the wideband SINR map, the sector with the maximum SINR is assigned to each specific pixel. All coverage areas of each sector within the ROI can be identified. This sector assignment will be used to place the number of UEs as discussed further.

3.2.1.4 UE Placement

The constant number of UEs per (macro and femto) sector[4] is selected for the UE placement. Due to the known sector assignment, these UEs are randomly dropped within the pixels (or coverage areas) of their corresponding (serving) sector. For instance, if

[4]Assume that there is a single sector per femto site.

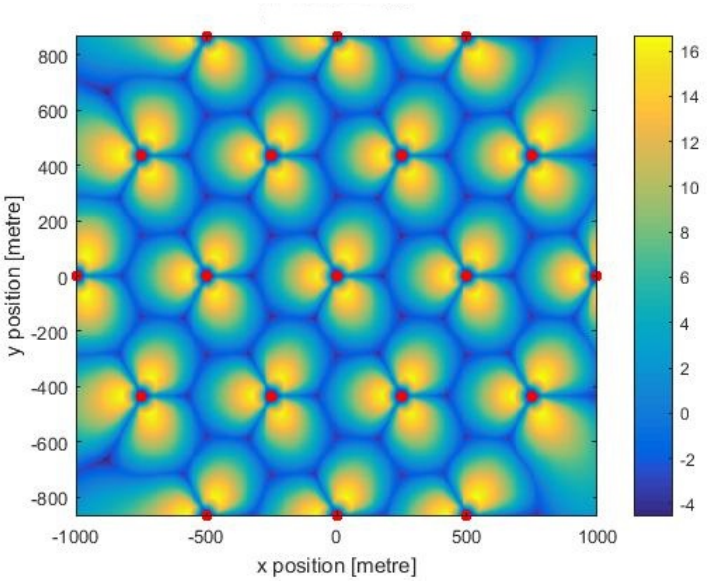

Figure 3.10: The wideband SINR map (in dB) with antenna gain, path loss and MCL.

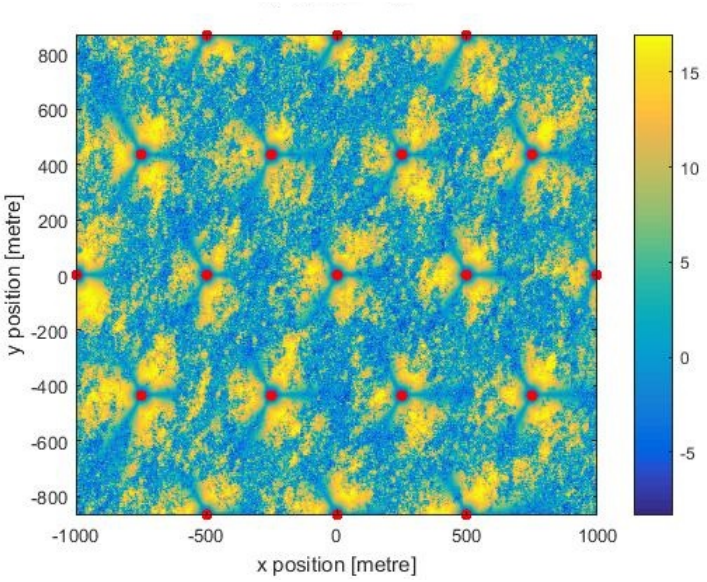

Figure 3.11: The wideband SINR map (in dB) with antenna gain, path loss, MCL and shadowing.

there are 2 attached UEs and 11 active (green) pixels for Sector 1 in Figure 3.12, only two of eleven pixels are randomly picked for these two UEs. Note that UEs are generated only for active (assigned) sectors.

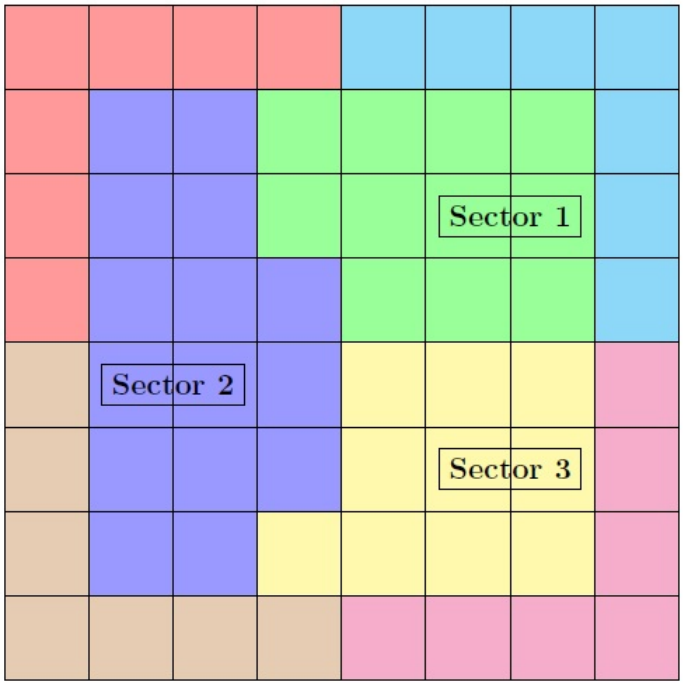

Figure 3.12: The sector assignment on a two-dimensional pixel map.

An example of UE placement in a heterogeneous network (homogeneous density of femtocells) is presented in Figure 3.13. 2 UEs per macro sector and 1 UE per femto sector are set for a good illustrative example. There are 4 of 57 macro sectors near the edge of ROI which are not assigned. If only active sectors are considered, there are 53 macro sectors and 33 femto sectors resulting in the generated 139 UEs (blue diamond markers).

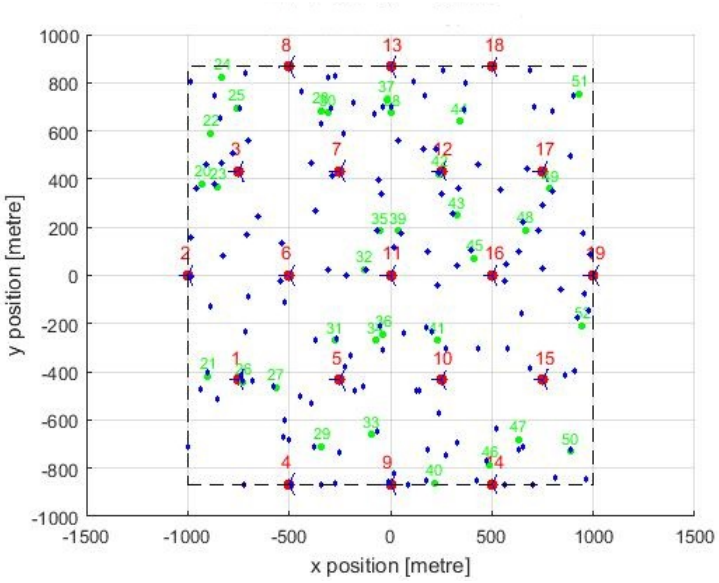

Figure 3.13: The UE placement for a heterogeneous network (139 generated UEs).

3.2.1.5 Small-Scale Fading

The next stage is to generate the small-scale fading based on power delay profile (PDP). Both uncorrelated and correlated fading can be considered in this simulation.

3.2.1.5.1 Power Delay Profile

According to [6], a choice of PDPs, including international telecommunication union (ITU) pedestrian (A and B), extended pedestrian B, vehicular (A and B) and typical urban (TU) channels, can be chosen for modelling. For example, the PDP of pedestrian A (PedA) channel is shown in Figure 3.14. These channel models have been recommended for the technical evaluation of radio transmission technologies by the ITU [55]. Additional 3GPP channel models [24], including extended pedestrian A (EPA), extended vehicular A (EVA) and extended typical urban model (ETU), could be added to the simulator in this thesis as well.

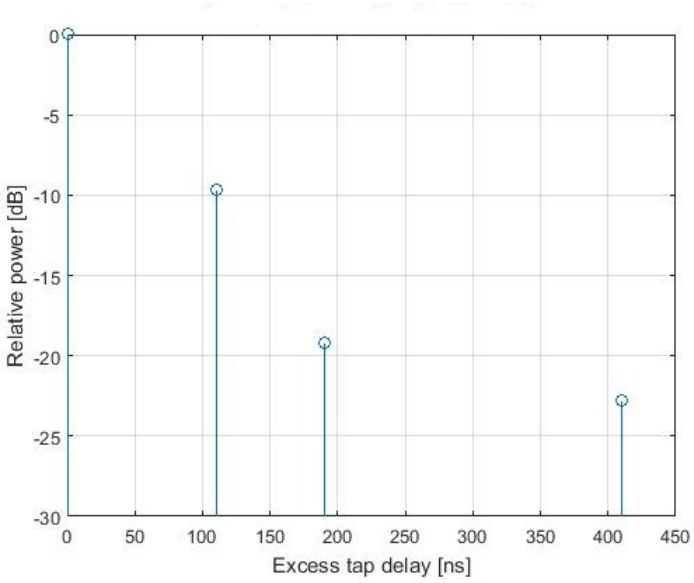

Figure 3.14: The power delay profile of PedA channel (4 taps).

3.2.1.5.2 Fading Generation

Subsequently, the Rayleigh fading channel coefficient is generated where either uncorrelated or correlated fading can be configured in the simulation setup. The fading generation of both methods is presented in this section. According to [56, 17], a well-known approach for modelling of uncorrelated fading is adopted. The independent in-phase (X_I) and quadrature (X_Q) components are two (uncorrelated) Gaussian random variables with zero mean and equal variance (σ^2). The signal envelope is then defined

$$|X(t)| = \sqrt{X_I^2(t) + X_Q^2(t)}, \tag{3.11}$$

where the envelope distribution is given by

$$f_{|X|}(x) = \frac{x}{\sigma^2} \cdot \exp\left(\frac{-x^2}{2\sigma^2}\right), \quad x \geq 0. \tag{3.12}$$

The signal phase is then determined

$$\Theta_X(t) = \arctan\left(\frac{X_Q(t)}{X_I(t)}\right), \tag{3.13}$$

where the phase distribution is considered as

$$f_{\Theta_X}(\theta_X) = \frac{1}{2\pi}, \quad \theta_X \in [-\pi, \pi). \tag{3.14}$$

Figures 3.15 and 3.16 show the distribution of simulated envelope and phase as compared with the theoretical probability density functions (pdf) from (3.12) and (3.14) in the case of uncorrelated fading, respectively. 4,000 realisations (the number of receivers by transmitters by random samples by taps) are used in this example. Hence, this proves that the simulated $X(t)$ has a Rayleigh-distributed envelope and uniformly-distributed phase.

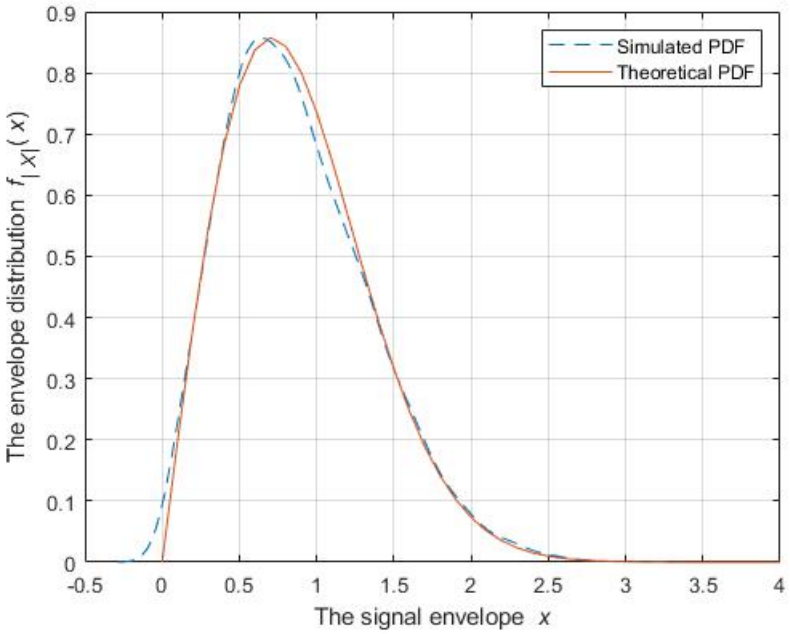

Figure 3.15: The pdf of signal envelope (the uncorrelated fading).

Alternatively, the Clarke and Jake's reference model is improved in [57] to generate the correlated fading. The randomness for random path gain (C_n), angle of incoming wave (α_n) and initial phase (ϕ_n) corresponding to the nth path is included in this generation. Firstly, the low-pass fading process of N propagation paths can be presented

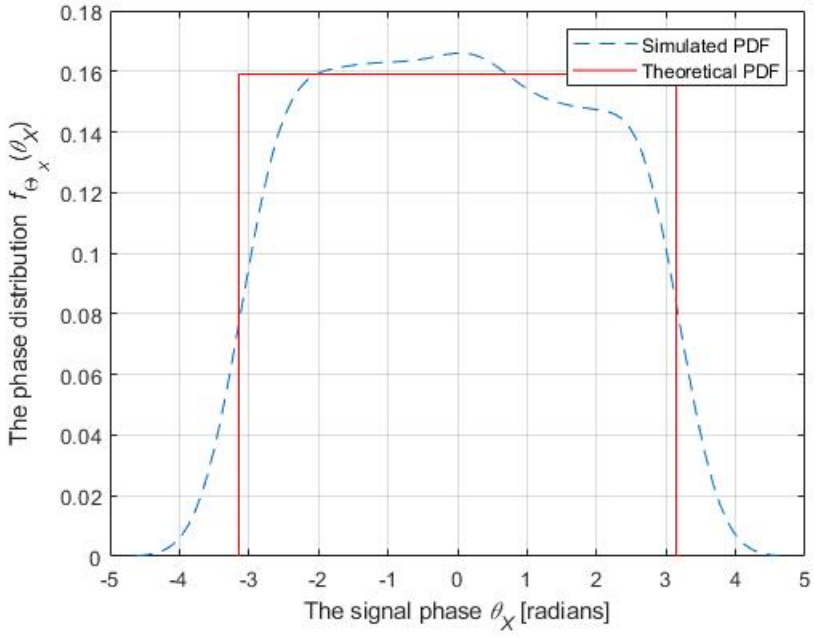

Figure 3.16: The pdf of signal phase (the uncorrelated fading).

as

$$g(t) = E_0 \sum_{n=1}^{N} C_n \exp\{j(\omega_d t \cos\alpha_n + \phi_n)\}, \tag{3.15}$$

where

$$\begin{aligned} C_n &= \frac{\exp(j\psi_n)}{\sqrt{N}}, \quad n = 1, 2, \ldots, N, \\ \alpha_n &= \frac{2\pi n - \pi + \theta}{N}, \quad n = 1, 2, \ldots, N, \\ \phi_n &= -\phi\frac{N}{2} + n = \phi, \quad n = 1, 2, \ldots, \frac{N}{2}, \end{aligned}$$

let $N/2$, E_0 and ω_d be an integer, a scaling constant and the maximum radian Doppler frequency, respectively. ψ_n, θ and ϕ are mutually independent random variables with the uniform distribution over $[-\pi, \pi)$. Furthermore, (3.15) can be rearranged as follows

$$\hat{g}(t) = \frac{E_0}{\sqrt{N}} \left\{ \sum_{n=1}^{M} \sqrt{2} e^{j\psi_n} \left[e^{j(\omega_n t + \phi)} + e^{-j(\omega_n t + \phi)} \right] \right\}, \tag{3.16}$$

where $M = N/4$ and $\omega_n = \omega_d \cos\alpha_n$. Then, the normalised low-pass fading process based on (3.16) is defined

$$X(t) = X_I(t) + jX_Q(t), \tag{3.17}$$

where

$$X_I(t) = \frac{2}{\sqrt{M}} \sum_{n=1}^{M} \cos(\psi_n) \cdot \cos(\omega_d t \cos\alpha_n + \phi),$$
$$X_Q(t) = \frac{2}{\sqrt{M}} \sum_{n=1}^{M} \sin(\psi_n) \cdot \cos(\omega_d t \cos\alpha_n + \phi).$$

and $\alpha_n = \frac{2\pi n - \pi + \theta}{4M}$ for $n = 1, 2, \ldots, M$. The pdfs of simulated envelope and phase in the case of correlated fading from (3.17) are illustrated in Figures 3.17 and 3.18, respectively. Similarly, the results appear to be the Rayleigh-distributed envelope and uniform phase.

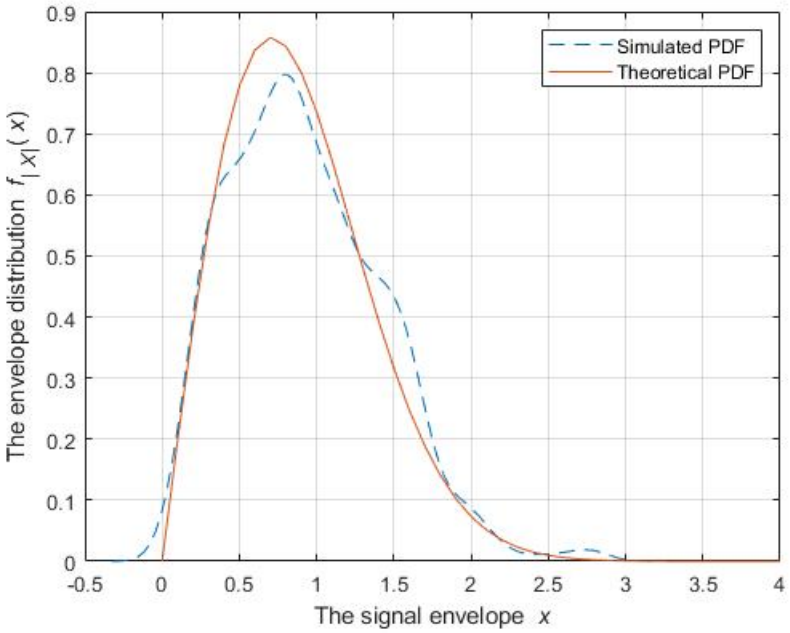

Figure 3.17: The pdf of signal envelope (the correlated fading).

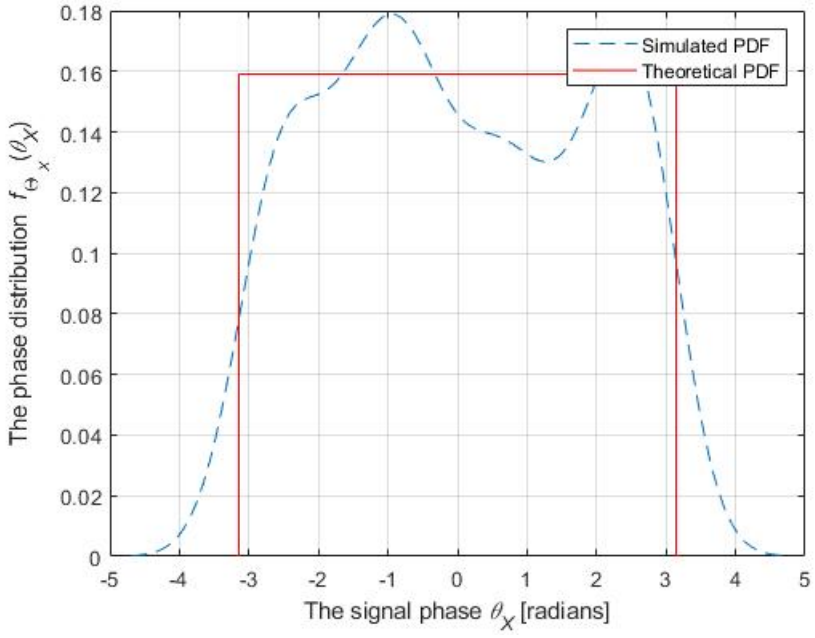

Figure 3.18: The pdf of signal phase (the correlated fading).

3.2.2 Main Simulation

The simulation model, including simulation flow and main simulation, is outlined in this section. This methodology was also published by the author of this thesis in [12].

3.2.2.1 Simulation Flow

The simulation flow is shown in Figure 3.19. The pre-generated data from Section 3.2.1 and related system parameters being the input are imported. Let CurrentTTI be the current transmission time interval (TTI) or subframe. The main simulation will be performed until reaching the simulation duration (SimLength). In each TTI, there is the number of operations such as scheduling in Figure 3.19 and the simulation results are then collected. After the main simulation is terminated, the results from each TTI are processed by the post-processing stage. For the output, UE throughput, fairness index and wideband SINR could be obtained by this simulation.

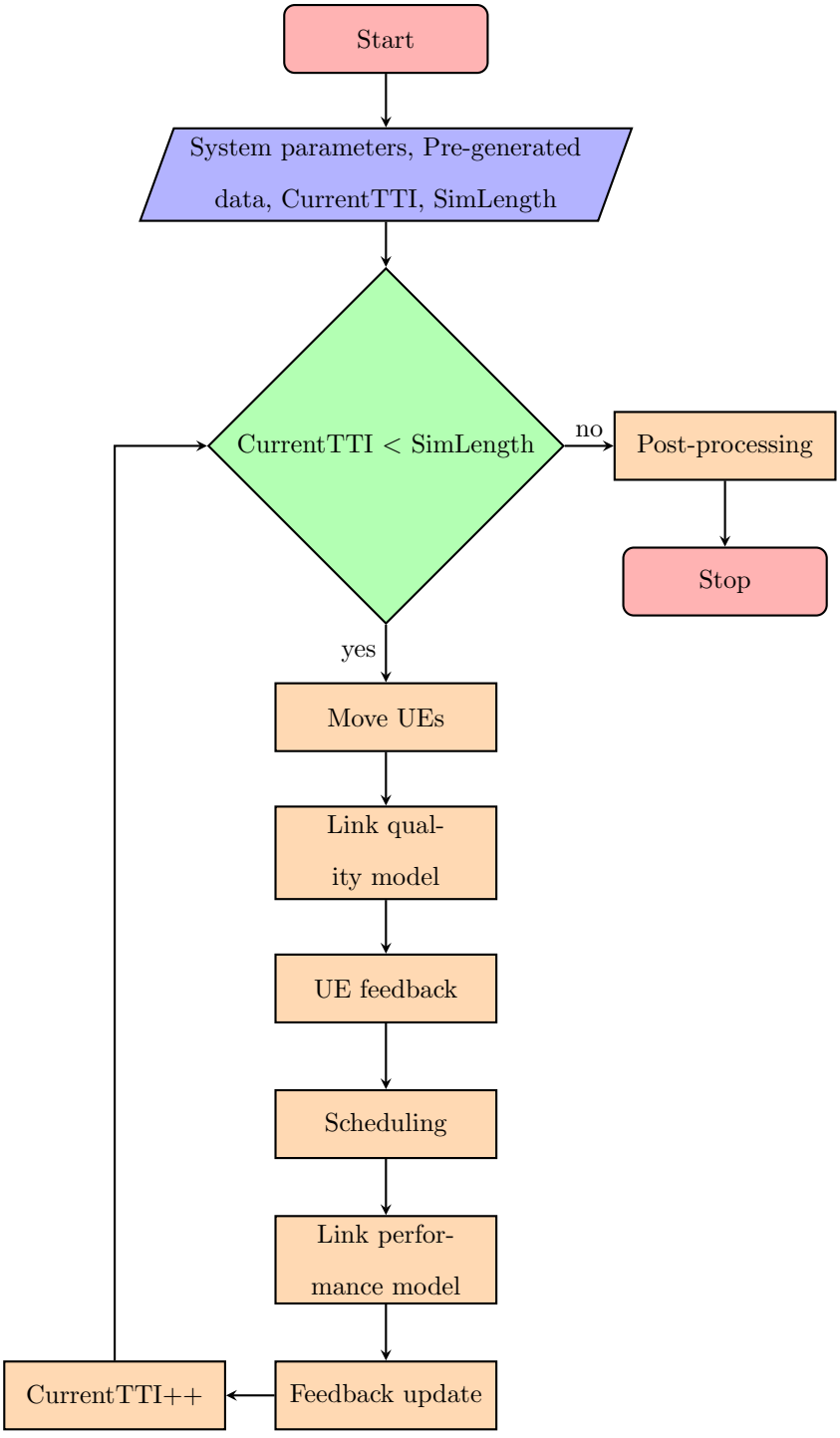

Figure 3.19: The simulation flow.

3.2.2.2 Main Simulation

The pre-generated data, including UE positions, large- and small-scale fading, is processed in the main simulation. There are six operational stages within each TTI as follows

a. Place/move UEs

- The initial UE positions for the first TTI are obtained from the UE placement.
- UE positions are randomly generated by a walking model as mentioned in Appendix A.
- Current UE positions are determined by UE positions from previous TTI.

b. Link quality model

- The large-scale fading is selected by current UE positions.
- The small-scale fading for each UE is determined by the current TTI.
- UE parameters such as transmission mode and RB grid are defined.
- Received (post-equalisation) SINRs and CQI feedback are calculated as described in Appendixes B and C, respectively.

c. eNBs receive and process the feedback from UEs

- The availability of UE feedback at eNB is checked.
- Current feedback is stored in the buffer for the next TTI.

d. eNBs schedule transmissions to the UEs

- RB allocation is performed, including round-robin, best-CQI and proportional fair.
- Homogeneous power allocation is selected.

- eNB signalling (Appendix D) is obtained such as CQI, transport block (TB) size and assigned RBs.

e. Link performance model (Appendix E)

- The output from link quality model (post-equalisation SINR) and scheduling (eNB signalling) is used.
- TB SINR, BLER and acknowledgment (ACK) are calculated, if any RBs are assigned.
- The feedback such as BLER and ACK is updated.

f. Update the UE feedback to the channel

- Related feedback is recorded in the buffer for post-processing and the following TTIs (Appendix E).

3.2.3 Post-Processing

The next stage is to process all results from the main simulation in Section 3.2.2. The performance metrics, including UE throughput, fairness index and wideband SINR, are described in this section.

3.2.3.1 UE Throughput

The average throughput of a given UE (in Mbps) can be defined as follows [6]

$$T_{\text{avg}} = \frac{B_{\text{total}}}{N_{\text{TTI}} \times L_{\text{TTI}} \times 10^6}, \tag{3.18}$$

where the total bit $B_{\text{total}} = \sum_{i \in A}(\text{ACK}_i \times \text{TB}_{\text{size},i})$. Let ACK_i and $\text{TB}_{\text{size},i}$ be the acknowledgment and the transport block size (in bits) on the ith TTI, respectively. Denote the set and number of accounted TTIs by A and N_{TTI}, respectively. The TTI without feedback is not considered. The TTI length (L_{TTI}) of 1 ms is set.

Note that UE throughputs derived from (3.18) are the main focus of interest and the main result of the developed simulator. The empirical cumulative distribution function (ecdf)[5] of UE throughputs is then determined, resulting in mean, edge and peak throughputs for the performance evaluation. According to [1], the terms edge and peak throughput which are the 5% and 95% points of the UE throughput ecdf have been widely employed to indicate the performance of cell edge and cell centre UEs, respectively. Therefore, these throughput statistics are used to summarise the UE throughput performance for comparison purposes throughout this thesis along with the full throughput distributions.

3.2.3.2 Fairness Index

To measure the equality of resource (throughput) distribution over N UEs, the fairness index is defined as [60]

$$J(\mathbf{x}) = \frac{(\sum_{i=1}^{N} x_i)^2}{N \sum_{i=1}^{N} x_i^2}, \tag{3.19}$$

where $\mathbf{x}$ is a throughput vector of length N. This index is restricted between [0,1]. 0 refers to the overall unfairness, whereas 1 means the overall fairness of throughput distribution. In other words, the same throughput could be offered to all UEs with the fairness index of 1.

3.2.3.3 UE Wideband SINR

According to [6], the wideband SINR of a given UE (in dB) can be determined

$$\gamma = 10 \log_{10} \left(\frac{P_{\mathrm{RX},0}}{P_N \cdot N_{sc} + \sum_{l=1}^{N_{\mathrm{int}}} P_{\mathrm{RX},l}} \right), \tag{3.20}$$

[5] An empirical cumulative distribution function (F_n) is the distribution function to model empirical (observed) data. For observations $\mathbf{x} = (x_1, x_2, \ldots, x_n)$, F_n is the fraction of observations less than or equal to a specific value of t in $\mathbf{x}$, that is, $F_n(t) = \frac{1}{n} \sum_{i=1}^{n} \mathbf{1}_{[x_i \leq t]}$, where n is the number of observations [58, 59].

where $P_{\mathrm{RX},i}$ is the received power (the index $i = 0$ for the desired part and $i = 1, \ldots, N_{\mathrm{int}}$ for the interfering parts). The power is attenuated by large-scale fading (path loss and shadowing). Let P_N be the thermal noise. N_{sc} is the number of subcarriers (or samples) per RB. This wideband SINR is calculated for each individual UE while the wideband SINR from (3.10) is computed for all sectors within the ROI (the two-dimensional map). Note that the ecdf of UE wideband SINRs is determined in just the same way a case of UE throughput does.

3.3 Simulation Verification

To verify the developed simulator, the simulation results from this tool are compared with the Vienna simulator. The network layout and simulation parameters are indicated. The ecdf of UE throughputs from (3.18) and wideband SINRs from (3.20) is used for this verification.

3.3.1 Network Layout

Figures 3.20 and 3.21 show the homogeneous network layout and UE placement between the Vienna and this developed simulators. The same ROI is investigated.

3.3.2 Simulation Parameters

The simulation parameters in Table 3.2 are the same for both simulators. Note that only UEs within the coverage area of central macro site are considered. This results in the network performance analysis without incurring border effects and the reduction of statistical sampling [7]. To obtain a statistically representative result of the average network performance, the simulation duration of 100 TTIs is used.

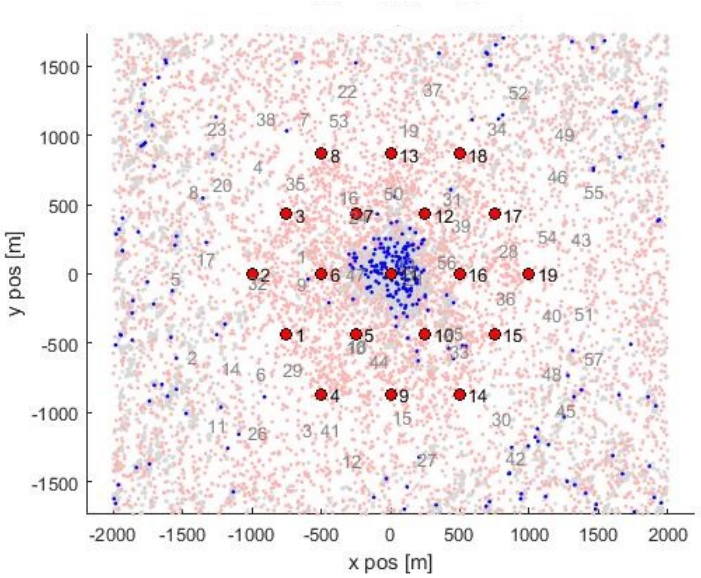

Figure 3.20: The network layout and UE placement (the Vienna simulator).

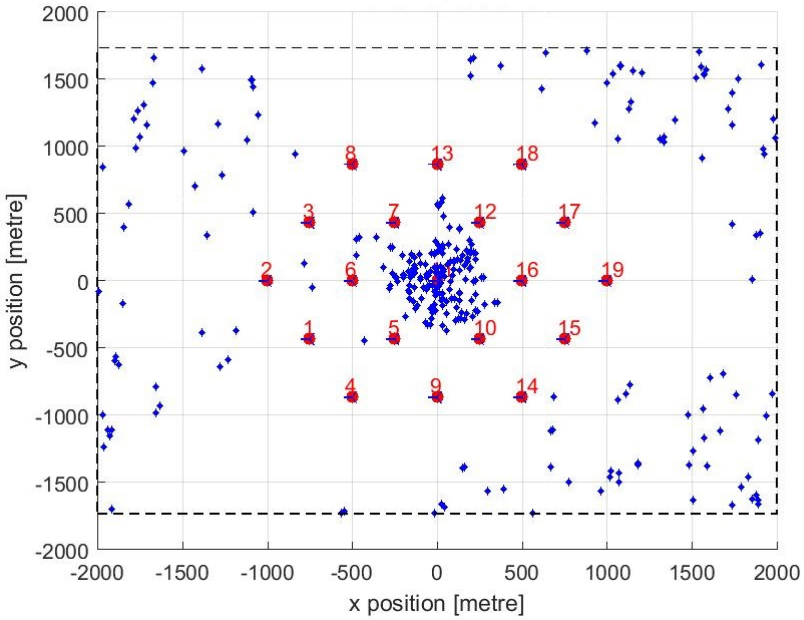

Figure 3.21: The network layout and UE placement (the developed simulator).

Table 3.2: Simulation parameters (reproduced from [7]).

Parameter	**Assumption**
Cellular layout	Hexagonal grid of 19 sites
Inter-site distance	500 m
Path loss model	$L = 128.1 + 37.6 \log_{10}(R)$
Lognormal shadow fading	$L_s \sim N(\mu, \sigma^2)$
Shadow fading mean	0 dB
Shadow fading standard deviation	10 dB
Shadow fading correlation	0.5 between sites, 1.0 between sectors
Antenna pattern (horizontal)	$A_{\mathrm{H}}(\theta) = -\min\left[12\left(\frac{\theta}{65^o}\right)^2, 15\mathrm{dB}\right]$
Carrier frequency	2.14 GHz
System bandwidth	1.4 MHz
Channel model	ITU Pedestrian A model
UE speed	5 km/h
Number of UEs	100 UEs per sector
Total BS TX power (P_{total})	46 dBm
Scheduling	Round-robin
Transmission mode	Single-input single-output (SISO)
Simulation length	100 TTIs

3.3.3 Results

The ecdf of UE wideband SINRs as mentioned in Section 3.2.3 is shown in Figure 3.22. All results from the developed tool are compared with the results of Vienna simulator.

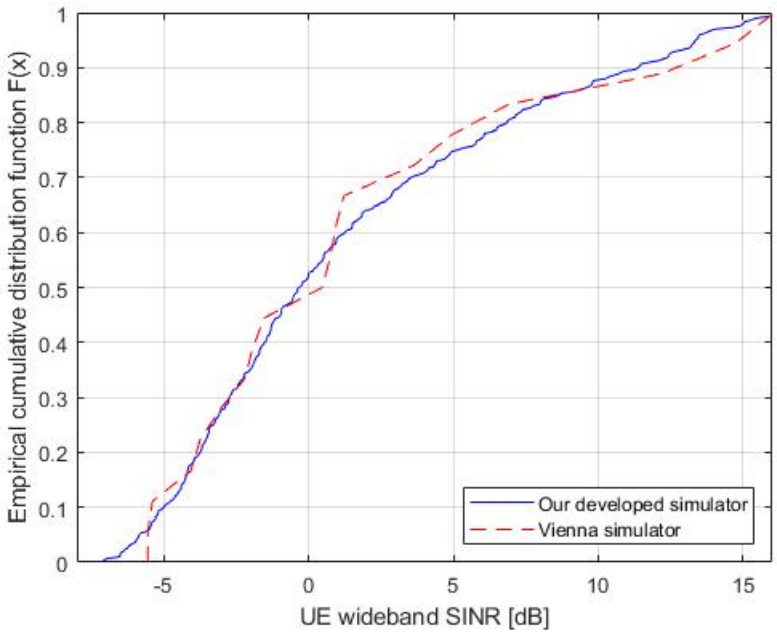

Figure 3.22: The ecdf of UE wideband SINR.

Furthermore, a comparison of UE throughput ecdf is illustrated in Figure 3.23. Key UE throughput statistics (peak, mean and edge) and fairness index are presented in Table 3.3. According to both UE wideband SINR and throughput results, a close match between these two simulators could be obtained.

3.4 Small Cell and Scheduling

After the simulation verification in Section 3.3, the scope of study is extended to the heterogeneous cellular network. The network layout and simulation parameters are discussed. Subsequently, the UE throughput is evaluated in connection with small cell

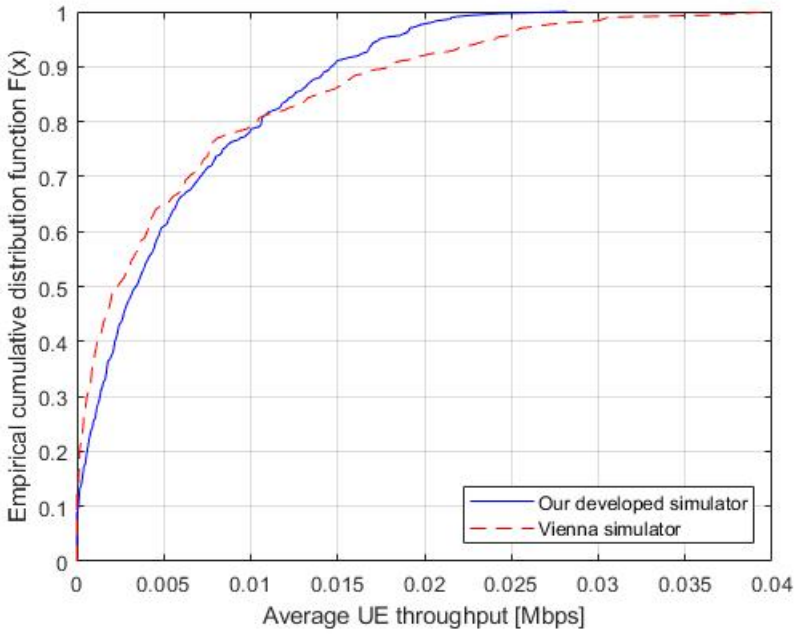

Figure 3.23: The ecdf of UE throughput.

Table 3.3: Performance metrics.

Performance metrics	**Our simulation**	**Vienna**
Peak throughput (kbps)	17.4	24.1
Mean throughput (kbps)	5.6	5.9
Edge throughput (kbps)	0	0
Fairness	0.4763	0.3569

deployments and scheduling techniques.

3.4.1 Network Layout

There are two network scenarios: homogeneous and heterogeneous networks. First, a homogeneous network, as shown in Figure 3.1, is considered. Second, a heterogeneous network with homogeneous density of femtocells as shown in Figure 3.2 is examined. Also, a heterogeneous network with a fixed number of femtocells per macro sector is investigated as illustrated in Figure 3.3. Note that the fading loss and UE placement are generated as discussed in Section 3.2.1.

3.4.2 Simulation Parameters

Tables 3.4 and 3.5 show the simulation parameters for macro and femtocell networks. Only femtocells and UEs within the coverage area of central macro site are considered in this simulation. Most simulation parameters are the same for both macro and femtocell networks except the network layout, path loss model, antenna pattern, the number of UEs and transmit power.

3.4.3 Results

To comprehend the impact of small cell deployments, the ecdf of UE throughput is evaluated while varying the homogeneous density (10 and 20 femtocells/km^2) and a constant femtocell per macro sector (1 and 2 femtocells per sector) as shown in Figure 3.24. All results are compared to the homogeneous network (macro-only) with the round-robin scheduler.

According to the results, the UE throughput can be enhanced. For instance, the peak throughput of the heterogeneous network with 2 femtocells per macro sector was around eight times as large as the homogeneous network. The key UE throughput metrics for these cases are presented in Table 3.6.

Table 3.4: Simulation parameters (macro network).

Parameter	**Assumption**
Cellular layout	Hexagonal grid of 19 sites
Inter-site distance	500 m
Path loss model	$L = 128.1 + 37.6 \log_{10}(R)$
Lognormal shadow fading	$L_s \sim N(\mu, \sigma^2)$
Shadowing mean	0 dB
Shadowing standard deviation	10 dB
Antenna pattern (horizontal)	$A_{\mathrm{H}}(\theta) = -\min\left[12\left(\frac{\theta}{65^o}\right)^2, 15\mathrm{dB}\right]$
Carrier frequency	2.14 GHz
System bandwidth	1.4 MHz
Channel model	ITU Pedestrian A model
UE speed	5 km/h
Number of UEs	30 UEs per sector
Total BS TX power (P_{total})	46 dBm
Scheduling	Round-robin and best-CQI
Transmission mode	SISO
Simulation length	50 TTIs

Table 3.5: Simulation parameters (femtocell network).

Parameter	**Assumption**
Cellular layout	Random placement
Inter-site distance	N/A
Path loss model	$L = 127 + 30\log_{10}(R)$
Antenna pattern (horizontal)	$A_{\mathrm{H}}(\theta) = 0$ dB
Number of UEs	2 UEs per sector
Total BS TX power (P_{total})	20 dBm

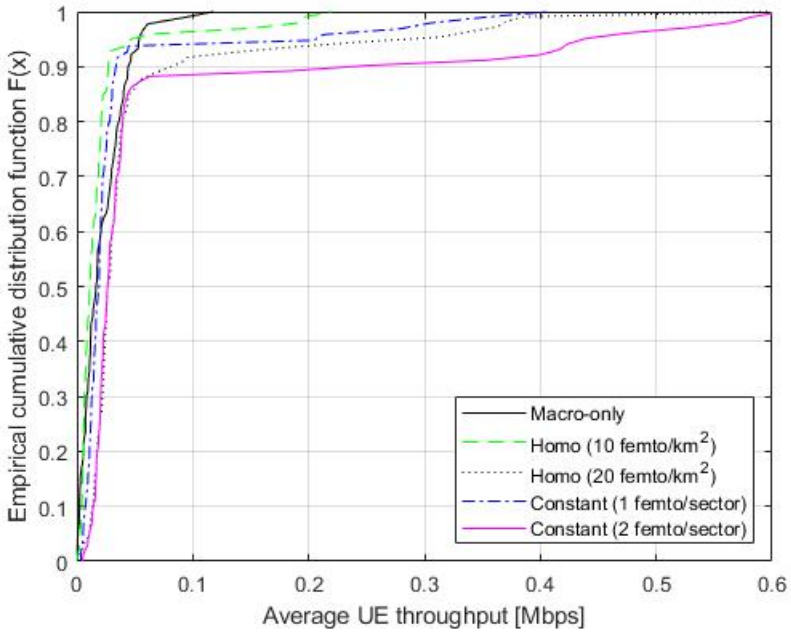

Figure 3.24: The ecdf of UE throughput (round-robin scheduling).

Table 3.6: UE throughputs (femtocell deployments).

Network scenario	**UE throughput (in kbps)**		
	Peak	**Mean**	**Edge**
Macro-only	54.2	22.1	0.816
Homogeneous (10 femtocells/km^2)	62.9	20.5	2.8
Homogeneous (20 femtocells/km^2)	313.5	53.3	11.4
Constant (1 femtocell/sector)	213.1	35.5	5.4
Constant (2 femtocells/sector)	438.9	74.3	11.4

Another issue of interest is the impact of scheduling. The ecdf of UE throughput under the round-robin and best-CQI schdulers is presented in Figure 3.25. Owing to the best-CQI, the peak throughput was enhanced for both homogeneous and heterogeneous (2 femtocells per sector) scenarios. A given RB was assigned to the UE with the best channel condition (or the maximum CQI) by this scheme. However, the round-robin outperformed the best-CQI in terms of edge throughput and fairness. Table 3.7 shows the UE throughput from all cases.

Table 3.7: UE throughputs (scheduling techniques).

Network scenario	**UE throughput (in kbps)**		
	Peak	**Mean**	**Edge**
Macro-only (round-robin)	54.2	22.1	0.816
Macro-only (best-CQI)	649.6	82.8	0
Macro-femto (round-robin)	438.9	74.3	11.4
Macro-femto (best-CQI)	737	185.5	0

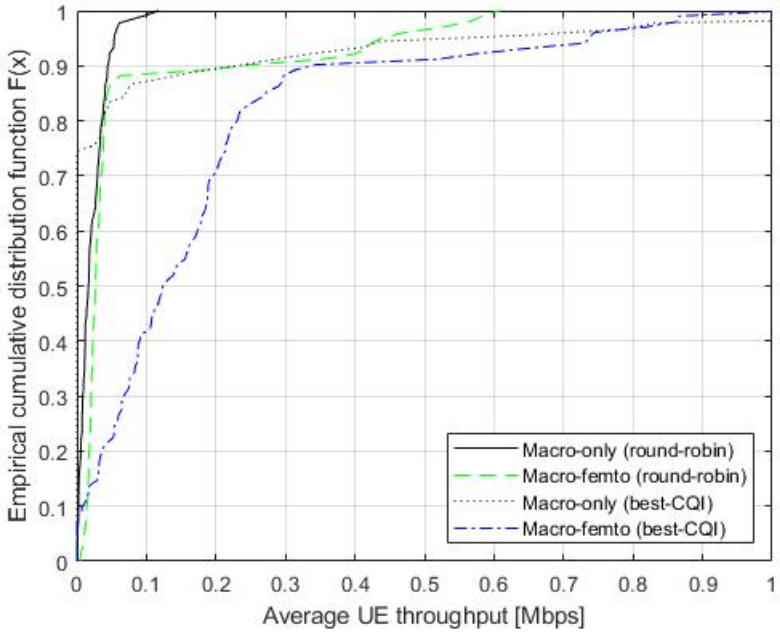

Figure 3.25: The ecdf of UE throughput (round-robin and best-CQI schedulers).

3.5 Summary

In this chapter, the SL simuation for cellular networks was discussed. Existing SL tools such as the Vienna SL simulator were identified. For the developed SL simulator in this thesis, system and simulation models were presented step-by-step. The results from this tool were compared with the reference tool for the simulation verification. Subsequently, homogeneous and heterogeneous LTE cellular networks in DL transmission were modelled to investigate small cell deployments and scheduling techniques in terms of UE throughput. According to the results, the performance such as peak UE throughput could be enhanced by means of femtocell deployments and best-CQI scheduler. However, this was at the expense of edge throughput and fairness as compared to the round-robin scheduler. A trade-off between throughput and fairness should be considered carefully in practice. In Chapter 4, resource allocation with CA, including CC selection and RB

scheduling, becomes the focus of attention. The performance is then evaluated using this developed SL simulator under various CA types, CC selection, frequency bands and scheduling techniques.

Chapter 4

Carrier Aggregation

In this chapter, the work of CA-based resource allocation is the focus published in [13]. The system model, including pre-generated data and CA capability, is first described. Subsequently, CC selection and RB scheduling are considered separately. Also, the simulation model, including simulation flow and parameters, is defined. The user throughput is then evaluated under different types of CA, CC selection, frequency bands and scheduling approaches.

4.1 System Model

The system model of a homogeneous network with CA is outlined. The pre-generated data such as large-scale fading are presented. Unlike Chapter 3, CA is included in the system model. Thus, different characteristics on each CC and CA capability are discussed as well.

4.1.1 Pre-Generated Data

The same network layout as shown in Figure 3.1 is selected to model a homogeneous network where only macro sites are considered. For the antenna gain, the antenna pattern from (3.1) is applied to each macro sector. The path loss model (in dB) can be

generalised as follows

$$L(R) = 40(1 - 4 \cdot 10^{-3} \cdot D_{hb}) \cdot \log_{10}(R) - 18\log_{10}(D_{hb}) + 21\log_{10}(f) + 80\text{dB}, \quad (4.1)$$

where R is the separation distance (in km) between the macro eNB and UE. Denote the carrier frequency (in MHz) and the eNB antenna height above the average rooftop level (in m) by f and D_{hb}, respectively. The antenna height of 15 metres is applied to (4.1). This results in the large-scale fading map formed by the antenna gain and path loss for a given macro sector on different CCs as illustrated in Figure 4.1. In this example, the inter-band non-contiguous CA is modelled where 2 downlink CCs from the 2100-MHz and 3400-MHz bands can be aggregated [24]. Because of the higher frequency, the maximum fading level of the 3400-MHz band (more than 140 dB in Figure 4.1b) is greater than the maximum fading level of the 2100-MHz band (below 140 dB in Figure 4.1a). Besides, the different bandwidth (5, 10, 15 or 20 MHz) with its corresponding transmit power (20 or 40 Watt) on each CC may be used [9].

The same method as discussed in Section 3.2.1 is used to generate the shadow fading and wideband SINR maps for each CC. The wideband SINR maps are then applied to obtain the sector assignment in Figure 4.2. In this way, the coverage area of each macro sector is identified. Not only sector index (1-57) but also CC index (1-2) with the maximum RSRP can be determined for each pixel on the map [6]. Subsequently, the constant number of UEs per sector is randomly placed and the same method for the small-scale fading is used as mentioned in Section 3.2.1.

4.1.2 CA Capability

To model the intra- and inter-band non-contiguous CA, there are offered 4 CCs with 5-MHz bandwidth each from either a single band or different combination of dual bands (900, 1800, 2100 and 3400 MHz[1]) on each sector. Due to the CA capability, less than 4

[1]The 3.4 GHz band is viewed as the spectrum from 3410 - 3600 MHz for mobile broadband and 5G services in the UK [61].

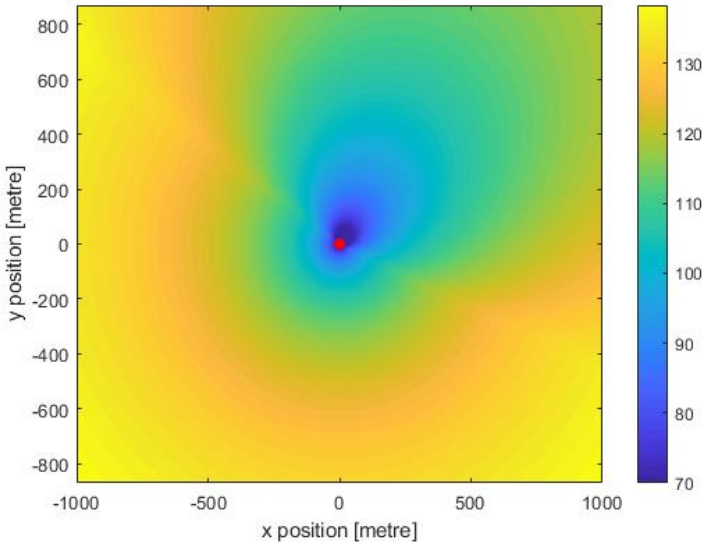

(a) The 2100-MHz band

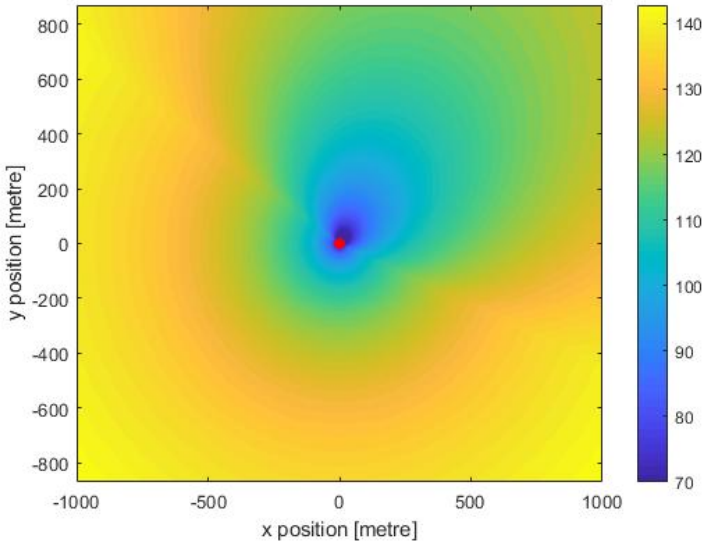

(b) The 3400-MHz band

Figure 4.1: The large-scale fading maps (in dB) for a macro sector (site number 11 and sector number 31) on different CCs: the maximum fading level of the 3400-MHz band is higher than the maximum fading level of the 2100-MHz band (the vertical colorbar).

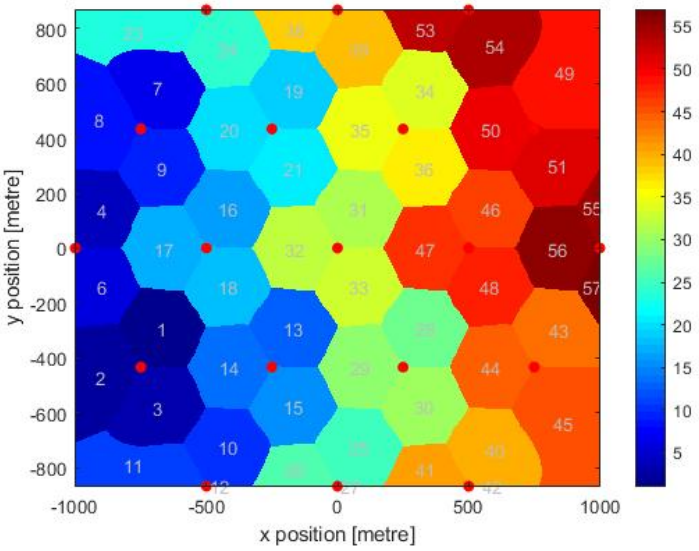

(a) The sector assignment without shadowing

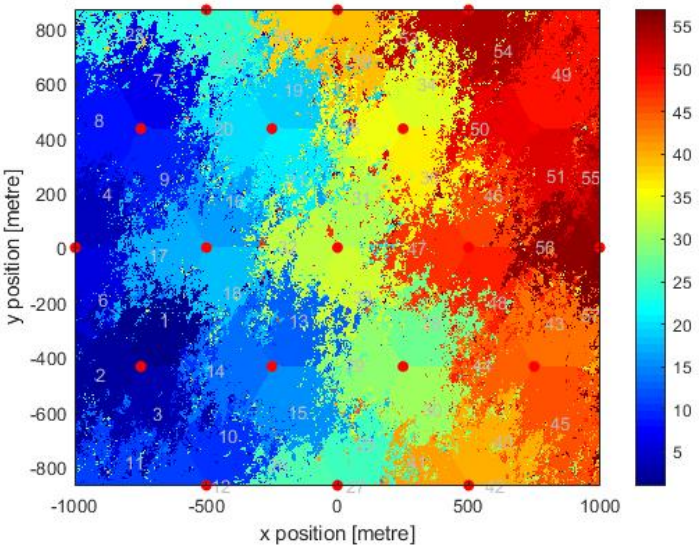

(b) The sector assignment with shadowing

Figure 4.2: The sector assignment (the sector index 1-57 on the colormap and vertical colorbar).

CCs may be allocated to each UE. In this study, there are two kinds of UEs, including LTE and LTE-A UEs. At each TTI, assume that only a single CC is used by a LTE UE while a LTE-A UE can access 2 CCs simultaneously. Note that the fraction of LTE/LTE-A UEs is able to be adjusted in the simulation.

4.2 Separate Resource Allocation

As discussed in Section 2.5.3, the CA-based resource allocation can be divided into CC selection and packet (or RB) scheduling. These two tasks are performed independently in this study. It is known as the separate resource allocation.

4.2.1 CC Selection

To assign a set of CCs to UEs, a list of CC selectors in this simulation is summarised in Table 4.1. Any CCs are picked regardless of channel condition by either RR or random selection while the channel quality is considered in the RSRP selection. This results in the simpler implementation in the case of RR and random approaches as compared with RSRP. Because of different CC selectors, the different load balance across CCs could be obtained. This point will be investigated further in Section 4.4.1.

Table 4.1: A list of CC selectors.

CC selector	**Approach**	**Channel condition**	**Benefit**
RR [25, 62]	Round-robin	No	Uniform CC load balance
Random [25, 62]	Random	No	Long-term CC load balance
RSRP [25, 37]	Maximum RSRP	Yes	Channel condition awareness

4.2.2 RB Scheduling

The next task is to allocate RBs to UEs on each CC. Table 4.2 shows a list of RB schedulers, including RR, best-CQI and PF, used in this study. The simplest RR scheduler has been widely used without the channel condition. For the best-CQI scheduler, the UE with highest CQI (or the best channel quality) is scheduled. In the PF scheduler the UE with maximum utility function will be scheduled first. This UE utility function with CA is defined in Section 2.5.3. In this way, the impact of RB scheduling will be considered in Section 4.4.3 as well.

Table 4.2: A list of RB schedulers.

RB scheduler	**Approach**	**Channel condition**	**Benefit**
RR [6, 31]	Round-robin	No	Simple implementation
Best-CQI [6, 31]	Greedy	Yes	High UE throughput
PF [6, 16]	Maximum utility function	Yes	Enhanced fairness

4.3 Simulation Model

In this section, the simulation flow and parameters used in Section 4.4 are described. Moreover, the performance metric is defined for the CA implementation.

4.3.1 Simulation Flow

The simulation flow is presented in Figure 4.3 where the CA selection stage is added to the flowchart in Section 3.2.2. All other stages have not been affected by this modification. The same operation can be provided for each CC. To support the CA scenario, the performance metric will be revised in Section 4.3.3.

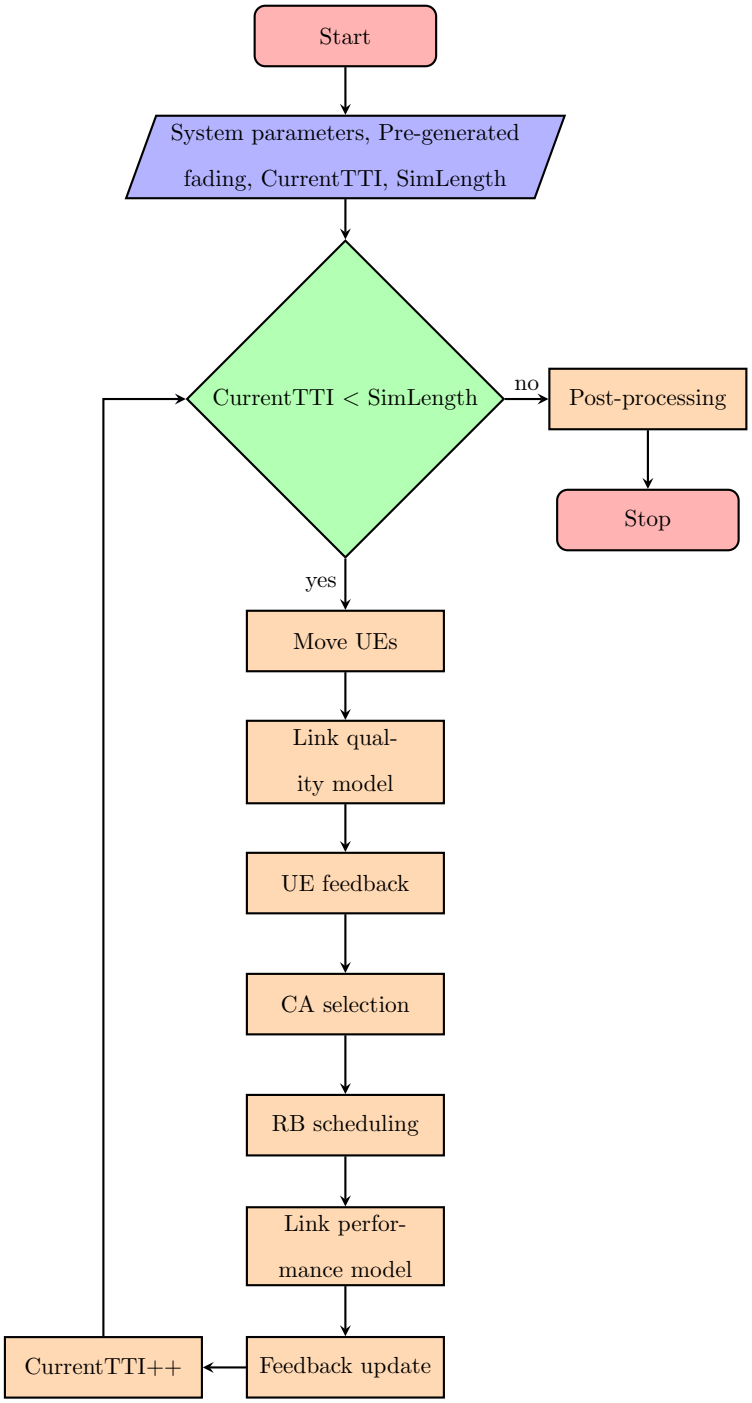

Figure 4.3: The simulation flow for CA implementation.

4.3.2 Simulation Parameters

Table 4.3 concludes the simulation parameters. Only UEs within the coverage area of the central site are investigated in this simulation. The simulation parameters in connection with the CA implementation are defined such as carrier frequencies (942.5, 1842.5, 2140 and 3505 MHz), bandwidth (5 MHz per CC) and CC selection (RR, random and RSRP). Besides, 50 percent of the total UEs in this simulation is the LTE-A UEs with CA capability.

4.3.3 Performance Metric

For the CA implementation, the average throughput of a specific UE (in Mbps) from (3.18) is redefined as

$$T_{\text{avg}} = \frac{B_{\text{total}}}{N_{\text{TTI}} \cdot L_{\text{TTI}} \cdot 10^6}, \tag{4.2}$$

where the total bit $B_{\text{total}} = \sum_{i \in A} \sum_{c \in C} (\text{ACK}_{i,c} \cdot \text{TB}_{i,c})$. Currently, $\text{ACK}_{i,c}$ and $\text{TB}_{i,c}$ are the acknowledgment and the transport block size (in bits) at TTI i and on CC c, respectively. Let A and C be the set of accounted TTIs and available CCs, respectively. N_{TTI} is the number of accounted TTIs and the TTI length (L_{TTI}) is 1 ms. In this way, the total bit from all supported CCs of each UE is used to calculate the average throughput in (4.2).

4.4 Results

The ecdf of average UE throughput based on (4.2) can be computed for the performance evaluation in connection with CA types, CC selection, frequency bands and RB scheduling.

Table 4.3: Simulation parameters.

Parameter	**Assumption**
Cellular layout	Hexagonal grid, 19 cell sites, 3 sectors per site
Inter-site distance	500 m
Path loss model	As mentioned in Section 4.1.1
Lognormal shadow fading	$L_s \sim N(\mu, \sigma^2)$
Shadow fading mean	0 dB
Shadow fading standard deviation	10 dB
Shadow fading correlation	0.5 between sites, 1.0 between sectors
Antenna pattern (horizontal)	$A_{\mathrm{H}}(\theta) = -\min\left[12\left(\frac{\theta}{65^o}\right)^2, 15\mathrm{dB}\right]$
Number of CCs	4 CCs per sector
Carrier frequency	942.5, 1842.5, 2140 and 3505 MHz
System bandwidth	5 MHz per CC
Channel model	ITU Pedestrian A model
UE speed	5 km/h
Number of UEs	10 UEs per sector (50% LTE-A UEs)
Total BS TX power (P_{total})	43 dBm
CC selection	RR, random and RSRP
Scheduling	RR, best-CQI and PF
Transmission mode	SISO
Simulation length	50 TTIs

4.4.1 CA Types and CC Selection

The impact of CA types and CC selection is considered. Figure 4.4 shows the ecdf of UE throughput resulting from the intra- (4 CCs on 2100 MHz) and inter-band non-contiguous CA (2 CCs on 2100 MHz and 2 CCs on 3400 MHz) under different CC selectors (random, RR and RSRP). The same RR RB scheduling is applied to all cases. For instance, the blue solid line refers to the throughput distribution of the intra-band CA with RSRP selection.

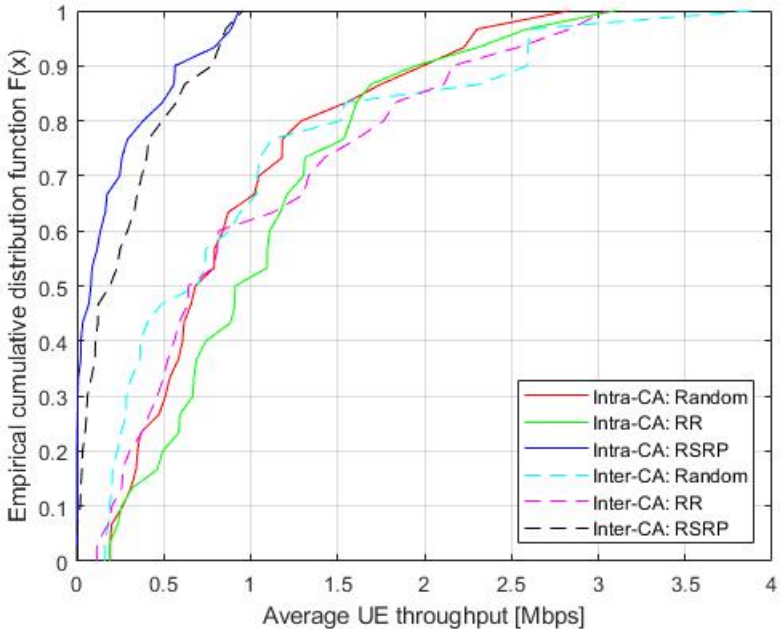

Figure 4.4: The ecdf of UE throughput under different CA types and CC selection.

According to the results, the mean and peak UE throughputs were notably enhanced by the random and RR CC selection. This improvement was obtained for both intra- and inter-band CA. For example, the peak throughputs of the RR selector (green solid and magenta dashed lines) were around three times as large as the RSRP selector (blue solid and black dashed lines). Table 4.4 concludes these simulation results. The fairness index mentioned in Section 3.2.3 is presented as well.

Table 4.4: UE throughputs under different CA types and CC selection.

Scenario	**UE throughput**			**Fairness**
	Peak (in Mbps)	**Mean (in Mbps)**	**Edge (in kbps)**	
Intra-CA: Random	2.3024	0.9452	199.2	0.6633
Intra-CA: RR	2.5879	1.1085	234.4	0.7179
Intra-CA: RSRP	0.8875	0.2107	0	0.3681
Inter-CA: Random	2.6064	0.9738	182.5	0.5237
Inter-CA: RR	2.8348	1.0508	180.4	0.6189
Inter-CA: RSRP	0.8557	0.2905	1.8	0.5195

To comprehend the impact of CC selection, the average number of assigned CCs per site per subframe[2] is shown in Figure 4.5. The corresponding CA types are listed in Table 4.5, that is, Type 1 is the intra-band CA with random selection while Type 6 is the inter-band CA with RSRP selection.

Table 4.5: CA scenarios.

Type	**CA scenarios**
1	Intra-band CA with random selection
2	Intra-band CA with RR selection
3	Intra-band CA with RSRP selection
4	Inter-band CA with random selection
5	Inter-band CA with RR selection
6	Inter-band CA with RSRP selection

Due to the random and RR selection, the load across different CCs (CC#1, CC#2, CC#3 and CC#4) could be balanced. The number of assigned CCs of each CC was

[2]There are 45 CCs in total resulting from 15 LTE UEs (15 $\times$ 1 CC) and 15 LTE-A UEs (15 $\times$ 2 CCs) in this simulation.

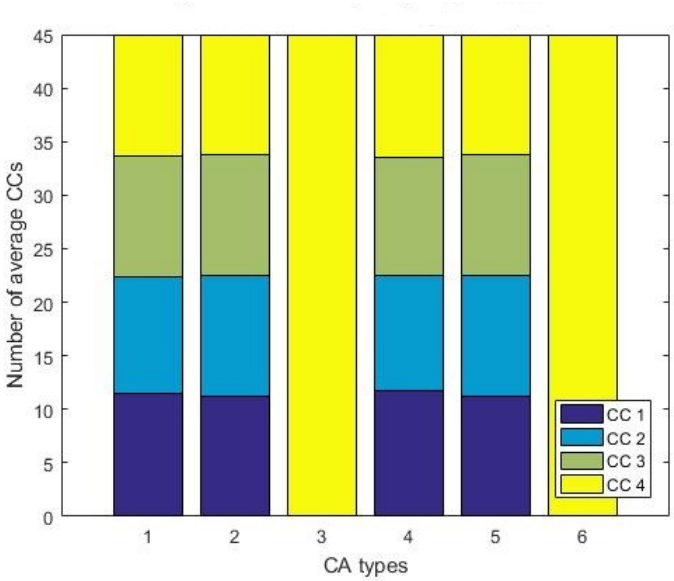

Figure 4.5: The average number of assigned CCs.

similar. In contrast to these two selectors, only the CC with maximum RSRP (CC#4) was picked by the RSRP selector. Thus, the undesirable load imbalance was obtained resulting in the degraded UE throughputs in Figure 4.4.

4.4.2 Frequency Bands

The UE throughput under different frequency bands is also investigated as shown in Figure 4.6. The first two CCs operate on 2100 MHz and the remaining two CCs may utilise either 900, 1800 or 3400 MHz. For instance, 900+2100 MHz (red and green solid lines) refers to the combination of 2100 and 900 MHz. Note that the appropriate combination of frequency bands should be considered further in connection with the available radio resource, deployment scenarios and hardware challenges (or limitations) in reality. Only the RR and RSRP CC selection are considered. Similarly, the RR RB scheduling is performed for all scenarios.

For each CC selector, the trends of UE throughput with different frequency bands were similar. For example, the throughput ecdfs (green solid, cyan dashed and black

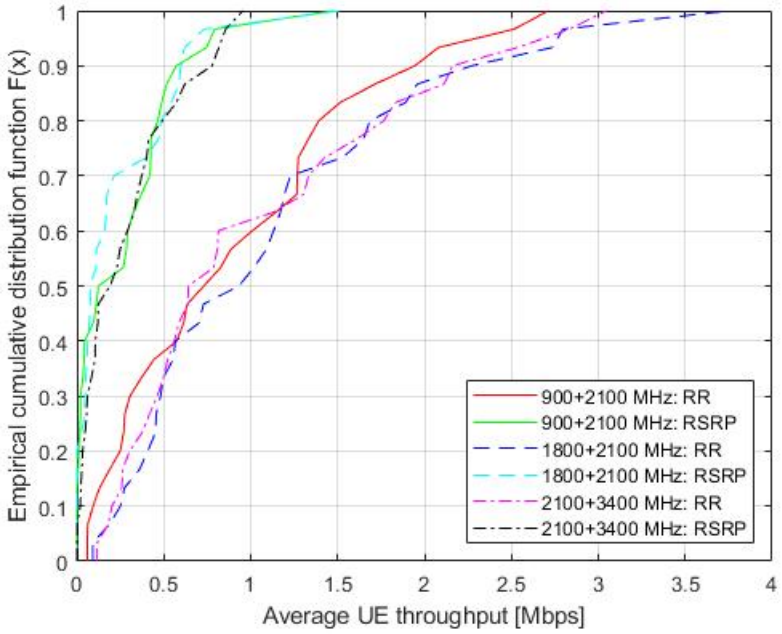

Figure 4.6: The ecdf of UE throughput under different frequency bands.

dash-dotted lines) from the combination of 2100 MHz and other three bands in the case of RSRP selection were nearly the same. In this way, there was the little variation of UE throughputs among these bands. These simulation results are summarised in Table 4.6.

4.4.3 RB Scheduling

The impact of RB scheduling, including RR, best-CQI and PF, is evaluated in Figure 4.7. The inter-band CA on 2100 and 3400 MHz is modelled. Only the RR and RSRP selectors are investigated. For instance, RR+RR (red solid line) is viewed as the combination of RR CC selector and RR RB scheduler.

According to the results, the best-CQI scheduling (green solid and magenta dashed lines) outperformed other RB schedulers for both CC selectors in terms of UE throughputs. For example, the peak throughput of the RR selector with best-CQI scheduler

Table 4.6: UE throughputs under different frequency bands.

Scenario	**UE throughput**			**Fairness**
	Peak (in Mbps)	**Mean (in Mbps)**	**Edge (in kbps)**	
900+2100 MHz: RR	2.5169	0.9293	62.2	0.621
900+2100 MHz: RSRP	0.7927	0.2797	0	0.4286
1800+2100 MHz: RR	2.7966	1.135	186	0.6274
1800+2100 MHz: RSRP	0.7321	0.2466	0	0.3638
2100+3400 MHz: RR	2.8348	1.0508	180.4	0.6189
2100+3400 MHz: RSRP	0.8557	0.2905	1.8	0.5195

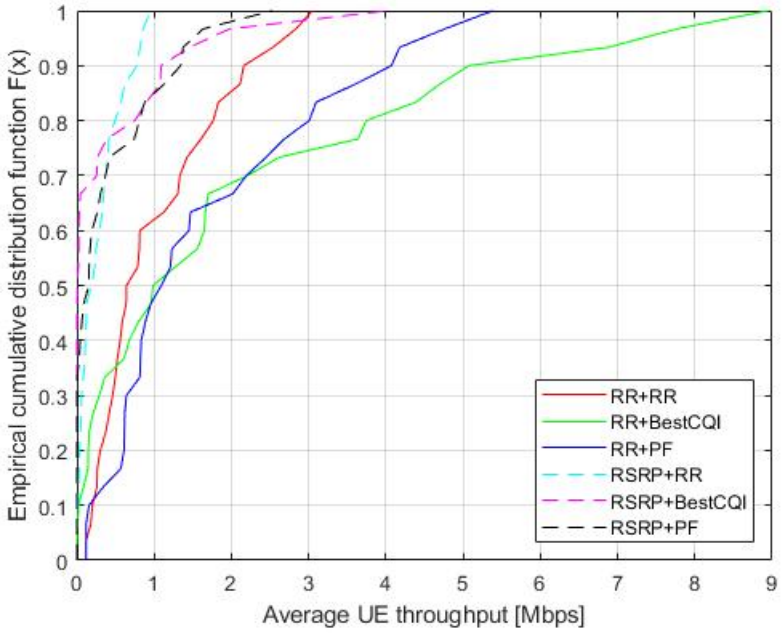

Figure 4.7: The ecdf of UE throughput under different scheduling approaches.

(green solid line) was almost three times as large as the RR selector with RR scheduler (red solid line). Although the UE throughput was notably increased by the best-CQI scheduler, there was the expense of fairness as compared with the RR and PF schedulers in Table 4.7. Therefore, the PF scheduling could be a reasonable choice to compromise between the performance and fairness consideration.

Table 4.7: UE throughputs under different scheduling approaches.

Scenario	**UE throughput**			**Fairness**
	Peak (in Mbps)	**Mean (in Mbps)**	**Edge (in kbps)**	
RR+RR	2.8348	1.0508	180.4	0.6189
RR+BestCQI	7.7628	2.1088	10	0.4305
RR+PF	4.759	1.7336	120	0.5868
RSRP+RR	0.8557	0.2905	1.8	0.5195
RSRP+BestCQI	1.9747	0.4115	0	0.1931
RSRP+PF	1.6305	0.4235	0	0.3237

4.5 Summary

The work in Chapter 3 was extended to CA. The DL homogeneous network was modelled by SL simulation where the CC selection and RB scheduling were implemented separately. The performance metrics, including UE throughput and fairness, were then evaluated under different CA types, frequency bands, CC selectors and RB schedulers.

To enhance the UE throughput, the CC load balance should be the first consideration. According to the results, the load across CCs could be balanced by either random or RR CC selection. Because of the undesirable load imbalance, UE throughput was degraded by the RSRP selector as compared with the two former CC selectors.

As mentioned in Chapter 3, the RB scheduling with CA should be selected in connection with the performance and fairness as well. Also, the computational complexity

may be considered in practice. For example, the UE throughputs could be significantly enhanced by the best-CQI scheduler. However, there was the cost of fairness and complexity as compared to the simplest RR scheduler. To compromise this issue, the PF scheduler could be another option presented in Section 4.4.3.

Note that the CA implementation could rise to the challenges of the radio design as outlined in Section 2.3. The RF design challenges of terminals are considered in connection with the CA type, CC configuration, coexisting networks, transmitter/receiver architectures and radio impairments [26]. The beam directions (patterns) for different CCs seem to be another challenge of the CA design to provide the desirable coverage across the service environment [25]. Moreover, although the joint CC selection and RB scheduling could offer the optimal performance, the reasonable (computational) complexity is required in practice. Therefore, these issues should be addressed and included in both modelling and real implementation of CA.

This CA-based simulator will be applied to the scenario of U-LTE where the resource allocation for the usage of unlicensed spectrum in a LTE heterogeneous network being the main aim of the project is modelled in Chapter 5. The revised system model and proposed resource allocation will be discussed step-by-step.

Chapter 5

Unlicensed LTE

As discussed in Section 2.4, the unlicensed spectrum can be used for the LTE network. For example, via the use of CA, the LTE licensed and the 5-GHz unlicensed spectrum are aggregated to improve the LTE data rate. This is known as the U-LTE deployment. However, this unlicensed spectrum may also be used by the WiFi network resulting in the unavoidable interference. Furthermore, the resource allocation in U-LTE could be complicated in connection with the coexistence between the LTE and WiFi networks as mentioned in Section 2.4.2. Therefore, to study this issue in detail, a DL heterogeneous network with U-LTE is modelled in this chapter. The system model, including pre-generated data and frame-based LBT, is first discussed. The proposed resource allocation, including CC selection and RB scheduling, is then described. Unlike the CC selection in Chapter 4, the CC selectors using the LTE transmission probability on CCs are presented. Subsequently, the simulation model, including simulation flow and parameters, is indicated. The proposed resource allocation is then evaluated in terms of user throughput.

5.1 System Model

The system model of a heterogeneous network with U-LTE is discussed. The pre-generated data such as the path loss model are first outlined. Moreover, the frame-based LBT used in this simulation is briefly described.

5.1.1 Pre-Generated Data

A heterogeneous cellular network, including macro and femto sites, is modelled as illustrated in Figure 3.3. A number of macro sites (red dots) with three sectors each are first generated. Subsequently, a single femto site (green dot) per macro sector is randomly dropped. For the antenna gain, the antenna pattern from (3.1) and the path loss model from (3.3) are applied to each macro sector. Unlike the macro network, the antenna pattern is assumed to be omnidirectional for each femto sector. Furthermore, the path loss model (in dB) based on [63] is expressed as

$$L_{\text{total}} = L(d_0) + N \log_{10} \frac{d}{d_0} + L_f(n), \tag{5.1}$$

where f is the operating frequency (in MHz). Denote the free-space path loss for a reference distance d_0 at 1 m by $L(d_0) = 20 \log_{10} f - 28$. N and d are the distance power loss coefficient and the distance (in m) between femtocell and UE, respectively. Let L_f and n be the floor penetration loss factor (in dB) and number of floors between femtocell and UE, respectively. Note that the number of floors is zero ($n = 0$) and the floor penetration loss factor is 0 dB ($L_f = 0$ dB) in this simulation. The path loss map (in dB) for a femtocell on a specific CC is illustrated in Figure 5.1. Additionally, a shadow fading map per (macro and femto) site on each CC is generated as mentioned in Section 3.2.1.

In this way, the wideband SINR map (in dB) on each CC can be shown in Figure 5.2. For instance, there are the CC number 1 in the 2-GHz licensed band and the CC number 2 in the 5-GHz unlicensed band. For other CCs on the same unlicensed band,

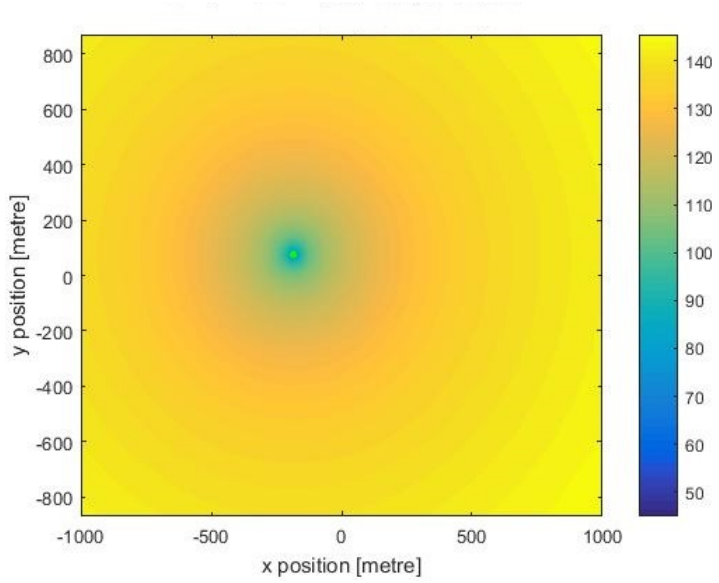

Figure 5.1: The path loss map (in dB) for a femtocell (site number 49) on a given CC (CC number 5).

the corresponding wideband SINR is similar to the map in Figure 5.2b. As discussed in Section 4.1.1, the coverage area of each (macro and femto) sector on the map can be identified, that is, there are 110 serving sectors in total[1]. Moreover, the same approaches from Section 3.2.1 for UE placement and small-scale fading are employed.

5.1.2 CA Capability

According to [24], a single CC with 5-MHz bandwidth in the 2-GHz licensed band is provided by each macro sector. Due to the CA, there are 5 CCs consisting of 1 CC with 5-MHz bandwidth from the 2-GHz licensed band and 4 CCs with 20-MHz bandwidth each from the 5-GHz unlicensed band offered by each femto sector. In this simulation, a macro

[1]There are 57 macro sectors and 53 femto sectors in this simulation. Only the active macro sectors are considered for the femtocell placement.

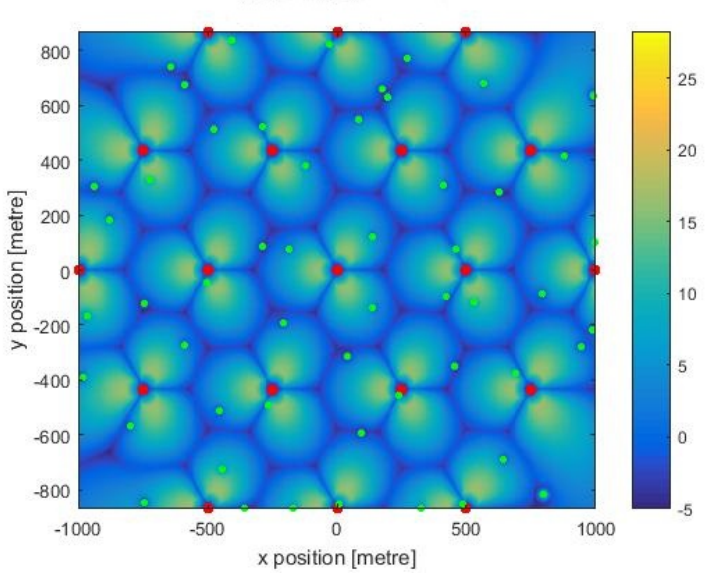

(a) The 2-GHz licensed band

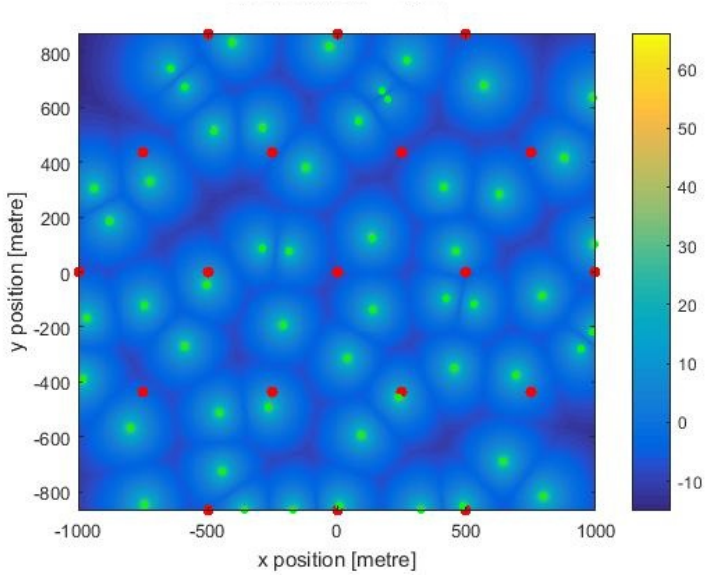

(b) The 5-GHz unlicensed band

Figure 5.2: The wideband SINR maps (in dB) without shadowing on different CCs.

UE can utilise only a licensed CC while a femto UE can access 2 of 5 CCs concurrently[2] at each subframe. Although an extra CC from the unlicensed band could be provided for the femto network, the unlicensed band may be shared by a number of WiFi devices. This leads to the undesirable interference between the LTE and WiFi networks. Thus, the coexistence approach as presented in Section 2.4.2 is strongly required for the U-LTE implementation.

5.1.3 Frame-Based LBT

Not only the LTE but also other network deployments may access the unlicensed spectrum. The coexistence of LTE and WiFi seems to be the first priority. The LAA could be a worldwide standard resulting from the frame- and load-based LBT schemes [30]. This coexistence approach stems from the CSMA/CA in WiFi. The CCA and discontinuous transmission (DTX) are the two main features of LBT.

Because of its fixed frame structure and easy implementation for the current LTE, the frame-based LBT is selected to model U-LTE in this simulation. For example, the corresponding LTE frame structure in the unlicensed spectrum is presented in Figure 5.3. A fixed frame period of ten subframes (or 10 ms) consisting of channel occupancy time (9 blue subframes) and idle time (a green subframe) is defined. The CCA is first performed to check whether the channel is free. If the channel is not busy, the equipment can start its transmissions immediately at the beginning of fixed frame period. Otherwise, it should wait until the next period and the CCA is then performed.

5.2 Proposed Resource Allocation

In this section, the proposed resource allocation with U-LTE is discussed. This task could be separated into CC selection and RB scheduling. Unlike Chapter 4, the coexistence

[2]There is a default CC from the 2-GHz licensed band and an extra CC from the 5-GHz unlicensed band for a femto UE.

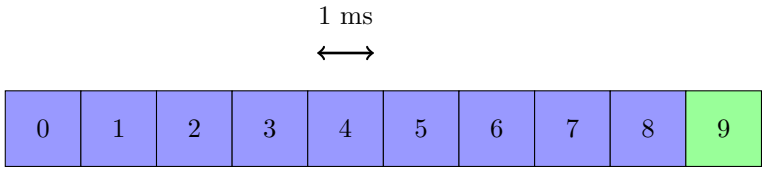

Figure 5.3: The frame structure of LTE in the unlicensed spectrum: occupied subframe (blue) and idle subframe (green).

between LTE and WiFi networks is required, that is, the frame-based LBT and CCA are applied to this simulation. The WiFi transmission condition is also used for this proposed resource allocation. In this way, the overall method of spectrum access in this work will be described in detail.

5.2.1 CCA

For the CCA, the energy detection (ED) has been widely employed [30, 64]. The channel is available if the total received energy on the channel is less than a specific (energy) threshold. This means the presence of WiFi in the U-LTE deployment is probably detected by the ED.

Although the ED appears to be an efficient CCA, the information of large-scale fading from all transmitters is needed by this ED approach [45]. Also, a large number of network elements and hidden node issue should be considered in practice. This could be the potential limitation when the ED is performed for both large-scale modelling and real implementation.

To the best of this author's knowledge, most related work of the CCA is derived from the ED where the energy threshold is specified based on the WiFi standard. Whereas this threshold may be changed by WiFi access points for better performances [45], there are still considerable questions that on how the energy threshold is appropriately adjusted in the U-LTE deployment. Besides, the ED scheme may operate inaccurately in the case of imperfect (energy) detection.

Therefore, a specific LTE transmission probability threshold is used instead of the energy threshold for the CCA in this simulation. A CC is free if its LTE transmission probability from (5.2) is greater than or equal to this transmission probability threshold.

5.2.2 Spectrum Access

The overall process of spectrum access for the U-LTE is described, in particular the proposed CC selection. Section 5.3.1 provides a brief description of this spectrum access as well.

First of all, the CCA is processed at the beginning of fixed frame period where the LTE transmission probability threshold is applied to evaluate the availability of CCs. Subsequently, the available CC(s) is selected for UEs. However, the conventional random, RR and RSRP CC selectors may not suit the U-LTE implementation. This is because the transmission condition of the WiFi network has not been included in the process of these CC selectors. In other words, not only the LTE but also the WiFi transmission condition should be considered for the CC selection in the U-LTE. For example, if the WiFi transmission probabilities and number of WiFi devices within the U-LTE deployment can be possibly acknowledged at the centralised LTE eNBs, the CC selection could be enhanced by means of these WiFi transmission conditions.

In this work, the novel CC selection for U-LTE is proposed where the LTE transmission probability on a CC derived from the WiFi transmission condition is applied to this CC selection. The CC idle probability of CC c is then obtained [49]

$$p_c = (1 - \tau_c)^{N_c}, \tag{5.2}$$

where c $\in \boldsymbol{C_U}$. Denote the set of CCs on the unlicensed band by $\boldsymbol{C_U}$. Let τ_c and N_c be the transmission probability of a WiFi device and number of WiFi devices on CC c, respectively. Based on [47], the transmission probability of a WiFi device is defined as

follows

$$\tau_c \triangleq \tau(p) \tag{5.3}$$

$$= \frac{2}{1 + W + pW \sum_{i=0}^{m-1} (2p)^i}, \tag{5.4}$$

where p is the conditional collision probability. The minimum contention window (W) and maximum backoff stage (m) are defined based on the 802.11 PHY specification. For example, the transmission probability of a single WiFi device from (5.3) is presented in Figure 5.4.

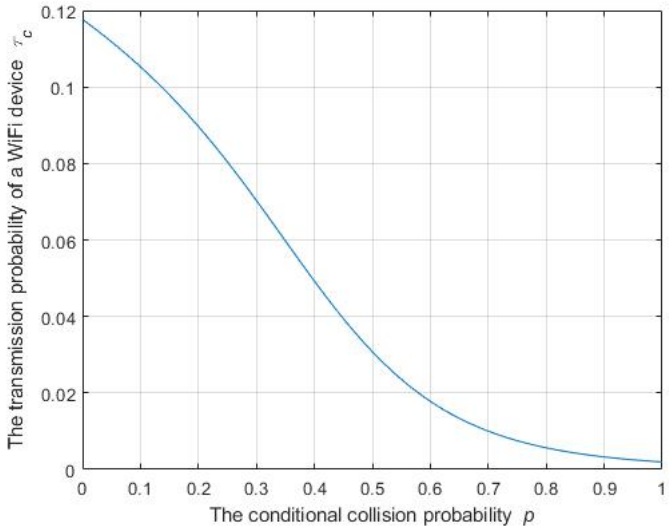

Figure 5.4: The transmission probability of a single WiFi device versus the conditional collision probability ($W = 16$ and $m = 6$).

For the transmission probability on a specific CC, Figure 5.5 shows the LTE transmission probability from (5.2) while the WiFi transmission probability ($p_w = 1 - p_c$) is illustrated in Figure 5.6. Both cases are displayed for the different number of WiFi devices on a given CC.

If the p_c is high, this means the number of WiFi devices on CC c is small resulting in the enough time for all WiFi devices to access this shared CC c with the LTE network.

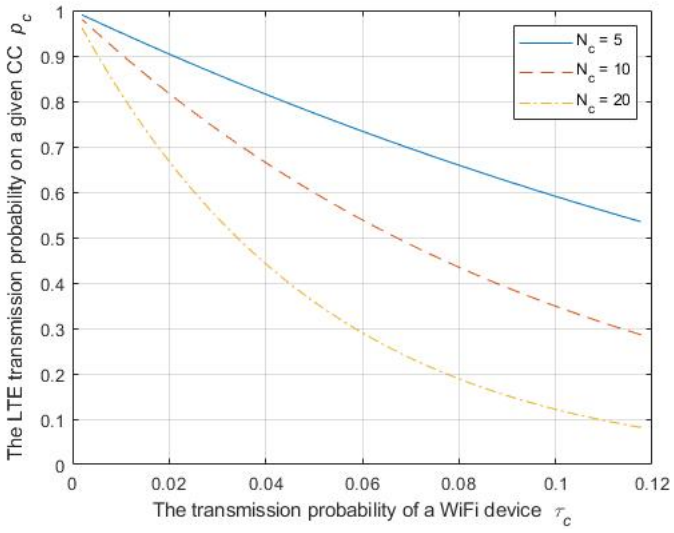

Figure 5.5: The LTE transmission probability on a specific CC versus the transmission probability of a single WiFi device.

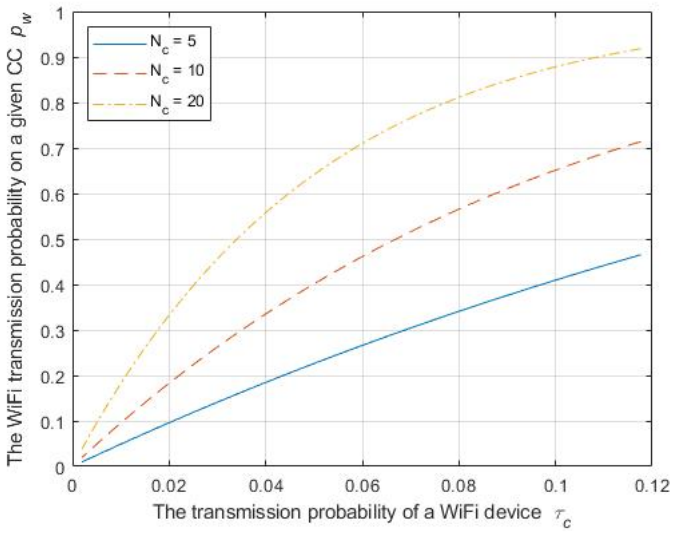

Figure 5.6: The WiFi transmission probability on a specific CC versus the transmission probability of a single WiFi device ($p_w = 1 - p_c$).

Hence, there is an opportunity for the LTE network to use the CC c as well. The high LTE throughput could be offered while the fairness between LTE and WiFi networks is maintained.

The CC selection for U-LTE is proposed as indicated in Algorithm 1. At the beginning of a fixed frame period (or every 10 ms), assume that the WiFi transmission condition, including τ_c and N_c, can be collected at the LTE eNB. Moreover, the hidden node problem is assumed not to occur here.

Denote the set of selected CCs on the unlicensed band for a LTE UE u by $\boldsymbol{C_S^u}$. $\Omega(\boldsymbol{C_U})$ and N_{UE} are the number of CCs on the unlicensed band and the number of UEs, respectively. The p_c from (5.2) is calculated for each CC on the unlicensed spectrum and the (transmission probability) threshold ε is adjusted. The p_c is then evaluated in connection with this ε. For instance, the CC cannot be utilised by any LTE UEs if its LTE transmission probability is smaller than the threshold (line 9 in Algorithm 1). Otherwise, the CC with the highest transmission probability is allocated to each LTE UE (line 14-15 in Algorithm 1). This proposed CC selection is called the maximum probability (MaxProb) approach in this work. Owing to the CA capability, the process will be terminated when the number of selected CCs ($\Omega(\boldsymbol{C_S^u})$) and the number of supported CCs of each LTE UE (N_{CC}^u) are equal.

Also, the RR and random CC selection with p_c are proposed. First, the LTE system can access the CC(s) if the LTE transmission probability is greater than or equal to the threshold ($p_c \geq \varepsilon$). Second, the CC selection may be modified (line 14-15 in Algorithm 1) where the CC(s) is selected to LTE UEs by either RR or random approaches.

Another task is to allocate RB(s) to LTE UE(s) on each individual CC after the CC selection. The RR, best-CQI and PF schedulers can be selected for the RB scheduling with CA as in Chapter 4. Therefore, any modification is not required for RB scheduling with U-LTE.

Algorithm 1 The CC selection with the maximum probability for U-LTE

1: Obtain p_c for $\forall c \in \boldsymbol{C_U}$
2: Make $\boldsymbol{C_S^u}$
3: $u \leftarrow 0$
4: $c \leftarrow 0$
5: **repeat**
6: $u \leftarrow u + 1$
7: **repeat**
8: $c \leftarrow c + 1$
9: **if** $p_c < \varepsilon$ **then**
10: This CC c cannot be used by LTE
11: **go to** 7
12: **else**
13: **repeat**
14: Select CC with highest p_c in $\boldsymbol{C_U}$ to UE u
15: Add the selected CC to $\boldsymbol{C_S^u}$
16: **until** $\Omega(\boldsymbol{C_S^u}) = N_{CC}^u$
17: **end if**
18: **until** $c = \Omega(\boldsymbol{C_U})$
19: **until** $u = N_{UE}$

5.3 Simulation Model

To model a heterogeneous network with U-LTE, the simulation flow and parameters are defined in this section.

5.3.1 Simulation Flow

Figure 5.7 shows the simulation flow for U-LTE implementation. The flowchart in Section 4.3.1 is extended by the addition of the CCA stage. As mentioned in Section 5.2, this CCA is performed every 10 TTIs where the LTE transmission probability on each CC from (5.2) is computed[3]. For the CA selector stage, these CC idle probabilities are first evaluated in connection with a fixed probability threshold. For example, the LTE transmission probability threshold of 0.5 is adjusted in this simulation. Subsequently, a set of active CCs is assigned to UEs. The MaxProb, RR and random CC approaches can be employed. Unlike the traditional CC selection, the LTE transmission probability on CCs is included in these three selectors. For the other stages, the same operation as in Chapter 4 is performed. For instance, the average throughput of a given UE within the post-processing stage is calculated based on (4.2).

5.3.2 Simulation Parameters

The simulation parameters for macro and femtocell networks are concluded in Tables 5.1 - 5.2, respectively. Some parameters are shared by both networks such as the ITU Pedestrian A channel model. Note that only femtocells and (macro and femto) UEs within the coverage area of central marco site are considered by this simulation.

[3]To determine the transmission probability of a single WiFi device (τ_c) in (5.3), let the conditional collision probability (p) be a single uniformly distributed random number in the interval (0,1). The minimum contention window (W) and maximum backoff stage (m) are 16 and 6, respectively.

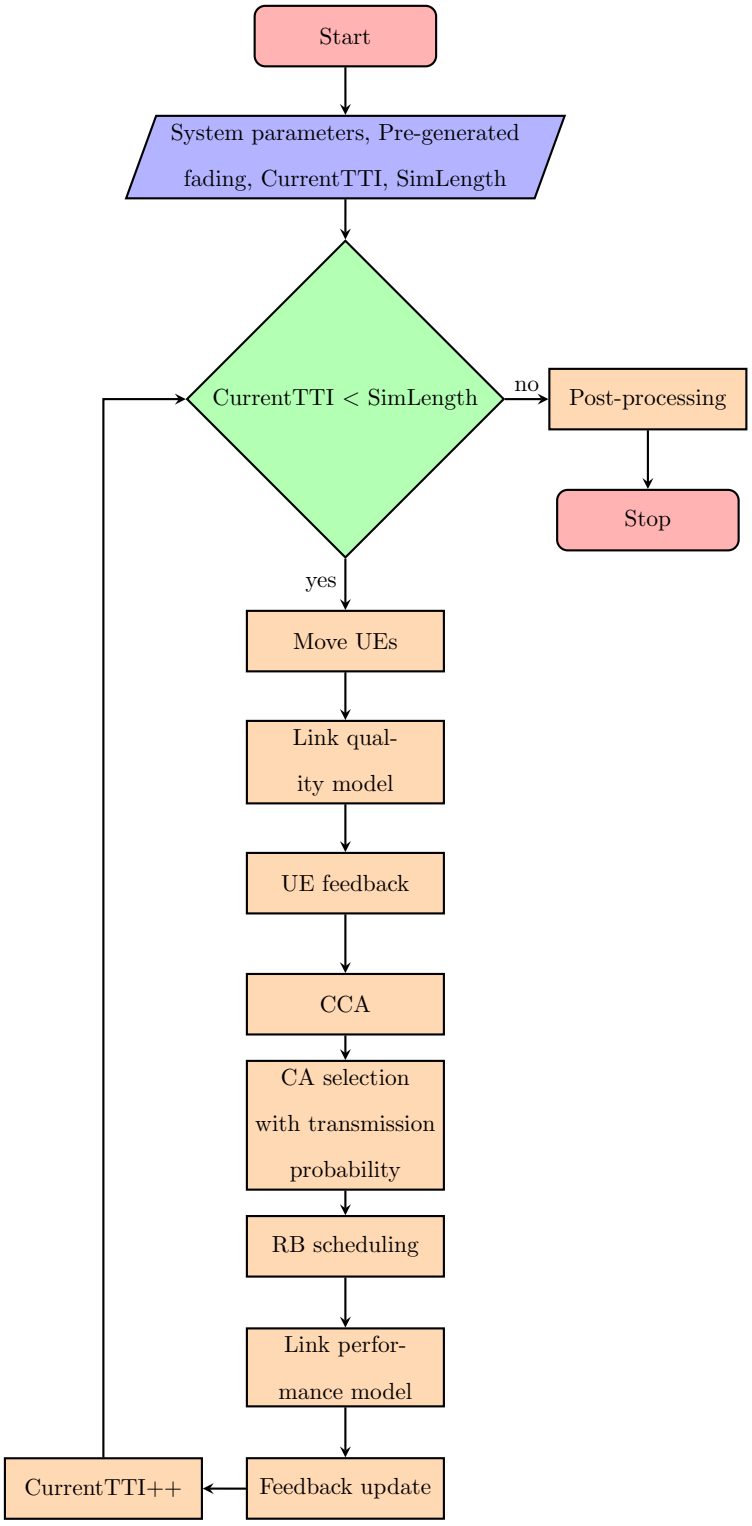

Figure 5.7: The simulation flow for U-LTE implementation.

Table 5.1: Simulation parameters (macro network).

Parameter	**Assumption**
Cellular layout	Hexagonal grid, 19 cell sites, 3 sectors per site
Inter-site distance	500 m
Path loss model	As mentioned in Section 5.1.1
Lognormal shadow fading	$L_s \sim N(\mu, \sigma^2)$
Shadowing mean	0 dB
Shadowing standard deviation	10 dB
Shadowing correlation	0.5 between sites, 1.0 between sectors
Antenna pattern (horizontal)	As mentioned in Section 5.1.1
Number of CCs	A CC per sector
Carrier frequency	2.14 GHz
System bandwidth	5 MHz
Channel model	ITU Pedestrian A model
UE speed	5 km/h
Number of UEs	10 UEs per sector
Total BS TX power (P_{total})	46 dBm
CC selection	RR, random and MaxProb
CC idle probability threshold (ε)	0.5
Scheduling	RR, best-CQI and PF
Transmission mode	SISO
Simulation length	50 TTIs

Table 5.2: Simulation parameters (femtocell network).

Parameter	Assumption
Cellular layout	Random placement
Femtocell density	A femtocell per macro sector
Inter-site distance	N/A
Path loss model	As mentioned in Section 5.1.1
Antenna pattern (horizontal)	As mentioned in Section 5.1.1
Number of CCs	5 CCs per sector
Carrier frequency	2.14 and 5.5375 GHz
System bandwidth	5 and 20 MHz
Number of UEs	2 UEs per sector
Total BS TX power (P_{total})	20 dBm

5.4 Results

The ecdf of UE throughput is determined for the performance evaluation. The impact of the proposed CC selection and RB scheduling is investigated in this section.

5.4.1 CC Selection

Figure 5.8 shows the UE throughput distribution under different CC selectors (RR, random and MaxProb). The same RR RB scheduling is applied to all scenarios. For example, the red solid line refers to the UE throughput distribution of MaxProb CC selection.

According to the results, the UE throughputs could be significantly increased by the RR CC selection as compared with other two CC selectors. For instance, both mean and peak throughputs of RR selector (blue dash-dot line) were around a twofold increase compared to MaxProb selector (red solid line). A summary of the key performance

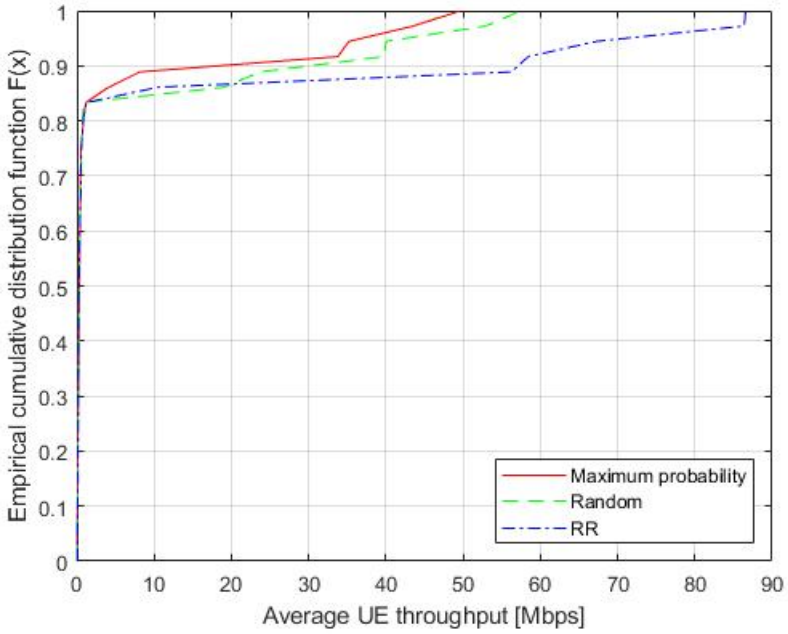

Figure 5.8: The ecdf of UE throughput under different CC selection.

indicators, including UE throughput and fairness index, is given in Table 5.3.

Table 5.3: UE throughputs under different CC selection.

Scenario	**UE throughput**			**Fairness**
	Peak (in Mbps)	**Mean (in Mbps)**	**Edge (in kbps)**	
RR	86.3794	10.4176	41.3	0.1492
Random	52.9572	6.7247	25.3	0.1593
MaxProb	43.5775	5.1138	37.7	0.1378

To explain the importance of CC selection, Figure 5.9 shows the average number of assigned CCs per site per subframe[4] under different CC selectors. Since the CC#1 has been configured as the default CC for both macro and femto UEs, there were the same

[4]There are 42 CCs in total resulting from 30 macro UEs (30 × 1 CC) and 6 femto UEs (6 × 2 CCs) in this simulation.

36 assigned CCs (30 macro UEs × 1 CC and 6 femto UEs × 1 CC) on CC#1 (blue bars) for all CC selectors.

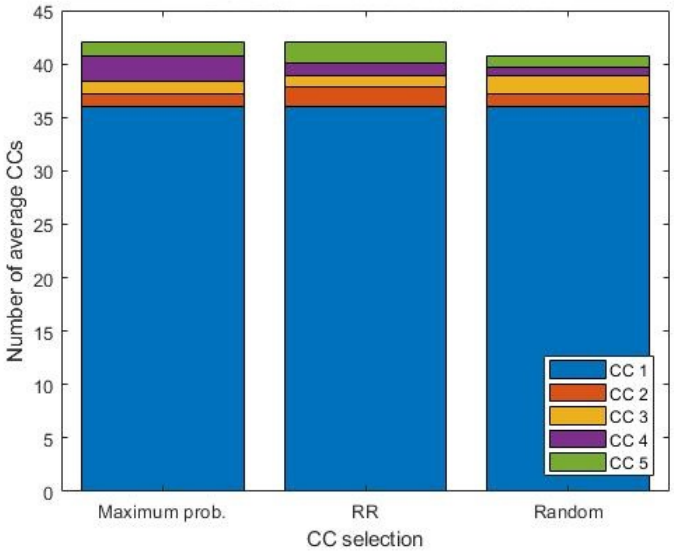

Figure 5.9: The average number of assigned CCs under different CC selection.

Because of the CA capability, the remaining CCs (CC#2 - #5) can be utilised by only femto UEs. As compared to the random and MaxProb CC selectors in Figure 5.9, the best load balance across CCs could be obtained by the RR CC selector (middle stacked bar) resulting in the higher throughputs as illustrated in Figure 5.8.

The CC load could be nearly balanced by the random selector (right stacked bar) as well. However, a few CCs were not randomly selected by this approach because the LTE transmission probabilities on these CCs were smaller than the transmission probability threshold at some moment in time (or TTI).

For the MaxProb selector (left stacked bar), the CC with highest LTE transmission probability was first picked. In this way, the load across CCs could not be balanced. For example, the number of assigned CCs on CC#4 (purple bar) of MaxProb selector was overallocated as compared to other three CCs. Owing to the undesirable load imbalance, this led to the lower throughputs in the case of both random and MaxProb selectors in

Figure 5.8.

5.4.2 RB Scheduling

RB scheduling is considered in this section. The UE throughput distribution under different RB schedulers (RR, best-CQI and PF) is illustrated in Figure 5.10. Note that the average UE throughput from both macro and femto networks (or the whole LTE network) is applied to the calculation of throughput ecdf. The same RR CC selection is performed for all cases.

According to the results, a similar trend of UE throughput under different RB schedulers was obtained. For instance, the mean throughput was approximately 10 Mbps while the peak throughput was higher than 80 Mbps for all scenarios. Key performance indicators are summarised in Table 5.4.

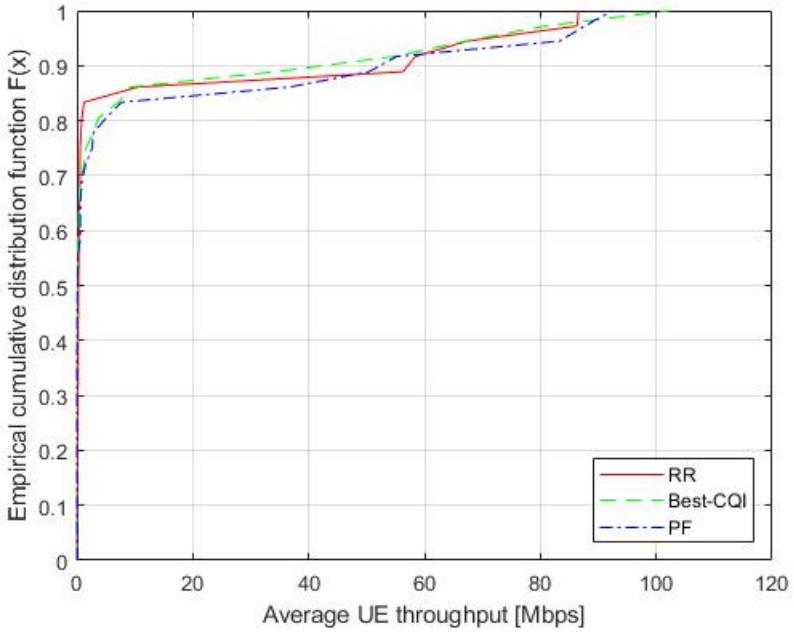

Figure 5.10: The ecdf of UE throughput under different schedulers.

To clarify the impact of RB scheduling, Table 5.5 shows the minimum, mean and

Table 5.4: UE throughputs under different RB scheduling.

Scenario	**UE throughput**			**Fairness**
	Peak (in Mbps)	**Mean (in Mbps)**	**Edge (in kbps)**	
RR	86.3794	10.4176	41.3	0.1492
Best-CQI	80.9442	10.2196	0	0.1454
PF	87.7313	11.9336	0	0.1697

maximum UE throughputs of each individual network. All UE throughputs of the femto network could be notably improved as compared with the macro network resulting from the CA capability. For the femto network, the best-CQI scheduler outperformed the other two RB schedulers in terms of the maximum UE throughput. In contrast, as compared to the best-CQI scheduler, the higher (minimum and mean) UE throughputs were offered by the RR and PF schedulers.

Table 5.5: UE throughputs of macro and femto networks.

Scenario	**Macro network**			**Femto network**		
	UE throughput (in Mbps)					
	Min	**Mean**	**Max**	**Min**	**Mean**	**Max**
RR	0.0402	0.3169	1.2328	10.5634	60.9211	86.5892
Best-CQI	0	0.6447	7.1992	9.2168	58.0941	102.3527
PF	0	0.795	7.7123	36.7626	67.6264	92.4382

5.5 Summary

In this chapter, the U-LTE heterogeneous network in DL transmission was modelled by SL simulation. The novel resource allocation, including CC selection and RB scheduling with the LTE transmission probability on CCs, was proposed. This proposed algorithm

was then evaluated under different CC selectors and RB schedulers.

To enable the LTE and WiFi networks to coexist in the unlicensed band, the CCA was first implemented. In this work, the LTE transmission probability threshold was used instead of the ED threshold approach. Unlike the conventional CC selection, the LTE transmission probability (or CC idle probability) on each CC derived from the WiFi transmission condition was used in the CC selection. This resulted in the proposed CC selectors, including RR, random and MaxProb. For the RB scheduling, the same RR, best-CQI and PF schedulers in Chapter 4 have been applied to this U-LTE scenario.

According to the results, the UE throughput was remarkably enhanced by the RR CC selector as compared to other proposed CC selectors. This was because the best CC load balance was obtained in the case of the RR selector. Owing to the LTE transmission probability threshold, a few CCs were not likely selected by the random selector. Furthermore, some CCs were probably overallocated by the MaxProb selector. This undesirable situation was similar to the case of the RSRP selector as presented in Chapter 4.

The (minimum, mean and maximum) UE throughputs between the macro and femto networks were compared. Due to the CA capability, all UE throughputs of the femto network were significantly magnified as compared with the macro network. For the impact of RB scheduling on the femto network, the highest UE throughput was obtained by the best-CQI scheduler. Meanwhile, the minimum and mean UE throughputs of either RR or PF schedulers were larger than the best-CQI scheduler. Therefore, it is still meaningful to emphasize that a compromise should be made between the performance, fairness and complexity in the choice of RB scheduling.

Chapter 6

Conclusion and Future Work

In this chapter, the conclusions, key results and main findings from this thesis are presented. Research challenges and future work are also suggested.

6.1 Conclusion

In this thesis, a new SL simulator of downlink LTE cellular networks based on the Monte Carlo simulation was developed. The small cell deployments, carrier aggregation and the use of unlicensed spectrum were modelled by this developed simulator. The performance metrics, including user throughputs and fairness index, were then evaluated in connection with these network scenarios.

In Chapter 3, both LTE homogeneous and heterogeneous networks were modelled by the developed simulator. To verify simulation results, the results from this developed tool were compared to the Vienna simulator [6] in the case of a homogeneous network. A close match between them was achieved in terms of UE wideband SINR and UE throughputs.

Small cell deployments and RB scheduling techniques were then investigated. Key UE throughputs were significantly improved by an increase of small cells (femtocells) and the usage of best-CQI scheduling, in particular the peak throughput. However, to

select a suitable RB scheduler, a tradeoff between UE throughput and fairness could be a potential challenge in practice.

In Chapter 4, the CA-based resource allocation, including CC selection and RB scheduling, was implemented. A homogeneous network was modelled by the developed simulator under different types of CA, CC selectors, operating frequency bands and RB schedulers.

The load across CCs could be balanced by either random or RR CC selection, resulting in the higher UE throughputs as compared to a maximum RSRP CC selector. Meanwhile, key UE throughputs were extremely increased by the best-CQI scheduler. A trade-off between UE throughput and fairness was still an important issue in the case of CA-based resource allocation. Furthermore, the computational complexity of the scheduling could be considered. A PF scheduler was probably selected as an alternative RB scheduling in practice.

In Chapter 5, the use of unlicensed spectrum for a LTE heterogeneous network was examined. To coexist LTE and WiFi networks in the unlicensed band, the frame-based LBT was included in the developed simulator. A novel resource allocation using the LTE transmission probability on CCs was proposed to facilitate the CCA and CC selection (RR, random and MaxProb selectors). The conventional RB scheduler (RR, best-CQI and PF schedulers) was then employed.

The best load balance across CCs was obtained in the case of a RR CC selector resulting in the enhanced UE throughputs. A comparison of UE throughputs between macro and femto networks was presented. Due to the CA, all key throughputs of the femto network could be significantly boosted. For the RB scheduling, although the best-CQI scheduler outperformed other schedulers in terms of the maximum UE throughput, there was the expense of its minimum and mean UE throughputs. Therefore, UE throughput, fairness and complexity were still the greatest challenge of RB scheduling in this U-LTE network scenario.

6.2 Future Work

In this section, research challenges and future work are suggested. First, the SL simulator developed in this thesis could be modified for future wireless network standards. According to [65], multiple frequency bands, ranging from the sub-6 GHz bands to millimetre wave (mmWave) bands, and flexible subcarrier spacing are used in 5G NR. Simulation modules, including frame structure and channel model, must be changed to support this latest standard. Also, massive MIMO, beamforming, use cases (eMBB, uRLLC and mMTC) and operation modes (non-standalone and standalone operation) appear to be the key driver which should be included in the SL simulation for 5G NR. For example, the modelling of the cooperation between LTE eNB and 5G gNodeB (gNB) in the non-standalone operation and the hybrid (analog and digital) beamforming are potentially developed [65].

Second, other channel parameters and performance metrics could be included in a future version of SL simulator. In additional to the RSRP, reference signal received quality (RSRQ) and SINR are probably key metrics to indicate the LTE channel qualities [66]. The relationship between RF conditions and throughput can be represented by them.

Third, future wireless networks become heterogeneous, that is, a macrocell tier is overlaid with small-cell tier(s). Although a network layout of hexagonal cells has been widely applied to design wireless cellular networks, this cellular concept may not suit heterogeneous cellular networks and network deployments in practice. Thus, the SL simulation based on stochastic geometry should be developed where the locations of network elements (base stations and user terminals) are modelled by point processes [67, 68]. Future network deployments such as massive IoT are probably analysed by this approach as well.

Fourth, the proposed resource allocation with U-LTE in Chapter 5 could be further

verified and extended for the modelling and real situation, respectively. For instance, it will be at least one million of devices per km^2 for mMTC [65] and the hidden node problem is unavoidable. Furthermore, a single framework of the unlicensed spectrum access for 5G NR has been developing [69]. The access to the unlicensed spectrum in 5G NR may be either a standalone or non-standalone (with the help of the licensed spectrum) bases. Hence, the coexistence mechanism of LTE, 5G NR and other RATs in the unlicensed spectrum could be examined and modelled by the SL simulation.

Fifth, resource allocation of 5G NR may be enhanced by machine learning and artificial intelligence (AI) [69]. This results in the efficient network optimisation in future wireless networks. For example, the sum-energy efficiency maximisation in interference networks and the system sum-rate maximisation in a massive MIMO network could be modelled by means of deep learning [70].

Finally, the time complexity should be considered for a large scale network. For instance, a network layout of cellular IoT is likely to be irregular and dense with a large number of IoT devices. Therefore, a lightweight simulator with the reasonable run-time is preferable to model such a network in practice. Moreover, a future version of SL simulator should be developed by free and open source software (FOSS). Software costs can be reduced while the source code is openly shared for a research collaboration.

Appendix A

Random Walk Model

Using a walking model, current UE positions are randomly generated by their corresponding positions from the previous TTI. The current position could be defined as follows

$$\text{UE\_pos}_{\text{current}} = \text{UE\_pos}_{\text{previous}} + V, \tag{A.1}$$

where the moving vector $V = \text{UE\_speed} \times [\cos(D)\sin(D)]$. UE_speed is the UE speed (in metres per TTI) and $D \sim \text{unif}(0, 360)$ is the UE direction (in degree).

Note that handover has not been supported where any UEs are attached to the same sector until the simulation is terminated. For example, a UE (red point) is served by sector 1 in the first TTI as illustrated in Figure A.1. The UE is moved and then may be served by the new sector in the next TTI. Therefore, it will be forced to randomly select one of available pixels within sector 1 (11 green pixels).

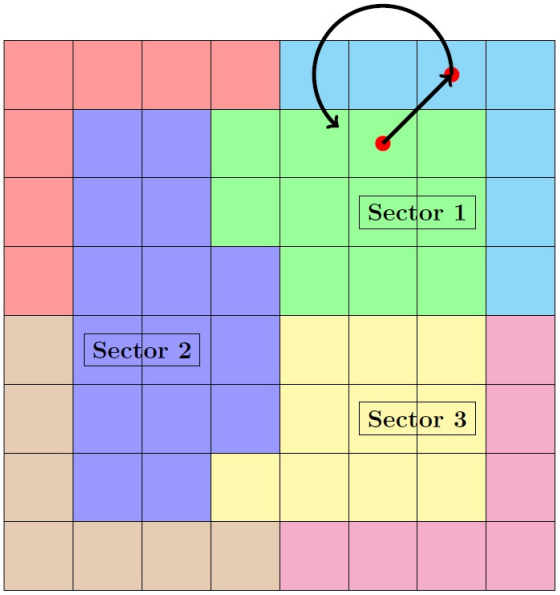

Figure A.1: The user moving.

Appendix B

Post-Equalisation SINR

The quality of signal is interpreted by the (per-subcarrier-and-subframe) post-equalisation SINR of data symbols with a block fading assumption. For example, the SINR of 12000 samples per TTI is required for the 20 MHZ LTE bandwidth (100 RBs and 12 subcarriers per RB). To reduce the complexity, the number of SINR samples can be decreased where a subset of the subcarriers is employed instead. According to [1], at least two subcarrier SINR values per RB ($2N_{\mathrm{RB}}$) are needed as shown in Table B.1.

Table B.1: The number of SINR samples for the link-to-system model (adapted from [1]).

System bandwidth (in MHz)	1.4	3	5	10	15	20
Number of resource blocks	6	15	25	50	75	100
Number of SINR samples	12	30	50	100	150	200

To calculate the SINR samples, the zero forcing (ZF) receiver could be considered. For SISO case, the SINR for a given subcarrier k can be defined as [71]

$$\gamma_k = \frac{P_{r,0}}{\frac{1}{|h_0|^2}\sigma_n^2 + \sum_{l=1}^{N_{\mathrm{int}}} \frac{|h_l|^2}{|h_0|^2} P_{r,l}}, \tag{B.1}$$

where h_0 and h_l are the channel coefficients resulting from the desired and interfering

signals, respectively. Let σ_n^2 be the receiver noise. The average received power is then

$$P_{r,i} = P_{t,i} \cdot G_{\text{antenna},i} \cdot L_{\text{pathloss},i} \cdot L_{\text{shadow},i}, \tag{B.2}$$

where the transmit power $P_{t,i}$ is scaled by the large-scale fading (antenna gain, path loss and shadowing). Denote the transmitting eNB by the index i, that is, the desired transmitter with $i = 0$ and the interferer with $i = 1, \ldots, N_{\text{int}}$ are considered. N_{int} refers to the number of interfering eNBs. Figure B.1 shows the post-equalisation SINR vector of a single UE from (B.1) under 1.4 MHz LTE system bandwidth (6 RBs). Only 12 SINR samples are required for the entire bandwidth.

```
>> SINR_postequal(1,:)

ans =

  Columns 1 through 7

  -11.2117  -11.0446  -10.7447  -10.3555   -9.9238   -9.4918   -9.0327

  Columns 8 through 12

   -8.7043   -8.4484   -8.2688   -8.1732   -8.1775
```

Figure B.1: The post-equalisation SINR vector (12 subcarriers/samples).

Appendix C

Link-to-System Mapping

According to [6], the link quality and link performance models are the main stage in the Vienna simulator as shown in Figure C.1. Also, the same models are implemented for the simulator developed in this thesis. After the equaliser, the subcarrier SINR vector $(\gamma_1, \ldots, \gamma_n)$ is measured from the link quality model. The next stage is the link performance model where only a set of allocated subcarriers is investigated. Due to a large number of subcarriers, the SINR vector is compressed into an effective SINR value (γ_{eff}). Then, this single γ_{eff} will be mapped into a single BLER value under each MCS. In fact, the LTE-defined CQI is used to identify the MCS. This process is known as link-to-system (L2S) mapping.

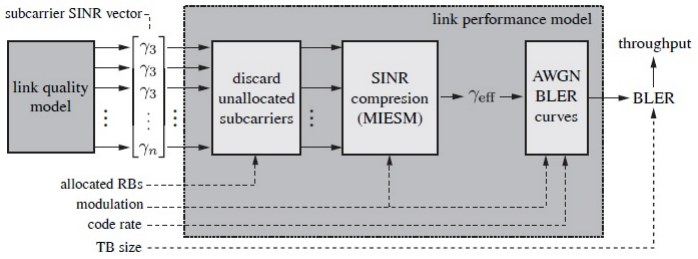

Figure C.1: The link quality and link performance models [1].

For the SINR compression or averaging, there are various approaches such as channel

capacity-based and exponential effective SINR mapping presented in [72, 31]. In this thesis, the MIESM has been selected. The SINRs are averaged in the mutual information (MI) domain and the average MI is then mapped into the effective SINR. The non-linear effective SINR mapping (ESM) averaging of MIESM is defined as [1]

$$\gamma_{\text{eff}} = I_k^{-1}\left(\frac{1}{N}\sum_{n=1}^{N} I_k(\gamma_n)\right), \tag{C.1}$$

where N is the length of SINR vector. Let $I_k(\gamma_n)$ be the bit-interleaved coded modulation (BICM) capacity for a modulation encoding k bits per symbol under given γ_n. This BICM capacity is defined as

$$I_k(\gamma) = k - \mathbf{E}\left\{\frac{1}{k}\sum_{i=1}^{k}\sum_{b=0}^{1}\sum_{z\in\mathcal{X}_b^i}\log\frac{\sum_{\hat{x}\in\mathcal{X}}\exp(-|Y-\sqrt{\gamma}(\hat{x}-z)|^2)}{\sum_{\tilde{x}\in\mathcal{X}}\exp(-|Y-\sqrt{\gamma}(\tilde{x}-z)|^2)}\right\}, \tag{C.2}$$

where $\mathcal{X}$ is the set of 2^k constellation symbols. Denote the set of symbols when bit i equals b by $\mathcal{X}_b^i$. Y is assumed to be complex normal with zero mean and unit variance. The BICM capacity under the 4-, 16- and 64-QAM modulations used in LTE is shown in Figure C.2.

Subsequently, γ_{eff} is mapped into a BLER value using AWGN SNR-to-BLER curves as illustrated in Figure C.3. The 15 BLER curves are precomputed and loaded from LL simulations. Furthermore, this results in the SINR-to-CQI mapping as shown in Figure C.4. The mapping at the 10% BLER point of BLER curves can be obtained.

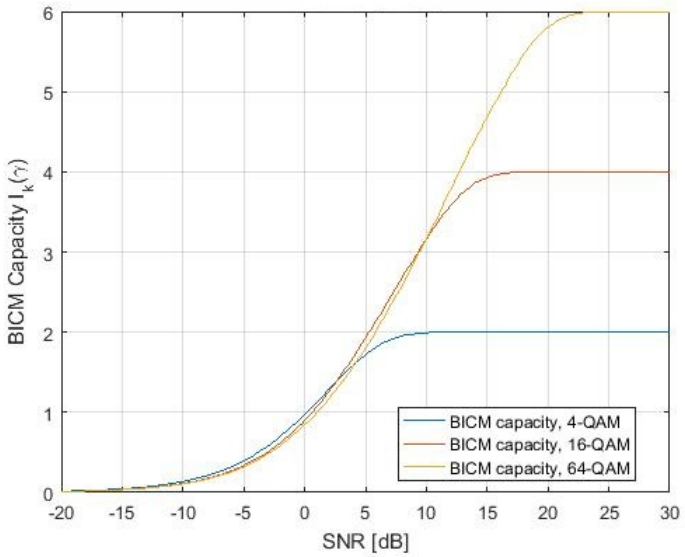

Figure C.2: BICM capacity curves in the LTE.

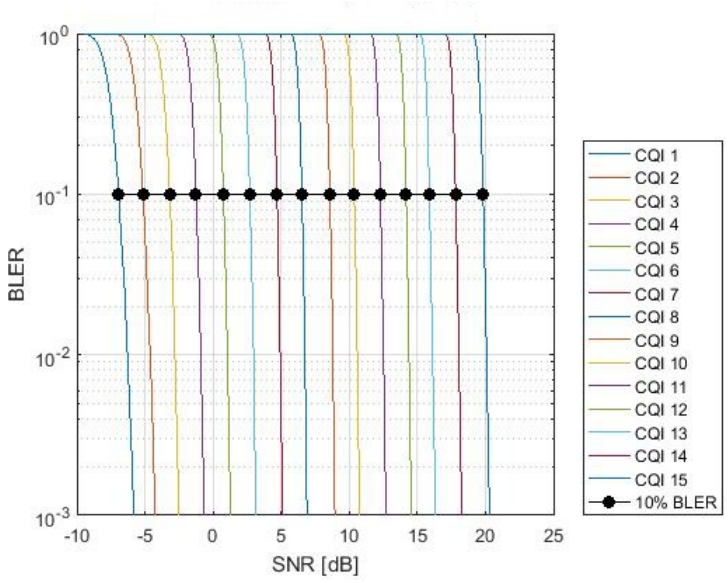

Figure C.3: AWGN SNR-to-BLER curves for the 15 LTE-defined CQIs.

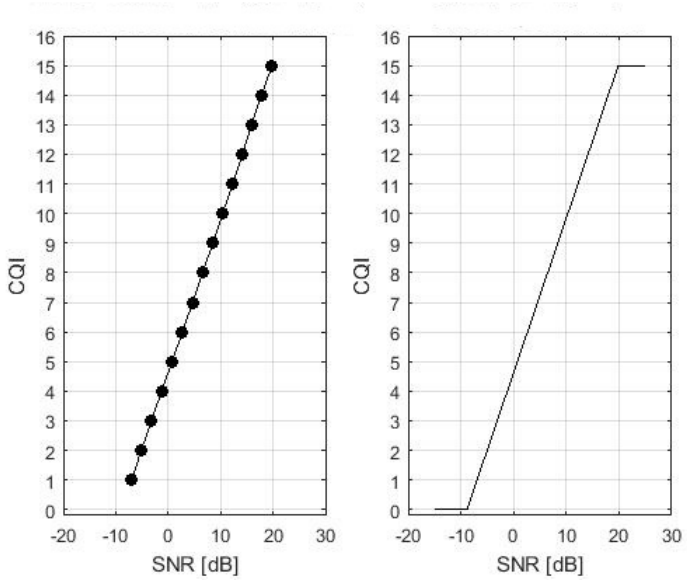

Figure C.4: The SNR-to-CQI mapping.

Appendix D

eNB Signalling

Due to the feedback from UEs (CQIs) and user allocation from the scheduler, the signalling from the eNB to each UE can be determined and listed as follows

- TB_CQI: CQI for the transmission of each codeword
- TB_size: Size of the current TB (in bits)
- num_assigned_RBs: Number of assigned RBs
- assigned_RB_map: Indicating the RBs of a specific UE
- assigned_power: Indicating the total power of a specific UE within the current TTI
- tx_mode: Transmission mode
- nLayers: Number of layers
- nCodewords: Number of codewords
- rv_idx: Redundancy version index (HARQ) for each codeword
- genie_TB_SINR: Estimated TB SINR as calculated by the eNB
- adaptive_RI: Carrier information necessary for the adaptive RI algorithm

For example, to obtain the TB size, the modulation order (modulation_order) and coding rate (coding_rate) from the look-up CQI table are selected based on the transmission CQI (TB_CQI). Also, the number of symbols per RB and number of assigned RBs (num_assigned_RB) are required for this calculation. The TB size is defined as [6]

$$\begin{aligned} \text{TB\_size} = \quad & (\text{sym\_per\_RB\_nosync} \times \text{num\_assigned\_RB} \\ & \times \text{modulation\_order} \times \text{coding\_rate} \times 2) - 24. \end{aligned} \tag{D.1}$$

This is the TB size without synchronization symbols (in bits) for two slots which is subtracted by 24 bits for the cyclic redundancy check (CRC). Let sym_per_RB_nosync be the number of non-synchronization symbols per RB.

Appendix E

Link Performance Model

Figure E.1 shows the link performance model. This final stage consists of

- Importing related information from previous stages (post-equalisation SINR vector and eNB signalling).
- If any RBs are assigned, layer mapping, TB SINR, BLER and ACK are determined.
- Updating feedback such as BLER and ACK.
- Storing related information for post-processing (performance metrics calculation).

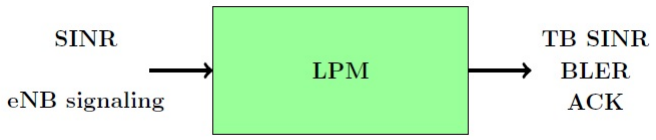

Figure E.1: The link performance model.

To obtain a single TB SINR (in dB), the post-equalisation SINR samples are averaged in connection with the corresponding TB CQI. Then, the TB SINR and TB CQI will be used to determine the BLER. For the acknowledgment, ACK = 1 if BLER <

rand(1,nCodewords) where rand(1,nCodewords) is an 1-by-nCodewords matrix of (uniformly distributed) random numbers. Otherwise, ACK is equal to zero.

At the end of each TTI, the information is stored in the feedback buffer of each UE as illustrated in Figure E.2. This buffer is required for the post-processing and operation of the following TTIs.

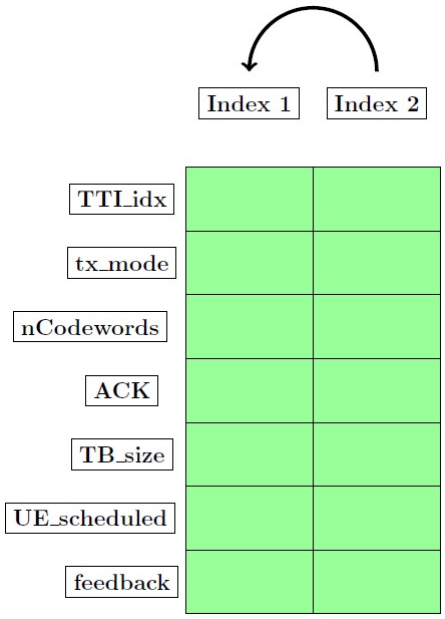

Figure E.2: The UE feedback buffer.

Bibliography

[1] J. Ikuno, "System Level Modeling and Optimization of the LTE Downlink," PhD thesis, Vienna University of Technology, 2013.

[2] Ofcom, "Connected Nations 2019," Ofcom, Tech. Rep., 2019.

[3] A. Ghosh and R. Ratasuk, *Essentials of LTE and LTE-A*. Cambridge University Press, 2011.

[4] A. Damnjanovic, J. Montojo, Y. Wei, T. Ji, T. Luo, M. Vajapeyam, T. Yoo, O. Song, and D. Malladi, "A survey on 3GPP heterogeneous networks," *IEEE Wireless Communications*, vol. 18, no. 3, pp. 10–21, jun 2011.

[5] H. Cui, V. C. M. Leung, S. Li, and X. Wang, "LTE in the Unlicensed Band: Overview, Challenges, and Opportunities," *IEEE Wireless Communications*, vol. 24, no. 4, pp. 99–105, aug 2017.

[6] M. Rupp, S. Schwarz, and M. Taranetz, *The Vienna LTE-advanced simulators : up and downlink, link and system level simulation*, 1st ed. Springer Singapore, 2016.

[7] X. Chu, D. Lopez-Perez, Y. Yang, and F. Gunnarsson, *Heterogeneous Cellular Networks: Theory, Simulation and Deployment*. Cambridge University Press, 2013.

[8] Ofcom, "Update on 5G Spectrum in the UK," Ofcom, Tech. Rep., 2017.

[9] 3GPP, "Evolved Universal Terrestrial Radio Access (E-UTRA); Further advancements for E-UTRA physical layer aspects (3GPP TR 36.814 version 9.1.0 Release 9)," 3GPP, Tech. Rep., 2016.

[10] 3GPP, "LTE; Requirements for further advancements for Evolved Universal Terrestrial Radio Access (E-UTRA) (LTE-Advanced) (3GPP TR 36.913 version 14.0.0 Release 14)," 3GPP, Tech. Rep., 2017.

[11] P. Alvarez, C. Galiotto, J. van de Belt, D. Finn, H. Ahmadi, and L. DaSilva, "Simulating dense small cell networks," in *2016 IEEE Wireless Communications and Networking Conference*. IEEE, apr 2016, pp. 1–6.

[12] N. Jinaporn, S. Armour, and A. Doufexi, "System-Level Simulation for Homogeneous and Heterogeneous Cellular Networks," in *2019 IEEE 89th Vehicular Technology Conference (VTC2019-Spring)*, 2019.

[13] N. Jinaporn, S. Armour, and A. Doufexi, "Performance Evaluation on Resource Allocation with Carrier Aggregation in LTE Cellular Networks," in *2019 IEEE 90th Vehicular Technology Conference (VTC2019-Fall)*, vol. 2019-Septe. IEEE, sep 2019, pp. 1–5.

[14] OpenSignal, "The State of LTE (February 2018)," Tech. Rep., 2018.

[15] 3GPP, "LTE; Evolved Universal Terrestrial Radio Access (E-UTRA) and Evolved Universal Terrestrial Radio Access Network (E-UTRAN); Overall description; Stage 2 (3GPP TS 36.300 version 14.2.0 Release 14)," 3GPP, Tech. Rep., 2017.

[16] D. Tse and P. Viswanath, *Fundamentals of Wireless Communication*, 1st ed. Cambridge University Press, 2005.

[17] A. Goldsmith, *Wireless communications*. Cambridge University Press, 2005.

[18] C. Ciochina and H. Sari, "A review of OFDMA and single-carrier FDMA," in *2010 European Wireless Conference (EW)*. IEEE, 2010, pp. 706–710.

[19] Keysight Technologies, "Concepts of Orthogonal Frequency Division Multiplexing (OFDM) and 802.11 WLAN," 2000. [Online]. Available: http://rfmw.em.keysight.com/wireless/helpfiles/89600B/WebHelp/Subsystems/wlan-ofdm/content/ofdm_basicprinciplesoverview.htm

[20] DreamCatcher, "ME1130 Essentials of LTE and LTE-Advanced," 2014. [Online]. Available: http://dreamcatcher.asia/cw

[21] K.-C. Chen and R. Prasad, *Cognitive Radio Networks*. Chichester, UK: John Wiley & Sons, Ltd, apr 2009.

[22] 3GPP, "LTE; Evolved Universal Terrestrial Radio Access (E-UTRA); Physical channels and modulation (3GPP TS 36.211 version 14.2.0 Release 14)," 3GPP, Tech. Rep., 2017.

[23] Alcatel-Lucent, "9362 ENTERPRISE CELL SERIES 2 V2.2 2100MHz W-CDMA SMALL CELL," Alcatel-Lucent, Tech. Rep., 2013.

[24] 3GPP, "LTE; Evolved Universal Terrestrial Radio Access (E-UTRA); User Equipment (UE) radio transmission and reception (3GPP TS 36.101 version 14.4.0 Release 14)," 3GPP, Tech. Rep., 2017.

[25] H. Lee, S. Vahid, and K. Moessner, "A Survey of Radio Resource Management for Spectrum Aggregation in LTE-Advanced," *IEEE Communications Surveys & Tutorials*, vol. 16, no. 2, pp. 745–760, jan 2014.

[26] C. Park, L. Sundström, A. Wallén, and A. Khayrallah, "Carrier aggregation for LTE-advanced: design challenges of terminals," *IEEE Communications Magazine*, vol. 51, no. 12, pp. 76–84, dec 2013.

[27] Y. Huang, Y. Chen, Y. T. Hou, W. Lou, and J. H. Reed, "Recent Advances of LTE/WiFi Coexistence in Unlicensed Spectrum," *IEEE Network*, vol. 32, no. 2, pp. 107–113, mar 2018.

[28] Qualcomm, "LTE in Unlicensed Spectrum: Harmonious Coexistence with Wi-Fi," San Diego, 2014.

[29] E. Almeida, A. M. Cavalcante, R. C. Paiva, F. S. Chaves, F. M. Abinader, R. D. Vieira, S. Choudhury, E. Tuomaala, and K. Doppler, "Enabling LTE/WiFi coexistence by LTE blank subframe allocation," in *IEEE International Conference on Communications*. Institute of Electrical and Electronics Engineers Inc., 2013, pp. 5083–5088.

[30] ETSI, "5 GHz RLAN; Harmonised Standard covering the essential requirements of article 3.2 of Directive 2014/53/EU (ETSI EN 301 893 V2.1.1)," Tech. Rep., 2017.

[31] F. Khan, *LTE for 4G mobile broadband : air interface technologies and performance*. Cambridge University Press, 2009.

[32] B. Sadiq, R. Madan, and A. Sampath, "Downlink Scheduling for Multiclass Traffic in LTE," *EURASIP Journal on Wireless Communications and Networking*, vol. 2009, no. 1, p. 510617, 2009.

[33] H. Lei, L. Zhang, X. Zhang, and D. Yang, "A Novel Multi-Cell OFDMA System Structure using Fractional Frequency Reuse," in *2007 IEEE 18th International Symposium on Personal, Indoor and Mobile Radio Communications*. IEEE, 2007, pp. 1–5.

[34] P. Ameigeiras, Y. Wang, J. Navarro-Ortiz, P. E. Mogensen, and J. M. Lopez-Soler, "Traffic models impact on OFDMA scheduling design," *EURASIP Journal on Wireless Communications and Networking*, vol. 2012, no. 1, p. 61, dec 2012.

[35] Y. Sun, W. Xiao, R. Love, K. Stewart, A. Ghosh, R. Ratasuk, and B. Classon, "Multi-User Scheduling for OFDM Downlink with Limited Feedback for Evolved UTRA," in *IEEE Vehicular Technology Conference*. IEEE, sep 2006, pp. 1–5.

[36] M. K. Muller, S. Schwarz, and M. Rupp, "QoS investigation of proportional fair scheduling in LTE networks," in *2013 IFIP Wireless Days (WD)*. IEEE, nov 2013, pp. 1–4.

[37] H. Tian, S. Gao, J. Zhu, and L. Chen, "Improved Component Carrier Selection Method for Non-Continuous Carrier Aggregation in LTE-Advanced Systems," in *2011 IEEE Vehicular Technology Conference (VTC Fall)*. IEEE, sep 2011, pp. 1–5.

[38] K. Arshad and S. Rostami, "Resource allocation for multi-carrier cellular networks," in *2018 IEEE Wireless Communications and Networking Conference (WCNC)*. IEEE, apr 2018, pp. 1–6.

[39] F. Wu, Y. Mao, S. Leng, and X. Huang, "A Carrier Aggregation Based Resource Allocation Scheme for Pervasive Wireless Networks," in *2011 IEEE Ninth International Conference on Dependable, Autonomic and Secure Computing*. IEEE, dec 2011, pp. 196–201.

[40] H.-S. Liao, P.-Y. Chen, and W.-T. Chen, "An Efficient Downlink Radio Resource Allocation with Carrier Aggregation in LTE-Advanced Networks," *IEEE Transactions on Mobile Computing*, vol. 13, no. 10, pp. 2229–2239, oct 2014.

[41] S. Rostami, K. Arshad, and P. Rapajic, "A joint resource allocation and link adaptation algorithm with carrier aggregation for 5G LTE-Advanced network," in *2015 22nd International Conference on Telecommunications (ICT)*. IEEE, apr 2015, pp. 102–106.

[42] S. Rostami, K. Arshad, and P. Rapajic, "Optimum Radio Resource Management in Carrier Aggregation Based LTE-Advanced Systems," *IEEE Transactions on Vehicular Technology*, vol. 67, no. 1, pp. 580–589, jan 2018.

[43] R. Ratasuk, M. A. Uusitalo, N. Mangalvedhe, A. Sorri, S. Iraji, C. Wijting, and A. Ghosh, "License-exempt LTE deployment in heterogeneous network," in *2012 International Symposium on Wireless Communication Systems (ISWCS)*. IEEE, aug 2012, pp. 246–250.

[44] R. Ratasuk, N. Mangalvedhe, and A. Ghosh, "LTE in unlicensed spectrum using licensed-assisted access," in *2014 IEEE Globecom Workshops (GC Wkshps)*. IEEE, dec 2014, pp. 746–751.

[45] A. Bhorkar, C. Ibars, and P. Zong, "Performance analysis of LTE and Wi-Fi in unlicensed band using stochastic geometry," in *2014 IEEE 25th Annual International Symposium on Personal, Indoor, and Mobile Radio Communication (PIMRC)*. IEEE, sep 2014, pp. 1310–1314.

[46] C. Chen, R. Ratasuk, and A. Ghosh, "Downlink Performance Analysis of LTE and WiFi Coexistence in Unlicensed Bands with a Simple Listen-Before-Talk Scheme," in *2015 IEEE 81st Vehicular Technology Conference (VTC Spring)*. IEEE, may 2015, pp. 1–5.

[47] G. Bianchi, "Performance analysis of the IEEE 802.11 distributed coordination function," *IEEE Journal on Selected Areas in Communications*, vol. 18, no. 3, pp. 535–547, mar 2000.

[48] H. Ko, J. Lee, and S. Pack, "A Fair Listen-Before-Talk Algorithm for Coexistence of LTE-U and WLAN," *IEEE Transactions on Vehicular Technology*, vol. 65, no. 12, pp. 10 116–10 120, dec 2016.

[49] H. Ko, J. Lee, and S. Pack, "Joint Optimization of Channel Selection and Frame Scheduling for Coexistence of LTE and WLAN," *IEEE Transactions on Vehicular Technology*, vol. 67, no. 7, pp. 6481–6491, jul 2018.

[50] MathWorks, "Monte Carlo Simulation," 2020. [Online]. Available: https://www.mathworks.com/discovery/monte-carlo-simulation.html

[51] ATDI, "ICS telecom EV." [Online]. Available: http://www.atdi.com/ics-telecom/

[52] 3GPP, "LTE; Evolved Universal Terrestrial Radio Access (E-UTRA); Radio Frequency (RF) system scenarios (3GPP TS 36.942 version 13.0.0 Release 13)," 3GPP, Tech. Rep., 2016.

[53] 3GPP, "3GPP TSG RAN WG4 (Radio) Meeting #51: Simulation assumptions and parameters for FDD HeNB RF requirements," 3GPP, San Francisco, Tech. Rep., 2009.

[54] H. Claussen, "Efficient modelling of channel maps with correlated shadow fading in mobile radio systems," in *2005 IEEE 16th International Symposium on Personal, Indoor and Mobile Radio Communications*, vol. 1. IEEE, 2005, pp. 512–516.

[55] ITU, "Recommendation ITU-R M.1225: Guidelines for evaluation of radio transmission technologies for IMT-2000," ITU, Tech. Rep., 1997.

[56] T. S. Rappaport, *Wireless communications : principles and practice*, 2nd ed. Prentice Hall PTR, 2002.

[57] Y. Zheng and Chengshan Xiao, "Simulation models with correct statistical properties for rayleigh fading channels," *IEEE Transactions on Communications*, vol. 51, no. 6, pp. 920–928, jun 2003.

[58] MathWorks, "Empirical cumulative distribution function," 2020. [Online]. Available: https://www.mathworks.com/help/stats/ecdf.html

[59] R Project, "Empirical Cumulative Distribution Function," 2020. [Online]. Available: https://www.rdocumentation.org/packages/stats/versions/3.6.2/topics/ecdf

[60] R. Jain, D.-M. Chiu, and W. Hawe, "A Quantitative Measure Of Fairness And Discrimination For Resource Allocation In Shared Computer Systems," *CoRR*, vol. cs.NI/9809, 1998.

[61] Ofcom, "Award of 2.3 and 3.4 GHz spectrum by auction," 2018. [Online]. Available: https://www.ofcom.org.uk/spectrum/spectrum-management/spectrum-awards/awards-archive/2-3-and-3-4-ghz-auction

[62] Y. Wang, K. Pedersen, T. Sorensen, and P. Mogensen, "Carrier load balancing and packet scheduling for multi-carrier systems," *IEEE Transactions on Wireless Communications*, vol. 9, no. 5, pp. 1780–1789, may 2010.

[63] ITU, "Recommendation ITU-R P.1238-9: Propagation data and prediction methods for the planning of indoor radiocommunication systems and radio local area networks in the frequency range 300 MHz to 100 GHz," Geneva, Tech. Rep., 2017.

[64] A. Mukherjee, J.-F. Cheng, S. Falahati, H. Koorapaty, D. H. Kang, R. Karaki, L. Falconetti, and D. Larsson, "Licensed-Assisted Access LTE: coexistence with IEEE 802.11 and the evolution toward 5G," *IEEE Communications Magazine*, vol. 54, no. 6, pp. 50–57, jun 2016.

[65] 3GPP, "Digital cellular telecommunications system (Phase 2+) (GSM); Universal Mobile Telecommunications System (UMTS); LTE; 5G; Release description; Release 15 (3GPP TR 21.915 version 15.0.0 Release 15)," 3GPP, Tech. Rep., 2019.

[66] 3GPP, "LTE; Evolved Universal Terrestrial Radio Access (E-UTRA); Physical layer; Measurements (3GPP TS 36.214 version 15.5.0 Release 15)," 3GPP, Tech. Rep., 2020.

[67] M. Haenggi, *Stochastic geometry for wireless networks.* Cambridge University Press, 2009.

[68] B. Błaszczyszyn, M. Haenggi, P. Keeler, and S. Mukherjee, *Stochastic Geometry Analysis of Cellular Networks.* Cambridge University Press, 2018.

[69] 3GPP, "3rd Generation Partnership Project; Technical Specification Group Services and System Aspects; Release 16 Description; Summary of Rel-16 Work Items (3GPP TR 21.916 version 0.1.0 Release 16)," 3GPP, Tech. Rep., 2019.

[70] A. Zappone, M. Di Renzo, and M. Debbah, "Wireless Networks Design in the Era of Deep Learning: Model-Based, AI-Based, or Both?" *IEEE Transactions on Communications*, vol. 67, no. 10, pp. 7331–7376, jun 2019.

[71] J. C. Ikuno, M. Wrulich, and M. Rupp, "System Level Simulation of LTE Networks," in *2010 IEEE 71st Vehicular Technology Conference.* IEEE, 2010, pp. 1–5.

[72] K. Brueninghaus, D. Astely, T. Salzer, S. Visuri, A. Alexiou, S. Karger, and G. Seraji, "Link Performance Models for System Level Simulations of Broadband Radio Access Systems," in *2005 IEEE 16th International Symposium on Personal, Indoor and Mobile Radio Communications*, vol. 4. IEEE, 2005, pp. 2306–2311.